Comprehensive Insights into Synthesis, Structural Features, and Thermoelectric Properties of High-Performance Inorganic Chalcogenide Nanomaterials for Conversion of Waste Heat to Electricity

Manjunatha Channegowda*, Rafiq Mulla, Yashaswini Nagaraj, Suraj Lokesh, Sachith Nayak, Sudeep Mudhulu, Chandresh Kumar Rastogi, Charles William Dunnill, Hari Krishna Rajan, and Ajit Khosla*

*Corresponding Authors
Manjunatha Channegowda - Department of Chemistry, RV College of Engineering, Bengaluru 560059, India; Centre for Nanomaterials and Devices, RV College of Engineering, Bengaluru 560059, India; Orcidhttps://orcid.org/0000-0003-0422-9614; Email: manjunathac@rvce.edu.in manju.chem20@gmail.com
Ajit Khosla - School of Advanced Materials and Nanotechnology, Xidian University, Xi'an, Shaanxi Province 710126, China; Orcidhttps://orcid.org/0000-0002-9868-0926; Email: khosla@gmail.com ajitkhosla@xidian.edu.cn

Authors
Rafiq Mulla - Energy Safety Research Institute, Swansea University, Bay Campus, Fabian Way, Swansea SA1 8EN, United Kingdom
Yashaswini Nagaraj - Department Chemical Engineering, RV College of Engineering, Bengaluru 560059, India
Suraj Lokesh - Department Chemical Engineering, RV College of Engineering, Bengaluru 560059, India
Sachith Nayak - Department Chemical Engineering, RV College of Engineering, Bengaluru 560059, India
Sudeep Mudhulu - Department of Chemical Engineering, National Taiwan University, Taipei 10617, Taiwan; Orcidhttps://orcid.org/0000-0003-0976-1853
Chandresh Kumar Rastogi - Centre for Advanced Studies, Lucknow, 226031 Uttar Pradesh, India
Charles William Dunnill - Energy Safety Research Institute, Swansea University, Bay Campus, Fabian Way, Swansea SA1 8EN, United Kingdom; Orcidhttps://orcid.org/0000-0003-4052-6931
Hari Krishna Rajan - Department of Chemistry, M. S. Ramaiah Institute of Technology, Bengaluru 560054, India; Orcidhttps://orcid.org/0000-0003-4939-2781

Abstract
Thermoelectrics are energy harvesters that can directly convert waste heat into electrical energy and vice versa. Currently, thermoelectric (TE) devices display lower efficiency as the materials used for construction possess a very low figure of merit (ZT). Therefore, understanding the structural features of materials, finding new materials, and analyzing their chemistry and physics play a vital role in enhancing their energy conversion efficiency. Among the different classes of TE materials, some inorganic chalcogenides are perfect candidates for power generation as they possess excellent TE properties. The objective of this review is to provide insights into structural features and innovative methods to obtain enhanced thermoelectric properties of selected inorganic chalcogenides. The review covers recent advances in preparation methods, structural features, and thermoelectric properties of selected metal selenides (Bi_2Se3, Ag_2Se, SnSe, etc.) and metal tellurides (Bi_2Te_3, SnTe, PbTe, etc.). The review also discusses the critical parameters for designing and optimizing the TE materials to obtain the required electrical conductivity (σ), Seebeck coefficient (S), and thermal conductivity (k). In addition, promising mechanistic approaches to be adopted for enhancing the efficiency of TE materials such as doping, alloying, and nanostructuring are discussed in detail. Finally, a summary that describes advancements in the materials design is provided with a prospect for future applications from these materials in the development of energy harvesting technology.

Keywords: Thermoelectricity; Thermoelectric properties; Thermoelectric devices, Chalcogenides; Selenides; Tellurides; Doped Materials

1. Introduction

The unprecedented socio-economic growth has led to an exhaustible usage of energy obtained from natural resources like coal, oil and other fossil fuels [1]. The rising energy demand, environmental problems caused by the use of coal and oil,and the associated fear of fuel extinction have resulted in a number of innovations that can effectively produce and utilize energy without or with minimum environmental pollution[2]. These innovations include the emergence of solar cells[3], hydrogen fuel cells[4], batteries[5], thermoelectric devices[6-7], etc. Statistically, more than 60% of generated energy is lost in vain due to insufficient energy harnessing technologies[8]. For example, only around 10% of the energy is produced by the combustion of petroleum fuels in automobiles, while the rest of it is lost as waste heat[9], or in case of steelworks, around 10^9 J of heat is wasted during the production of 1 tonne of crude

steel.[10] Therefore, there are continuous efforts to develop of new technologies as well as there is a growing interest in enhancement of conversion efficiency of existing ones.[11-12] Among these technologies, thermoelectrics is one of the attractive and rapidly developing energy harnessing methods that can effectively convert waste heat into useful electric power.[13-15]

As depicted in figure 1, the thermal energy lost during the production of electricity in the power plant, inefficient usage of fire energy for domestic purposes, metallurgy reactions in hot furnaces, automobile engines, space rocket engines, etc. could be efficiently converted to useful green electricity. In these scenarios, the TE technology can be a viable, green and sustainable technology for the power generation from waste thermal energy. TE technology also helps address issues such as the global energy crisis, environmental pollution and for the development of sustainable energy generation technologies. Itcan be a promising technology and could be effectively used to achieve three important sustainable development goals, such as SDG-7 (Ensure access to affordable, reliable, sustainable and modern energy), SDG-11 (Make cities inclusive, safe, resilient and sustainable), and SDG-13 (Take urgent action to combat climate change and its impacts) as proposed by United Nations[16-18].

TE materials utilise temperature difference across the material to generate electric voltage [8],providing a method for direct conversion of waste heat into electricity.[9-10] Therefore, it is perceived as a green technology that can contribute to the reduction of global carbon emission and energy economy. [19] TE devices serve as an eco-friendly energy conversion technology along with several advantages of relatively smaller sizes, high reliability, environmental friendliness, and capabilities of working under broad working temperature ranges.[20] However, at present, the efficiency of these devices is not good enough to meet with the Carnot efficiency[21-22].

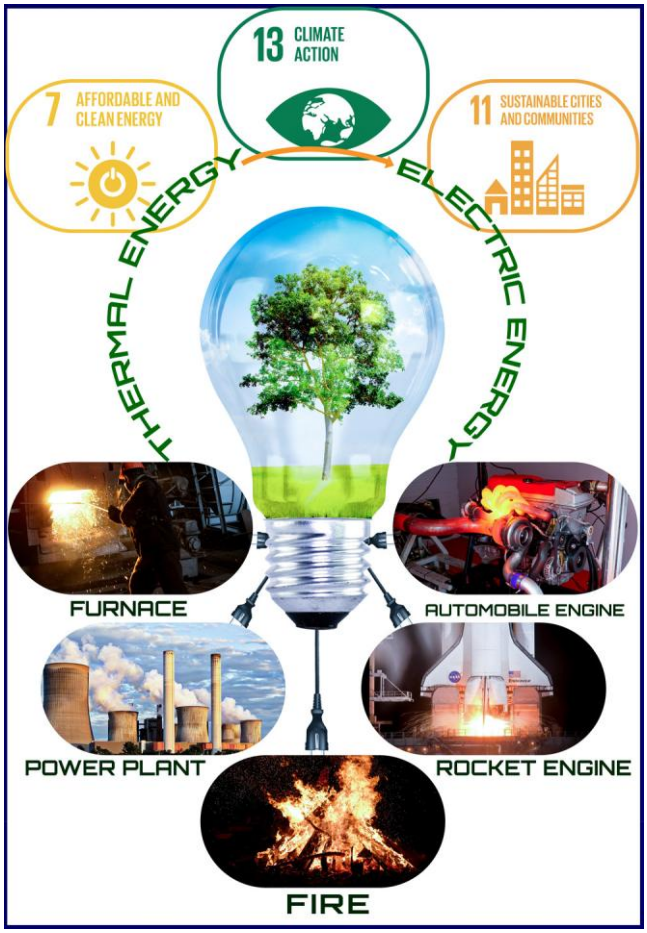

Figure 1. Representing the Sources of thermal energy for electricity generation using TE technology and its ability to achieve SDSs (7, 11 and 13).[23-26]

In order to enhance performance of TE materials and devices, different novel strategies are being used to develop new materials for the application. It is well-known that the quantum confinement effects in nanoscale materials found to exhibit exciting opto-electronic and physical properties. Semiconductor nanostructures have greatly contributed to the growth of nanotechnology due to their high surface to volume ratio and tunable band gap [27]. This attractive class of materials has been used in many functional nanodevices including sensors[28-29], transistors[30], solar cells[31], electro catalyst [32], photocatalyst[33-34], adsorbents[35-36] and nano-generators[37].

The working of thermoelectric devices is based on three effects namely, Seebeck effect [38], Peltier effect [39] and Thomson effect [40]. In TE generators, the conversion of heat to electricity is quantified by a dimensionless quantity known as the "Figure of Merit" (ZT). The Figure of Merit is defined as

$$ZT = \frac{\sigma S^2 T}{k} \qquad [1]$$

where 'σ' is the electrical conductivity, 'S' is Seebeck coefficient, 'k' is thermal conductivity of the material at the respective characteristic temperature 'T'. Thus, any TE material with good performance characteristics must possess high values of 'σ' and 'S' while 'k' must be as low as possible. The general rule of thumb therefore is the larger the 'ZT', the better the TE properties exhibited by the material. The improvement of 'ZT' values can be achieved by introducing nanoscale precipitates and compositional irregularity into existing materials, which provide abundant grain boundaries or defects that can significantly assist in reducing lattice 'k' while maintaining a relatively high power-factor (PF = $\boldsymbol{\sigma S^2}$), as represented in the Equation (1). Recent progress has resulted in a high 'ZT' value of about 2 with a projected efficiency of 20%, which is expected to have a significant impact on the energy production and conservation sectors[41]. Currently, TE materials that are of keen interest are Bi_2Te_3, [42] PbTe,[43] Bi_2Se_3,[44] PbSe,[45] SnTe,[46] $Ge_{0.95}Bi_{0.05}Te$,[47] $Ge_{1-x-y}Ta_xSb_yTe$,[48] half-Heusler compounds like $Ti_x(Zr_{0.5}Hf_{0.5})_{(1-x)}NiSn$ (x = 0–0.7) [49] or BXGa (X - Be,Mg and Ca),[50] skutterudites, Mg_2X (X - Si, Ge, Sn), ternary compounds (e.g., MgAgSb, BiCuSeO) [51], binary compounds - oxides like ZnO, $SrTiO_3$[52] or $NaCo_2O_4$[53], nitrides like BN [54], copper chalcogenides,[55] ScN [56] or $C_3\ N_4$ [57], etc.

Recent developments in the TE research suggest that some of the metal chalcogenides based on selenides and tellurides have significantly better performance as compared to other materials. In this review, we have made an effort to present a comprehensive overview of the most prominent metal chalcogenide TE materials that include some of the selected metal selenides and tellurides. This article also highlights the various fabrication processes and performance analysis of different electrical and thermal parameters that determine the TE efficiency.

2. Historical background of thermoelectricity

The period from 1820 to 1920 is regarded as the century of early study of thermoelectricity[58]. Those initial years have witnessed the discovery and development of the thermoelectric science by several scientists in Europe and Russia with Berlin being the prime centre of major research activity.Thomas Johann Seebeck, in 1821-1823 observed that a circuit constructed from two dissimilar metals, having junctions exposed to different temperatures deflected a compass magnet[59]. Seebeck originally attributed this deflection to the induced

magnetism by the difference in temperature and related it to the earth's magnetic field. However, it was later realised that the magnet was deflected by an electric current produced from thermoelectric force. This phenomenon of generating electrical potential from temperature difference is popularly called the Seebeck effect.

In 1851, Gustav Magnus hinted that the 'S' is a thermodynamic state function by discovering that the developed electric potential does not depend on the temperature distribution along the metals. Seebeck also made a qualitative list of different elements, metals, and alloys on the basis of their relative Seebeck effect. The Seebeck effect was quantitatively characterised (μV/K) and 'σ' of many metalsand alloys was identified correctly in 1910 by Werner Haken from the support of Becquerel's studies on ZnSb and CdSb. This identification helped classification of some good thermoelectric materials such as Sb_2Te_3, Bi_2Te_3, $Bi_{0.9}Sb_{0.1}$, SnTe, Cu-Ni alloys.

The Peltier effect, regarded as a contrast of the Seebeck effect, was observed by a French physicist Jean Charles Athanase Peltier in 1834. He found that heating or cooling effects at the junction of two dissimilar metals by passing an electric current through the circuit. The effect was further studied by Lenz, who in 1838 postulated that drop or rise in the temperature of the junction depends on the direction of current flow. It was stated that the heat energy generated or absorbed at the junction is proportional to the magnitude of electric current with the Peltier coefficient being the proportionality constant.

In 1858, William Thomson provided the most comprehensive explanation of the Seebeck & Peltier effects and described the relationship between them, which is well-known as theThomson effect. According to Thomson, heat is either liberated or absorbed when an electric current flows in a material which is kept under a temperature difference.He further postulated that this heat energy is proportional to temperature gradient across the material with the Thomson coefficient being the proportionality constant; which is related thermodynamically to the 'S'.

The 'ZT', which necessitates that good thermoelectric materials should possess large 'S', high 'σ' and low 'k', was developed from the constant property model. This model was first used by Edmund Altenkirch to obtain the efficiency and performance of a thermoelectric generator (1909) and a cooler (1911) respectively, under optimised design & operating conditions[60-61]**.** The concept of 'ZT' was employed byAbram Fedorovich Ioffe in 1949 to develop the modern history of thermoelectricity that made it into the classical textbooks of "Semiconductor Thermoelements" and "Thermoelectric Cooling" in 1956[62].H. Julian Goldsmid was a pioneer who used 'ZT' as a quality factor and identified the importance of

high mobility and effective mass combination and low lattice 'k' in semiconductors. He found that when semiconductors are properly doped, they can become good TE materials [63].

The period from 1950s to present is treated as Renaissance Era in the field of thermoelectrics as it has markeda great progress in research and development of thermoelectric materials to achieve higher 'ZT' values and better device efficiency. During this period, first-generation thermoelectric materials with a 'ZT' value of 0.8-1.0 and conversion efficiency (η) of 5-6% were developed. After years of study into improving 'ZT', better 'ZT' values at high temperatures were achieved thatresulted in the development of second-generation thermoelectric materials with 'ZT' values ranging from 1.3 to 1.7 and a 10% increase in device efficiency**.** The development of third generation of thermoelectric materials is currently under progress with new fabrication technologies that have been successful to achieve a higher 'ZT' of 1.8-2 and a further improved performance with efficiency of 15-20%. This group of materials is currently being developed and represents the future of thermoelectric technology[64].

3. Terminologies in Thermoelectricity

- Figure of Merit ('ZT') – It is a dimensionless number used to measure the performance of a thermoelectric device considering the characteristic properties of material used in the device.
- Seebeck Coefficient (S) – It is the measure of the magnitude of an induced thermoelectric voltage in response to a temperature difference across a material, as induced by the Seebeck effect expressed in volts per kelvin.
- Electrical Conductivity (σ) – It is the measure of material's ability to conduct electric current and it is a reciprocal of electrical resistivity expressed in siemens per metre.
- Thermal Conductivity (k) – It is the rate at which heat is transferred by conduction through a unit cross-section area of a material, when a temperature gradient exists perpendicular to the area expressed in watts per metre kelvin.
- Carrier Concentration (n) – It is the number of charge carriers present in unit volume of the material.
- Electron Mobility (μ) – It is a measure of electron movement in a material under an electric field.

4. Heat to Electricity Conversion Mechanism

The exponential growth of energy demand leading to numerous development and research innovations in energy harnessing technologies [65]. Majority of industrial processes and natural

processes that involve usage of thermal energy also result in loss of energy as heat. This energy loss must be judiciously utilized for improvement of overall energy economy, andto achieve this, thermoelectricity can be a promising technology to do it effectively[66]. TE materials consist of free electrons or holes which act as carriers of both charge and heat. The mobile charge carriers diffuse from the hot end to the cold end when a temperature gradient is applied. If the material is p-type, positive charges get accumulated at the cold end resulting in a positive potential. Similarly, if the material is of n-type, a negative potential is developed, as illustrated in Figure 2 that depicts the movement of electrons and holes in p-type and n-type materials, respectively, induced by the temperature gradient [67-68].

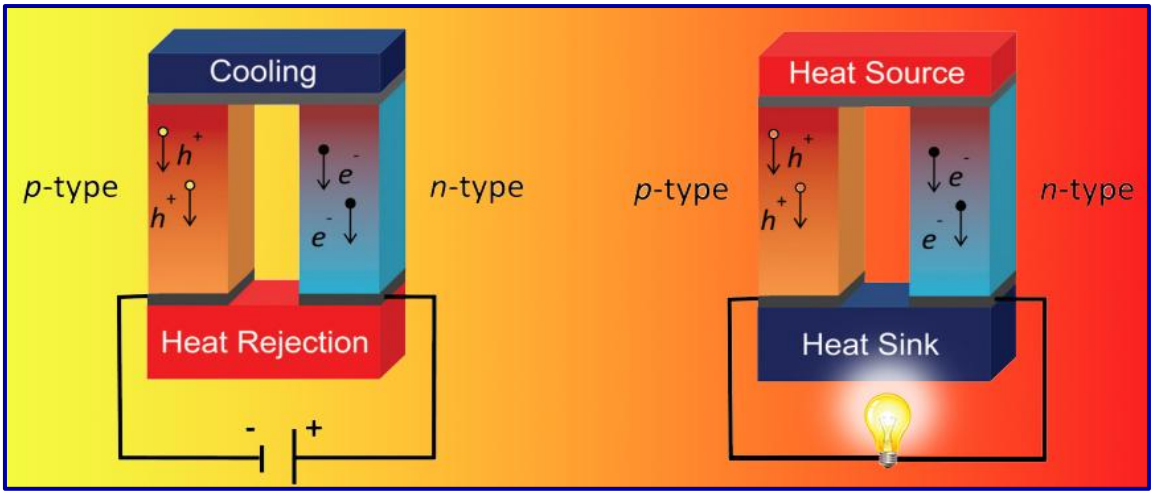

Figure 2. Representation of the TE effect in (left) a Peltier cooler and (right) a TE generator. Charge carriers move from one end of the thermocouple, carrying entropy and heat towards the other end. Both n- and p-type materials are necessary for a complete device. (Reprinted with permission from [68] Copyright © 2020, The Royal Society of Chemistry)

A thermoelectric generator (TEG) is a solid-state device that uses the Seebeck effect to convert heat energy into electricity. It consists of several pairs of p- and n-type materials (called as TE legs) that are connected in series through electric conductors. The temperature difference on each TE leg generates a small electric potential, such electric potentials from all the conductors added up to generate sufficient voltage from the TEG. The representative scheme of energy conversion is shown in Figure 2. [68].

The Seebeck effect describes the cause of potential build up is due to diffusion of charged carriers driven by temperature gradients present across the material. Charge carriers move from the hot end to cold end of material leading to gradient in charge carriers, which is balanced by an electric field that produces electric potential in the material. The magnitude of this effect is realised by the magnitude 'S', given by equation (2) which may be either

positive or negative depending upon the majority of charge carriers available for diffusion in the material. It is defined as

$$S = \frac{\Delta V}{\Delta T} \qquad (2)$$

where 'ΔV' is the potential developed and 'ΔT' is the temperature gradient applied.

The Seebeck effect is affected by factors such as (a) density of states(DOS) of carriers, where sharply changing DOS improves the 'S', (b) transmissivity of material, allows more electrons to pass through the potential barriers, (c) mean free path, which defines the scattering of electrons and (d) temperature, when the ratio of grain size to length of a material is high the increase in temperature becomes more significant [69].

On the other hand, the Peltier effect, discovered by French scientist Jean-Charles-Athanase Peltier in 1834, is considered to be the inverse of the Seebeck effect. A heating or cooling effect can be observed when an electric current passes through a circuit made up of two distinct conductors, resulting in a temperature change at the junction regions. This generation of temperature difference between the junctions of the two conductors is known as the Peltier effect [70].

As discussed above, equation (1) theoretically demands that the TE materials should possess large 'S' and 'σ' while the 'k' must be as low as possible to obtain enhanced 'ZT' values. However, these requirements are in practical,limited by Weidemann- Franz law and the Pisarenko relation. Additionally, all the three parameters are a function of carrier concentration,therefore, cannot be tuned independently [71]. Thus, there exists a complex relationship between the thermoelectric parameters that help understand these parameters in more detail, are outlined by equations (3), (4) and (5).

$$S = \frac{8\pi^2 {k_B}^2}{3eh^2} m^* T \left(\frac{\pi}{3n}\right)^{\frac{2}{3}} \qquad (3)$$

$$\sigma = ne\mu = \frac{ne^2\tau}{m^*} \qquad (4)$$

$$\kappa_{tot} = \kappa_{lat} + \kappa_{ele} = \kappa_{lat} + L\sigma T \qquad (5)$$

Where 'k_B' is Boltzmann constant, 'h' is Planck constant, 'n' is carrier concentration, 'm*' is carrier effective mass, 'T' is temperature,'τ' is the relaxation time, 'e' is charge of carriers, 'κ_{tot}', 'κ_{lat}' and 'κ_{ele}' are total, lattice, and electrical thermal conductivities, respectively, and 'L' is the Lorentz number. Past decades have seen notable progress in the field of

thermoelectricity with enhanced 'S' and reduced 'k'. The enhanced values of 'ZT' are achieved by employing diverse strategies such as engineering of band structure to enhance 'S' and synthesis of hierarchical structures to reduce 'k'. Such strategies have resulted in different and new kind of thermoelectric materials as shown in Figure 3. Figure 3 depicts various thermoelectric materials that are in the spotlight along with their maximum 'ZT' values, cost, and cost effectiveness (which is defined as ratio of 'ZT' to cost).

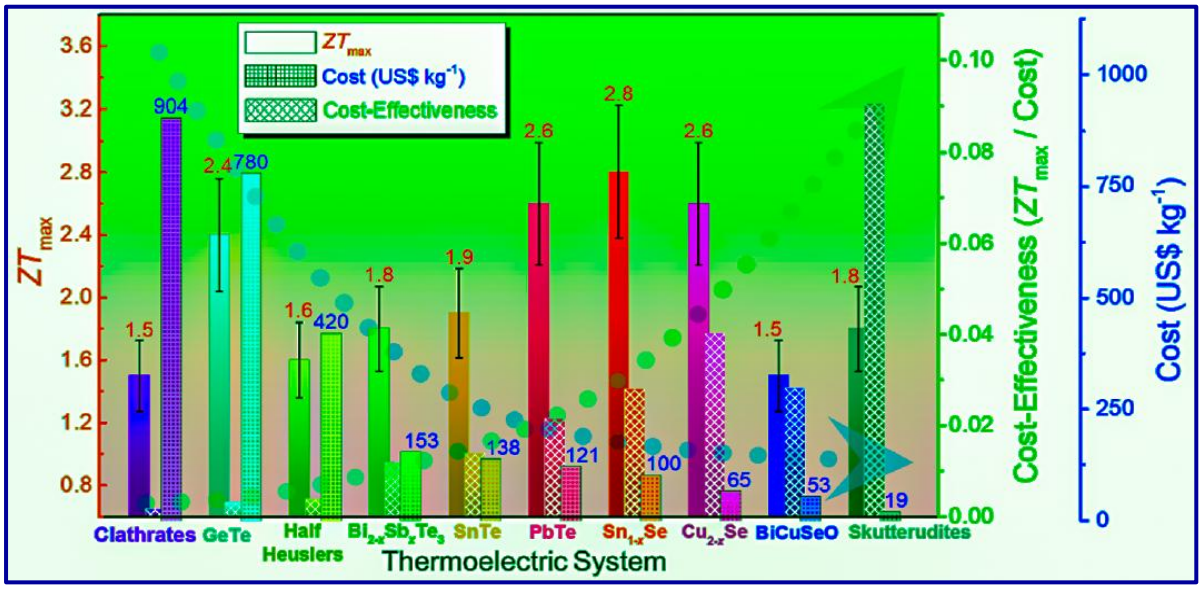

Figure 3. 'ZT' values for state-of-the-art TE materials in the last 10 years. (a) Reported maximum 'ZT' values ('ZTmax') with error bars, calculated cost, and calculated cost-effectiveness ('ZTmax'/cost) (Reprinted with permission from [72] Copyright © 2020, American Chemical Society)

In the past decade, attempts have been made to explore materials like clathrates, GeTe, half-Heuslers, $Bi_{(2-x)}Sb_xTe_3$, SnTe, PbTe, $Sn_{(1-x)}Se$, $Cu_{(2-x)}Se$, BiCuSeO, and skutterudites owing to their better thermoelectric properties. It can be observed thatthe cost of materials reduced significantly with subsequent enhancement in cost effectiveness of these materials that is attributed to the innovative and rigorous research focus on thermoelectrics.

5. Inorganic chalcogenide nanostructures for thermoelectrics

Metal chalcogenide-based thermoelectric materials have a higher TE performance than metal oxides due to the strong covalent nature of interatomic bonds resulting from poor electro-negativity. When compared to other thermoelectric materials, their high atomic weight helps reduce 'k'. Furthermore, the relative ease with which chalcogenides form various structures provides an excellent platform for studying and enhancing thermoelectric performance. Metal

chalcogenide-based thermoelectric materials are also superior in terms of material manufacture and operation costs[73-74].

Nanostructures of binary chalcogenides exhibit improved thermoelectric properties in comparison to their bulk counterparts because of the enhanced power factor (PF) obtained due to quantum confinement boosting the density of states around Fermi level and decreasing the lattice 'k' resulting in effective phonon scattering at grain boundaries. Further, effective scattering of minority charge carriers at the grain boundaries of nanostructures helps achieve improved thermoelectric properties like higher 'S' as compared to the bulk counterparts. Many of the chalcogenides based compoundshave tuneable electronic band structures and variable phonon transport properties, and also possess higher thermal stability, which makes them the best choice for TE materials.

5.1. Metal selenides

The transition metal selenium based compounds with semiconductor behaviour form metal chalcogenides belonging to group I-VI,which have attracted significant attention due to their exceptional physical and chemical properties [75]. Selenide based materials exhibit a wide range of variation in crystal structure, conduction type (electronic and ionic), band gap, and phase configuration (single phase or polymorphism) [76]. Selenides outperform in thermoelectric properties which is believed to originate from their large size and mass. Based on simple chemical intuition, a larger and heavier Selenium (Se) atom in M_xSe_y(M is metal) compounds indicate a smaller difference in electronegativity between 'M' and 'Se', resulting in a more covalent character of the M-Se bond[77]. Therefore, the electronic band must be sharp due to smaller effective mass and higher carrier mobility. A smaller band gap is also a consequence of an appreciable overlap of orbitals of 'M' and 'Se'. The described characteristics of M-Se bond formation led to a high PF for thermoelectric devices and an inherent decent value of 'σ' [41, 78]. Chalcogenides are easily available in different structures which open up further scope for the study to enhance their thermoelectric performance. They are favourable for both n-type and p-type doping which draws more attention towards them[79].

The conventional inorganic TE materials have quite a wide range of uses in the thermoelectric industry. The aim of this section is to provide an overview and the most current progress of prominent metal selenides due to their eco-friendly nature, earth abundance and capability to exhibit remarkable thermoelectric properties under appropriate conditions[74]. The fabrication of metal selenide based thermoelectric materials can be

categorized into three major methods such as wet chemical synthesis, high-temperature fabrication, and chemical/physical deposition. This section covers a discussion on different material fabrication strategies and thermoelectric properties of some important groups such as (a) bismuth selenide, (b) silver selenide, (c) tin selenide, and some other promising selenides.

(a) *Bismuth selenide (Bi_2Se_3)*: Bismuth selenide (Bi_2Se_3) is a semiconductor that has all the characteristics required for a best performing thermoelectric material. Being a tellurium-free compound, Bi_2Se_3 also possesses good thermoelectric properties at low temperature range (10K – 350K) [80]. It is a narrow bandgap semiconductor with high carrier mobility and layered structure [81] due to which it exhibits properties of topological insulators.As it has layered structures bonded by van Der Waals force, foreign atoms can be introduced to enhance its TE performance.

(b) *Silver selenide (Ag_2Se)*: Silver selenide is a narrow bandgap intrinsic semiconductor with an orthorhombic crystal structure that undergoes a phase transition at ~ 406 K and forms a superionic cubic phase [82]. It exhibits exceptional thermoelectric properties at room temperature and its abundance availability makes it a better choice[83]. At low transition temperature, silver selenide provides a good platform for thermoelectric properties to be manipulated.

(c) *Tin selenide (SnSe)*: Tin selenide is a medium temperature range thermoelectric compound with narrow bandgap and layered structure [84]. Itslayered structure with van Der Waals and tight covalent bonds result in high anisotropic properties and low 'k' [85]. SnSe has attracted significant attention for research due to its low toxicity, high earth abundance and excellent energy conversion efficiency [86].

5.1.1. Wet chemical synthesis

Thermoelectric nanomaterials can be synthesised in a number of ways, among which solution based synthesis methods are quite easy and cost-effective. Samanta *et al.*[87] reported a simple and low-temperature solution phase method to fabricate ultrathin nanosheets of BiSe and Bi_4Se_3. The synthesis process provides a method for few-layer 2D nanosheets of different topological materials from (Bi2)m(Bi2Se3)n homologous series with a general and facile synthesis route.[87] The fabricated nanosheets are ultrathin in nature having 1-3 layers of thickness and 1-2 μm in lateral dimension (Figure 4) and these structures exhibit ultralow κ_{lat} of about 0.24-0.27 W/mK because of significant phonon scattering at heterostructured interfaces of BiSe and Bi_4Se_3. These heterostrctured nanosheets hold great promise for low thermal conductivity applications.

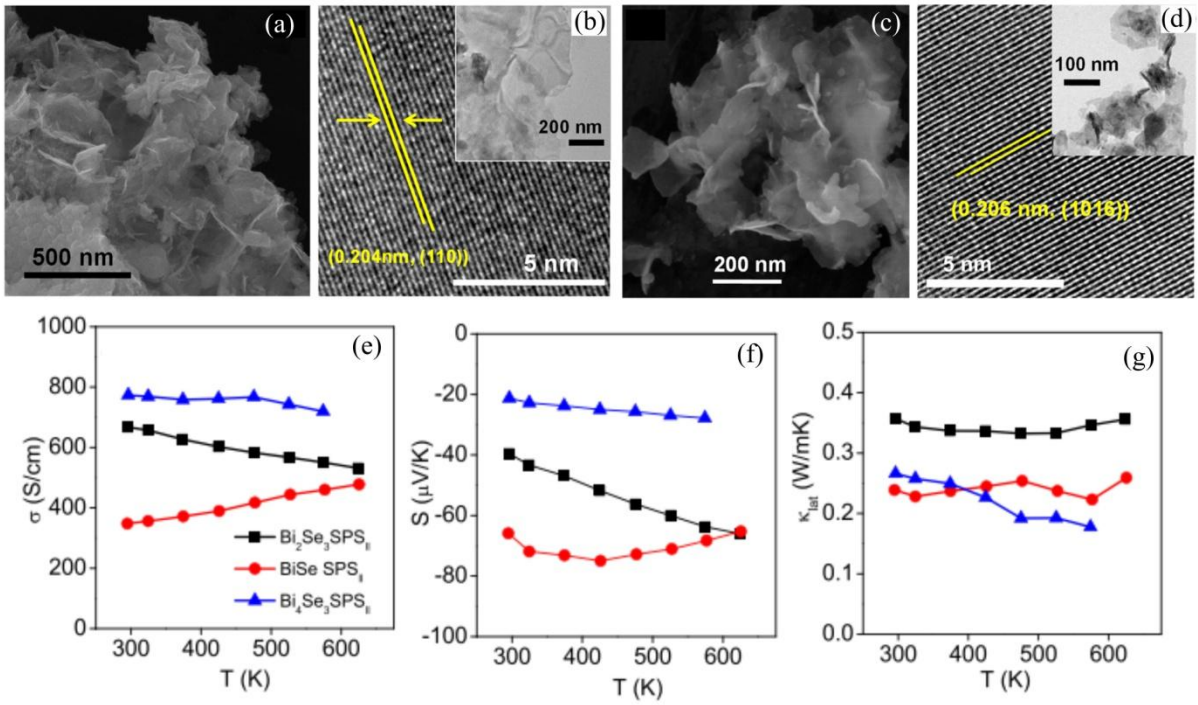

Figure 4. (a & b) FESEM and HRTEM images of BiSe nanosheets. (c & d) FESEM and HRTEM images of Bi4Se3 nanosheets. Temperature dependent (e) electrical conductivity, (f) Seebeck coefficient, and (g) lattice thermal conductivity of Bi_2Se_3, BiSe, and Bi_4Se_3 nanosheets. Reprinted with permission from[87] Copyright © 2020, American Chemical Society)

Masood *et al.*[73] followed a simple low temperature wet chemical reduction method to synthesise Bi_2Se_3 nanomaterials of particle size ranging 100-300 nm. The study confirms the formation of ultrathin sheet-like structure and it is evident that formation of high purity single crystalline Bi_2Se_3 nanosheets with non-uniform size distribution was observed. They showed that 'σ' of Bi_2Se_3 remains constant initially but increases with increase in temperature 'T' which may be attributed to low charge carriers and less thermal excitation at low temperatures. The variation of 'σ' affects 'S' which initially increases with increase in 'T' and then reaches a maximum of −95 μV/K at 150ºC and continues to decrease with further increase in 'T'. The variation in carrier concentration due to thermal excitation might be the reason for the trend displayed by 'S'. PF also shows a similar deviation as 'S'. PF initially increases with 'T', reaches a maximum of 1.55 μW/cm-K² at 150 °C and then decreases with further increase in 'T'. Tumelero *et al.*[88] used electrodeposition method to form nanostructures with 200-400 nm particle size. The measurements showed that 'S' is negative which confirms that Bi_2Se_3 allows n-type conduction due to Se vacancies. Under the use of standard electrolyte, a 'PF' of 61 mW/cm-K² was observed. Kadel *et al.*[89] followed a simple

hydrothermal method to synthesise Bi_2Se_3 particles which had flake-like structure and depicted a particle size of around 300 nm. Authors observed that 'PF' increases with increase in temperature which can be attributed to dependence of 'σ' on temperature and thus increase in semiconductor nature of Bi_2Se_3. The maximum value of 'PF' obtained was 1.52 $\mu W/mK^2$ at 523 K. They also showed that 'S' was also temperature dependent and increases with increase in temperature which is due to quantum confinement effect. The maximum value of 'ZT' obtained was 0.096 at 523K. In addition, other methods like co-precipitation [90], successive ionic layer adsorption and reaction (SILAR) [91], and vapour-solid technique [92] have been identified to successfully synthesize nanostructures ranging from 20-200 nm size.

Andzane *et al.*[92] also proved that doping of bismuth selenide with dopants like antimony would have an influencing effect on its phase resulting in hexagonal phase. It was also noticed that nanostructures with flake-like [89] or plate-like [92] morphology showed better thermoelectric performance. Similarly, Musah *et al.*[93] have reported a co-doping approach of indium and antimony into Bi_2Se_3 to create a manifold enhancement in the TE performance. The resulting compounds have shown a high figure of merit (ZT = 0.47) at 473 K for a doping concentration of 0.1 at%.

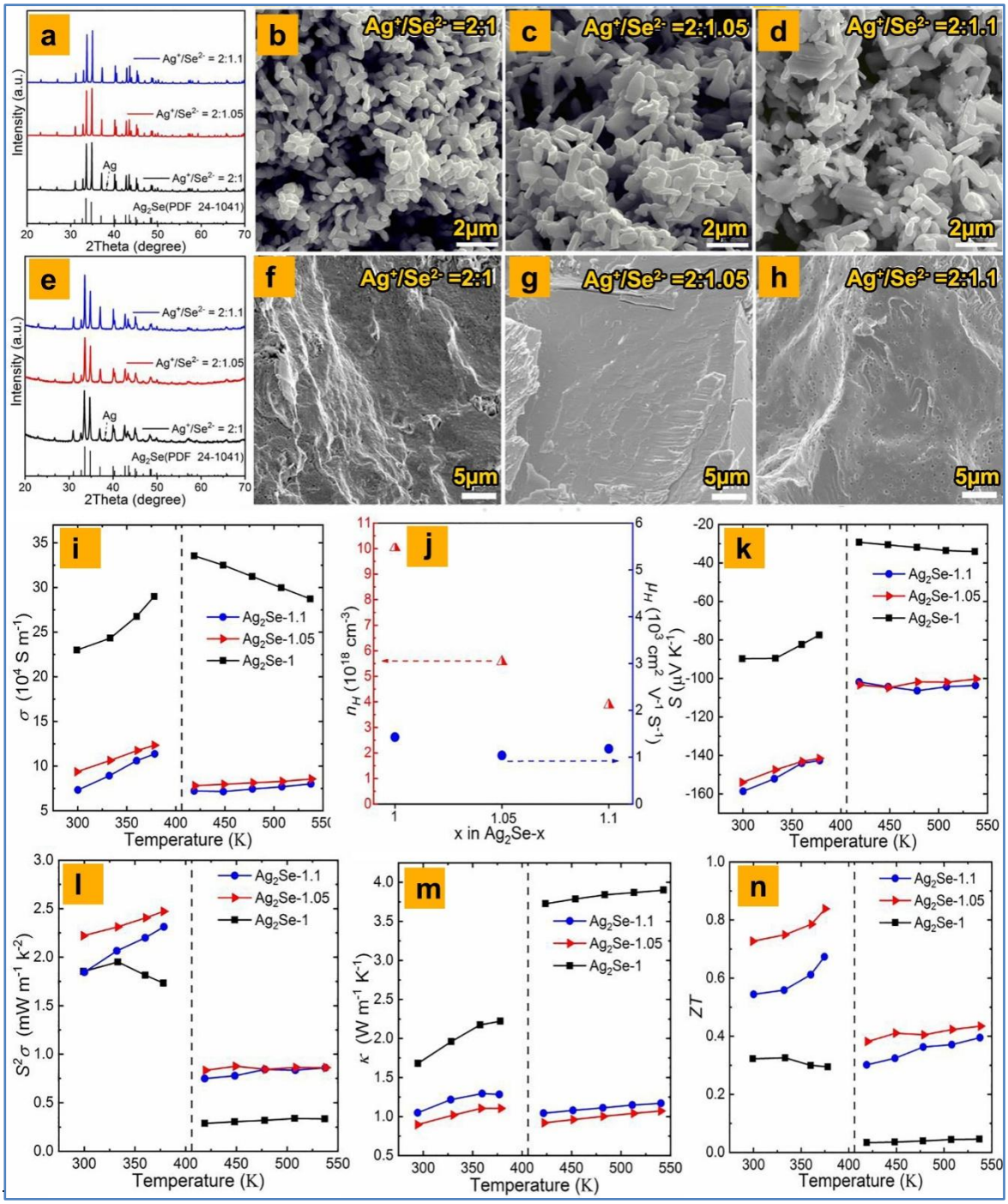

Figure 5. (a) XRD pattern, (b-d) SEM images of as obtained products of Ag_2Se with varying precursor concentrations. (e) XRD pattern, (f-h) SEM images collected from fractured Ag_2 Se pellets along the direction perpendicular to pressing Ag_2 Se, The Ag^+/Se^{2-} molar ratios utilised in the syntheses are labelled in the images. Temperature-dependent thermoelectric properties of Ag_2Se-x (x = 1, 1.05, 1.1) pellets: (i) 'σ', (k) 'S', (l) 'PF', (m) 'k', and (n) 'ZT'. (j) gives the room temperature Hall carrier concentration and mobility of Ag_2 Se-x pellets. (Reprinted with permission from [82] Copyright © 2020, Elsevier) The vertical dashed lines indicate the phase transformation temperature reported for Ag_2Se [94].

Wang *et al.*[82] used a solution-based synthesis method which is less energy consuming compared to melting and annealing methods but requires the usage of surfactant or organic

solvents. The Ag_2Se was prepared by dissolving silver nitrate in deionised water followed by boiling in an oil bath. This solution was added to a mixture of different concentrations of Selenium (Se) and Sodium Borohydride ($NaBH_4$). The obtained mixture was cooled in the Argon atmosphere and products of 0.3 - 2 µm were obtained as evident from Figure 5(b,c,d).The (X-ray diffraction) XRD and SEM images as shown in Figure 5(a) confirm the presence of both Ag and Se. These products were sintered to form pellets by spark plasma sintering (SPS) and the sintered products showed a fractured surface with no specific morphology as seen in Figure 5(f,g,h). The study showed that XRD peaks of as-prepared nanomaterial after sintering decreases as seen in Figure 5(e), which is attributed to reduction in silver content and hence can be concluded that sintering helps in completion of reaction. The reduction in k after sintering as observed from Figure 5(m) is due to the porous structure of the as-synthesised silver selenide which enhances the phonon scattering. The '**σ**' increases from 7.81×10^{4} Sm^{-1} at 420 K to 8.57×10^{4} Sm^{-1} at 540 K as seen in Figure 5(i) which was realized by hall measurement (shown in Figure 5(j)) of carrier concentration. The 'S' decreases with increase in 'T' till phase transition and remains unchanged further as depicted in Figure 5(k). The maximum value of 'S' (−103µV/K) was attained over a temperature range of 420–540 K. This blend of high 'S' and lower '**σ**' was accredited to obtain a high 'PF' of 2.47 $mWm^{-1}K^{-2}$ at 380K and from Figure 5(l), it can be seen that 'PF' also shows same trend as 'S' with temperature.

Lim *et al.*[95]prepared silver selenide by colloidal synthesis method. Oleyl amine (OLA) was degassed at 140℃ and heated to 180℃ which was added with silver nitrate ($AgNO_3$) and Se powder and allowed to react for 30 min at 180℃ with subsequent cooling. Ligand displacement using ammonium thiocyanate (NH_4SCN) was used to eliminate organic surfactant attached to the particles. The size of particles as-obtained was in the range of 16-32 nm. They observed that 'σ' and 'S' showed a steady increase and decrease respectively for the temperature variation from room temperature to 389 K. The maximum value of 'PF' obtained was 2.34 mW/mK^2.

Huang *et al.*[96] synthesised a nanocomposite of SnSe and rGO by heating a solution mixture to its boiling point with addition of sodium hydrogen selenide (NaHSe) and boiled for 2h. The solution mixture was an aqueous solution of tin chloride with NaOH and $NaBH_4$ added with GO, dispersed in water by ultrasonication, at room temperature. TEM results showed that SnSe nanoplates were bound to rGO sheets. Authorsobserved p-type conduction of rGO with positive value of 'S' which initially increases but then decreases with further increase in temperature due to bipolar effects. 'σ' initially increases and then decreases with increase in

temperature for doped SnSe. For nanocomposites, SnSe/rGO has a higher value of 'σ' compared to that of SnSe/GO_m (modified) which is greater than that of SnSe/GO [94, 96]. 'k' of SnSe decreases due to surface oxidation by exposure to air [93]. 'k' of doped products decreases due to increased interfaces which cause lattice phonon scattering, carrier scattering and also enhance defects. Due to the above-mentioned effects of 'S' and 'σ', it is concluded that higher values of 'PF' are obtained at low temperature range and a peak value of 'ZT' of 0.91 was attained at 823 K for SnSe/rGO-0.3 composition.

Protsak *et al.*[86] followed a similar method to prepare nanocomposites of SnSe with GO and modified GO. In contrary, Chandra *et al.*[97] synthesised SnSe nanosheets by heating up mixture of precursors, capping agent and morphology controlling agent to 200^oC in N_2 atmosphere and doped it with Bi using Bi-neo decanoate precursor. Figure 6(a, g) shows the folded structure of the synthesised nanosheets before and after doping Bi on SnSe nanoparticles as characterised by SEM. The thickness of the sheet was found to be 1.18nm as confirmed by Atomic Force Microscopy (AFM) is depicted in Figure 6(b, h). The 2-D structure of nanosheets prior doping was further understood by TEM and TEM images as shown in Figure 6(c, d) and the same was observed after addition of Bi as seen in Figure 6(i, j). The obtained specimens were studied under selected-area electron diffraction (SAED) as displayed in Figure 6(e, k) to support the information that specimens are single crystalline in nature. Homogenous placement of Sn, Se and Bi atoms was investigated using scanning transmission electron microscopy (STEM) along with EDAX as depicted in Figure 6(f, l). All the discussed nanomaterial specimens showed orthorhombic phase and their crystal structure was altered by doping with transition metals like copper and bismuth. Maintaining structure and composition during heat treatment, findings of Chandra *et al.*[97] agreed with variation of thermoelectric properties with temperature as discussed above. 'σ' increases with increase in temperature but decreases with increase in dopant concentration as seen in Figure 6(m). 'S' decreases with increase in 'T' but increases with increase in dopant concentration as shown in Figure 6(n). Considering both the trends, Figure 6(o) depicts the variation of 'PF' with temperature. 'k' decreases with both increase in temperature and dopant concentration as displayed in Figure 6(p, q). Calculating 'ZT' with all the above properties, 'ZT' also increases with increase in T and decreases with increase in dopant concentration as shown in Figure 6(r). Hence, they were successful in obtaining an electrically conductive n-type $Sn_{0.94}Bi_{0.06}Se$ with high 'S' value of -285 μV/K at 719 K and 'PF' of 100 μW/mK² at 719 K at higher temperatures.

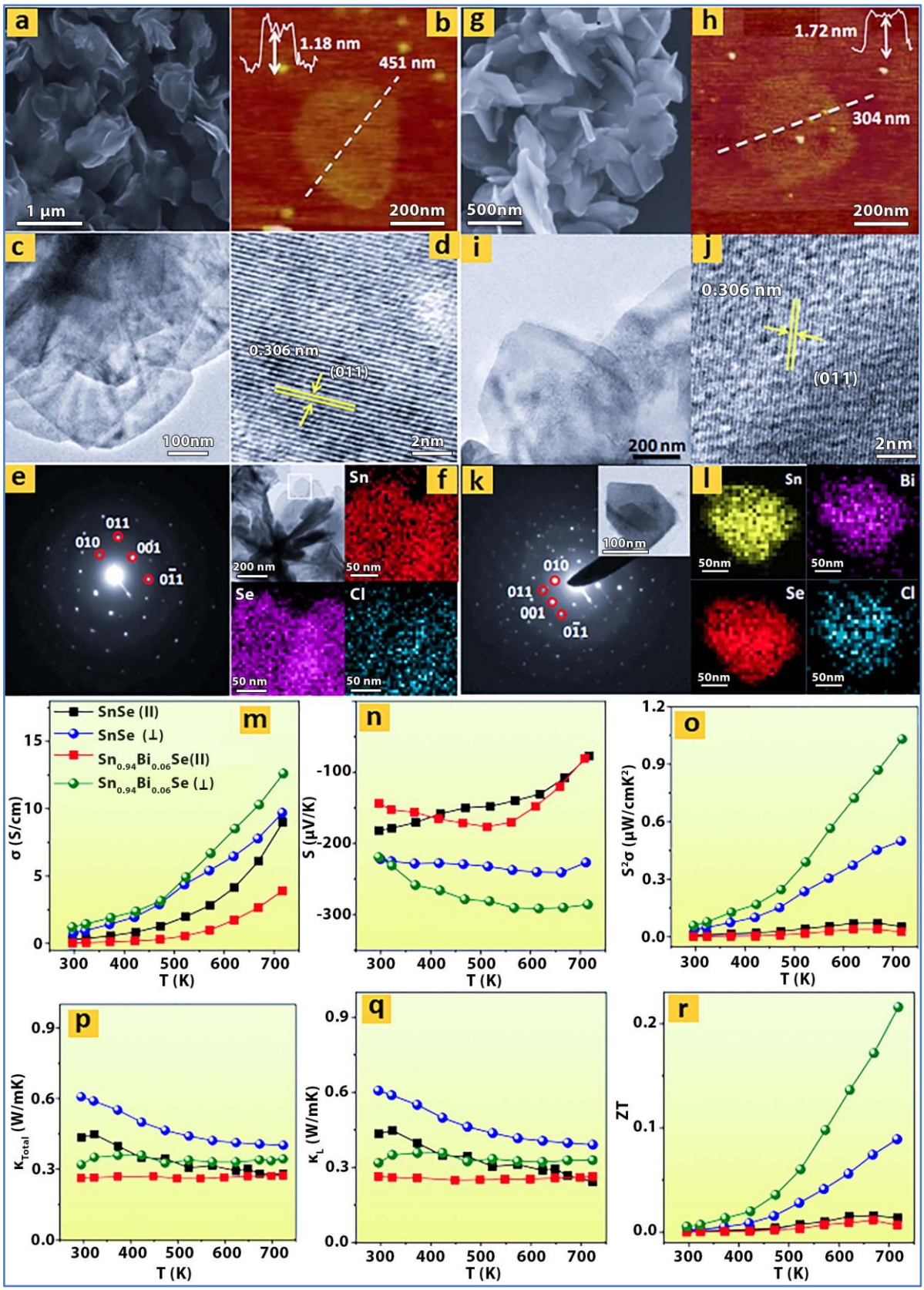

Figure 6. (a) FESEM, (b) AFM, (c) TEM, (d) HRTEM images (e) SAED pattern, (f) STEM image of synthesised SnSe nanosheets and EDAX color mapping for Sn, Se and Cl. (g) FESEM, (h) AFM, (i) TEM, (j) HRTEM images, (k) SAED pattern, inset of (l) shows the STEM image of $Sn_{0.94}Bi_{0.06}$Senanosheet and EDAX color mapping of Sn, Se, Bi and Cl.

Temperature dependent m) σ; n) S; o) PF; p) κ_{total}; q)κ_L; and r) ZT; of SnSe and $Sn_{0.94}Bi_{0.06}Se$ nanosheets. (Reprinted with permission from [97] Copyright © 2018, American Chemical Society)

5.1.2. High temperature fabrication

High temperature fabrication methods such melt growth and spark plasma sintering (SPS) provide a straightforward way to fabricate TE compounds in bulk quantity with precise control of composition. These methods are also very effective in doping of impurities into host material. The effects of impurity atom doping on TE properties of selenide based compounds have been reported in several studies. Bohra *et al.*[98] synthesized Bi_2Se_3 bulk alloys by vacuum melt method followed by vacuum hot-pressing process. The developed compounds have shown the synergetic combination of ultra low thermal conductivity (~0.7 W/mK), high Seebeck coefficient (~168 μV/K), and a very low resistivity (~15 μΩ-m). These multi-scale hierarchical Bi_2Se_3 compounds have shown an impressive ZT of 0.96 at 370 K. Very recently, Hegde *et al.*[99] have studied the effects of Sn and Te co-doping on the TE properties of Bi_2Se_3. The single crystals of $(Bi_{1-x}Sn_x)_2Se_{2.7}Te_{0.3}$ have been obatined via a melt-growth technique using elemental precursors, tin, bismuth, selenium, and tellurium. Authors found a 6 times reduction in resistivity of the doped compounds, and a high ZT of 0.32 has been observed in $Bi_2Se_{2.7}Te_{0.3}$ at 400 K, which is ~7 times larger than that of Bi_2Se_3.Bayesteh *et al.*[100] have fabricated via SPS method. The as developed compounds have shown a large power factor of 800 $\mu W/mK^2$ and a ZT of 0.14 at 300K. Gao *et al.*[83]observed that carrier concentration of product decreases after annealing which might be due to reduction of silver content or due to energy filtering effect on nano-sized interfaces between Ag and Ag_2Se. It was also observed that carrier mobility was doubled after annealing which was due to enhanced crystallinity and decreased carrier concentration leading to weak scattering. Due to this decrease in carrier concentration and increase in carrier mobility, 'σ' decreased which enhanced the PF.

Samanta *et al.*[81] experimentally studied the crystal structure as shown is figure 7(a) of bismuth selenide and confirmed that it exhibits mainly two phases, orthorhombic and rhombohedral phase, which arises due to the use of additives such as tartaric acid or glycerol [88]. Ingots of BiSe were synthesized by mixing stoichiometric amounts of starting elements such as Bi, Sb, and Se in quartz ampoules at 1123 K. They observed that 'k' of Bi_2Se_3 decreases with increase in temperature as shown in Figure 7(f) which can be due to boundary scattering of phonons. The maximum value of 'S' as seen in Figure 7(d) was -80 μV/K at 425 K and a high 'ZT' of 0.8 was observed in figure 4(h) at 425 K. It was also observed that, with

increase in concentration of dopant, 'σ' and 'k' decrease whereas 'S' increases, thus increasing the 'PF' of Bi_2Se_3 with increase in dopant concentration (Figure 7(c,d)). Therefore, Bi_2Se_3 qualifies as a good thermoelectric material and represents further there is lot of scope for study to enhance'PF' by exploiting the temperature dependence of 'σ', 'k' and 'S', by addition of suitable dopants.

J. He *et al.*[101] synthesised Ag_2Se composite by zone melting at a high temperature of 1123 K to obtain particles of size 10-100 nm. All these prepared nanomaterials displayed orthorhombic phase and underwent phase transition when temperature was increased above 403 K during measurement of material properties. They also observed that carrier mobility decreases with increase in dopant concentration which is attributed to increase in carrier concentration with dopant concentration due to massive Se vacancies. The maximum value of 'ZT' of 0.92 was attained at 820K. Doping does not have much effect on the value of 'S' whereas the value 'k' of the silver selenide has decreased with increase in temperature and also with increase in dopant concentration.

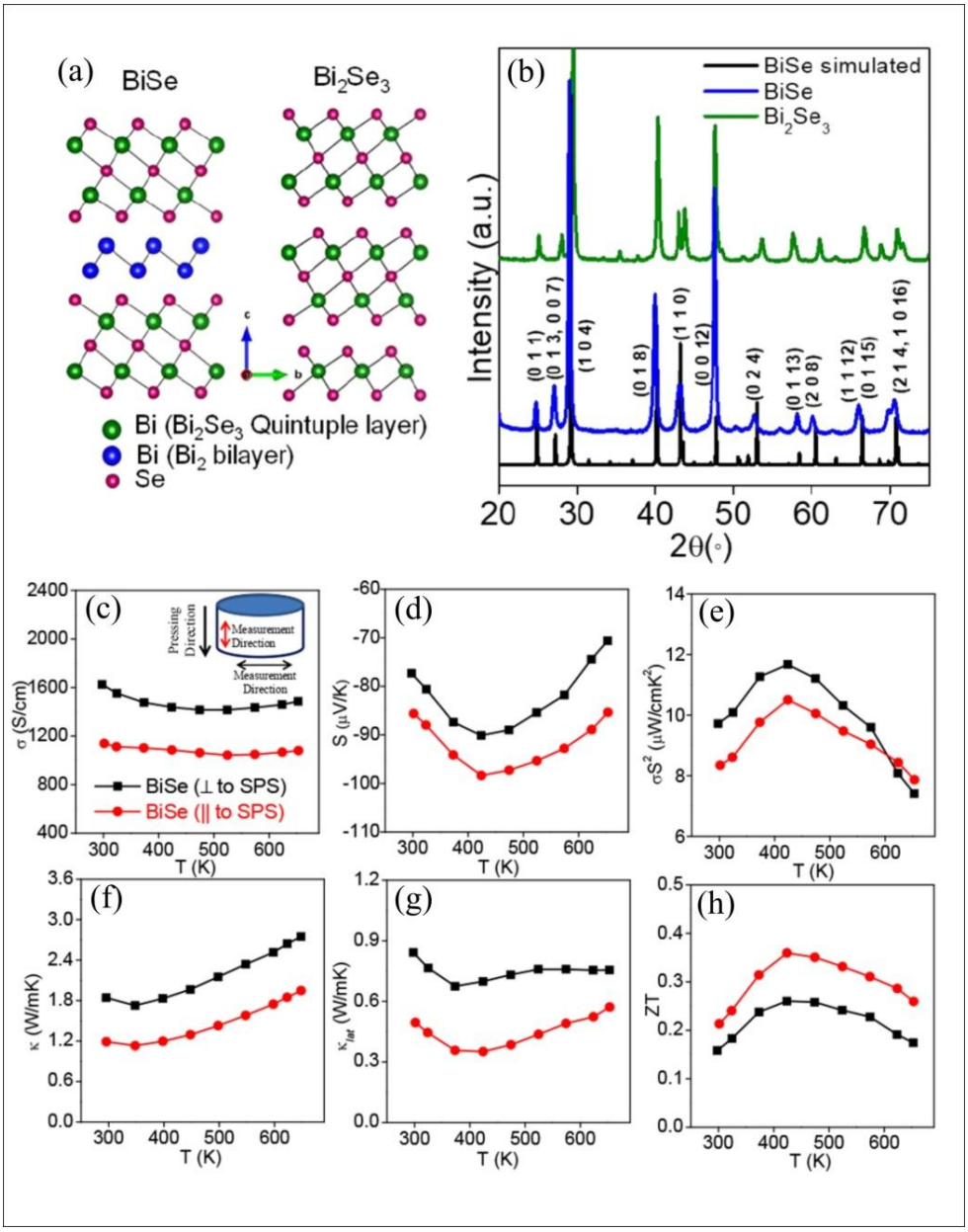

Figure 7. (a) Crystal structures and (b) powder XRD patterns of BiSe and Bi_2Se_3; Temperature dependent (c) 'σ', (d) 'S', (e) PF (σS^2), (f) total 'k', (g) lattice 'k_{lat}' and (h) 'ZT' of BiSe measured parallel and perpendicular to SPS pressing directions. Inset in (d) shows schematic of thermoelectric measurement directions, along the pressing direction (red, ||) and perpendicular to pressing direction (black, ⊥). (Reprinted with permission from [81] Copyright © 2018, American Chemical Society),

Though the above discussed selenide compounds show remarkable properties, there are few other selenide compounds which exhibit excellent thermoelectric properties [102-103]. Owing to the complex synthesis and fabrication methods, attention has been drawn towards other

selenide compounds to be used as alternate TE materials. The above discussed materials show effective thermoelectricity in low or medium temperature ranges but there are remarkable materials that show high performance at wide temperature range like PbSe and Cu_2Se [102].

Wu, Wei, and Li *et al.*[104] explained that PbSe shows p-type conduction due to oxidation of Pb and its loss during processing that generate Pb vacancies and hence extra hole carriers. They synthesised PbSe by mechanical alloying (MA) which gave PbSe that exhibited a high 'ZT' of 0.83 at 673K which was improved by excess Pb stoichiometry over low and mid-temperature range. Zhao *et al.*[105] showed that doping of PbSe matrix with metals like Na and CdS would be an effective technique to reduce its 'k' to 0.57W/mK at 923K to obtain a good 'ZT' of 1.6 at 923K. Liu *et al.*[106] explained that the 'S' can be increased while 'k' can be decreased significantly by critical scattering of electrons and phonons during the phase transition in Cu_2Se. They synthesised Iodine-doped Cu_2Se that was largely temperature dependent and were successful in achieving 'ZT' of 2.3 at RT due to critical scattering effect. Zhao *et al.*[107] alloyed 'S' at Se sites by melt quenching method at 1123 K and annealing for 8 days due to which carrier concentration is significantly increased but carrier mobility is decreased, thus 'k' and 'σ' is decreased. Therefore, a high 'ZT' of 2 at 1000 K was achieved, which is one of the impressive values reported in recent years. With Cu doping, Wang *et al.*[108] showed that 'S' becomes more negative depicting n-type conduction. As temperature and concentration of dopant increases, the value of 'S' decreases whereas Ge *et al.*[84] observed that 'S' increases till 700 K and then decreases with further increase in temperature. With increase in dopant concentration, 'σ' increases as fermi level gets shifted lower into valence bands compared to pure SnSe [84]. Maximum effectiveness of the doped material was found to be at 1% Cu doping on SnSe as authorised by a maximum 'PF' of 1.96 mW/mK^2 and a maximum 'ZT' of 0.75 at 300 K. Zhang *et al.*[85] noticed that 'S' decreases with increase in temperature and always showed positive value for SnSe due to p-type conduction which was attributed to the energy filtering mechanism at grain boundaries. The highest value of 'ZT' obtained was 1.08 at 805 K.

All these studies suggest that the SnSe can become a promising material for thermoelectric applications. Further, the compound is quite suitable for modifying its TE properties by compositional variations, synthesis of divergent morphologies or doping with metals like Bi, Cu, Cl, etc. For example, $SnSe_2$/SnSe composites of promising performance were prepared by the melting−quenching process by Shu *et al.*[109]. Here, authors have studied the influence

of Cl doping on the TE properties of the nanocomposites. The observed data showed that the Cl doping modifies the charge distribution and decreases the energy barrier at interfacial regions between the two phases, as a result, a maximum ZT of 0.56 at 773 K has been achieved from the 6% Cl-doped $SnSe_2$/SnSe nanocomposites.

Fabricating SnSe on different base materials to utilise its maximum efficiency is still a progressive study and provides a platform for new experimental studies [110]. Although silver selenide is an attractive TE material, more studies required in order to understand its TE properties in detail, which will assist enhance 'σ'. This can be achieved by using different synthesis methods and effectively exploiting the temperature dependence of preparation methods. Research on manipulation of thermoelectric properties of Ag_2Se compounds at high temperatures is imperative for their effective use in device fabrication and for practical applications.

5.1.3. Chemical/Physical deposition

With chemical/physical deposition methods, the film composition, morphology, and crystallinity can be varied by controlling deposition parameters during the process. These methods are also capable of producing different phase materials in binary and tertiary systems. Jindal *et al.*[111] used thermal evaporation technique in vacuum to fabricate thin films of Ag_2Se with particle size 36.2 nm. Authors discussed the dependence of 'σ' on temperature. 'σ' increases with increase in temperature till 120 ℃ and then decreases abruptly which is due to intrusion of cubic phase in orthorhombic lattice structure exhibiting liquid-like behaviour. Maximum value of 'σ' was observed to be 6.37×10^4 S/m attained at 90 ℃. The value of 'S' rises till 90 ℃ and then decreases due to variation in carrier concentration along with 'T'. The maximum value of 'S' obtained was -73.14 μV/K at 90℃. Due to 'S' and 'σ' variations, 'PF' also shows similar trend and maximum value of 'PF' was ~341.06 $\mu W/mK^2$ at 90 ℃.

Wu *et al.*[112] showed that 'σ' of Bi_2Se_3 can be enhanced by introduction of graphene by 1D texturing. They successfully obtained a maximum 'ZT' of 1.03. The comparative study between bismuth selenide and graphene doped bismuth selenide via various structural and graphical analysis is depicted in figure 8 (a-h). Jia *et al.*[113] used co-evaporation technique to prepare SnSe films from pure tin (Sn) and Se on Al_2O_3 substrate in Argon atmosphere with source temperature of Sn at 1100^{o}C and Se at 195^{o}C. Employing different molar ratios of Sn:Se and different substrate temperature, films with different compositional phases were obtained. A specimen of SnSe/34%$SnSe_2$ showed that nanosheets were randomly dispersed

whereas a specimen of SnSe/46%$SnSe_2$ showed petal-like nanosheets and another specimen of SnSe/71%$SnSe_2$ exhibited round nanosheets. All specimen samples contained roughness and size of nanosheets in the range 200-300 nm. Thus, different phase induction into SnSe affected morphology of the nanomaterial and hence its properties. They observed that in the SnSe/X%$SnSe_2$ (X=30-80%) composite pure SnSe phase showed positive 'S' indicating p-type conduction. Whereas with increase in $SnSe_2$ content the number of n-type carriers increases and changes the conductivity type of Sn-Se films due to which negative 'S' value are obtained that increases with increasing temperature. It was shown that 'S' increases with increase in temperature for lower $SnSe_2$ concentrations and decreases with increase in temperature for higher $SnSe_2$concentrations due to increase in carrier concentration. At 34%c$SnSe_2$, the value of 'S' reached a maximum of −257.46 μV/K at 250 °C which is due to decrease in carrier concentration caused by compositional variation. The highest 'PF' was calculated to be 155 μW/mK² at 250 °C. Recently, Burton *et al.*[114] have fabricated porous networks of thin film SnSe nanosheets using a simple thermal evaporation method. The developed films exhibited an unprecedentedly ultra-low thermal conductivity of 0.08 W/mK around 400 K, indicating materials' potential for better thermoelectrics.

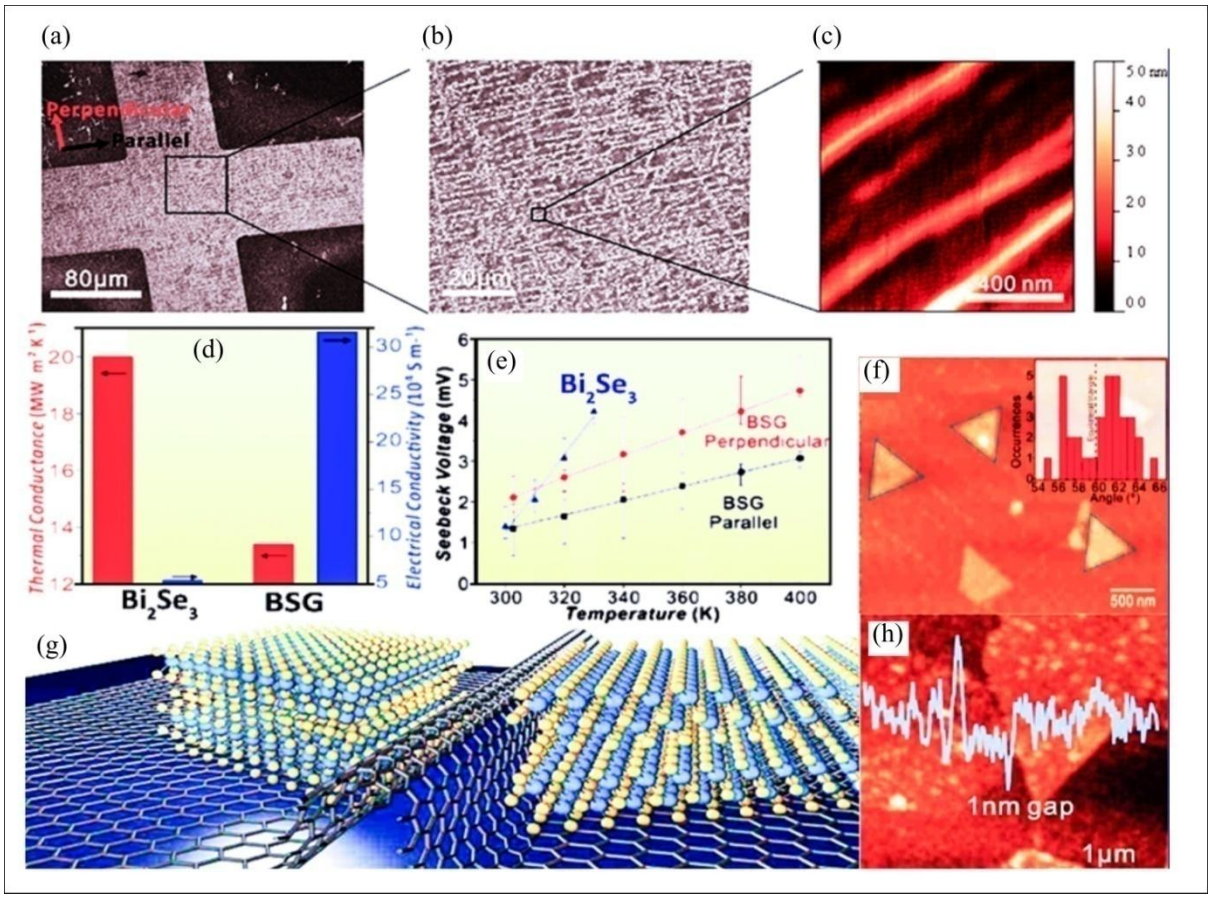

Figure 8. (a) Cross-electrode structure to measure data, (b) zoom-in SEM image, and (c) AFM image of wrinkled graphene. (f) AFM characterization of BSG grown for 3 minutes (inset) distribution of internal angles of BSG flakes showing deviation from ideal angle. (d) 'σ' (blue bar) and thermal conductance (red bar) of Bi_2Se_3 and BSG. (e) Seebeck voltage of Bi_2Se_3 (blue-triangle), BSG in the parallel (black square) and perpendicular direction (red circle) (directions indicated in panel j), (g) schematic of the Bi_2Se_3/graphene/Bi_2Se_3 heterojunction. (h) AFM close-up and height profile of interface between two Bi_2Se_3 flakes, (Reprinted with permission from [112] Copyright © 2019 American Chemical Society)

5.2 Metal tellurides

Metal tellurides have outstanding properties and potential applications in magnetic, thermoelectric, optic, catalytic, biological and electric fields[115-116]. There are numerous studies on metal telluride nanostructures that are systematically focused on the synthesis of various morphologies such as nano plates, nano rods, nano wires, nano flakes, and so on. To obtain metal telluride nanostructures with different structures and morphology, there are several synthesis techniques that have been investigated such as colloidal routes such as solvothermal/hydrothermal methods, thin film deposition techniques, high temperature material fabrication, etc[117]. The fabrication of metal telluride based materials can be categorized into three major methods such as wet chemical synthesis, high-temperature fabrication, and chemical/physical deposition. This section covers a discussion on different material fabrication strategies and thermoelectric properties of some important groups such as (a) bismuth tellurides, (b) lead tellurides, (c) tin tellurides, and some other promising tellurides.

(a) *Bismuth telluride (Bi_2Te_3)*: Bismuth telluride is one of the best and commercially used compounds for thermoelectric power production and refrigeration because of its intrinsically high 'σ' and low 'k' at ambient temperature[118-119]. Further improved performance has been observed from nanostructured Bi_2Te_3 as compared to its bulk counterpart, and also from doping with impurities. Hierarchical nanoparticles, nanorods, nanoplates, and nanobelts are used as building elements in hierarchical Bi_2Te_3-based nanostructures with unique morphologies[120].Recent developments in thermoelectric research suggest that Bi_2Te_3 is one of the successful and most efficient n-type thermoelectric materials around ambient temperature. As a result, current research focus is on the fabrication of Bi_2Te_3 nanoparticles, as well as the doping of other elements and filler materials into Bi_2Te_3 nanoparticles, such as graphene, silver, and carbon nanotubes, to obtain further enhancements in its thermoelectric properties.

(b) *Lead telluride (PbTe)*: Lead telluride and their alloys are among the most efficient thermoelectric materials for moderate temperature applications. By enhancing the 'PF' via band engineering, the PbTe system can be optimised for power generation applications. Much emphasis has been paid to the production of diverse morphologies of PbTe. Also, PbTe is frequently alloyed with Sn to produce alloyed SnTe with high thermoelectric characteristics.

(c) *Tin telluride (SnTe)*: At ambient temperature, Tin Telluride (SnTe) exhibits a low band gap of 0.18 eV and a significant energy separation of 0.35 eV. Because of its potential for waste heat recovery, thermoelectric performance enhancement of SnTe has received a lot of attention [121]. Tin chalcogenides have been significantly researched upon lead-free and less hazardous nature, in addition to their potential for waste heat recovery[122-123].

Simultaneously, efforts are still being made on these telluride based products to develop diverse combinations or alloys by doping with metals. Other compounds with good thermoelectric capabilities across a large temperature range, such as Sb_2Te_3, Ag_2Te, $Cu_{1.75}Te$ are also covered in the discussion.

5.2.1. Wet chemical synthesis

Synthesis of Bi_2Te_3 nanoparticles can be done in numerous ways as mentioned in Table 1. Bao *et al.*[124] followed the simple solvothermal method to obtain the texture-dependent hexagonal nanostructures of size 200-500 nm. They showed that the as-prepared nanomaterial of low 'k' (1.2 W/mK) due to strong phonon scattering at room temperature which could explain the increased density of interfaces and dislocations due to the step-like structure.

Hyun *et al.*[125] showed that Tellurium nanostructures were obtained by using wet-chemical synthesis approach to obtain Bi_2Te_3 nanowires and used graphene oxide as filler material to obtain Graphene based Bi_2Te_3 nanowires of size 100 nm to 1 µm. Individual graphene sheets are randomly spread across the two distinct Bi_2Te_3 matrices, as shown by red arrows in the FESEM images of both Bi_2Te_3 powder depicted in Figure 9(a,b) and Bi_2Te_3 NW in Figure 9(c,d) composites of before and after sintering with 10% graphene content respectively. They discovered that there were no stronger diffraction peaks for graphene in the XRD patterns of Graphene/Bi_2Te_3 because the intensity of graphene was very weak. Hence the XRD pattern shows a stronger (0 1 5) peak attributed to Bi_2Te_3 and the intensity of Bi_2Te_3 decreases as

graphene concentration increases, which explains that the graphene concentration influences the XRD patterns. Values of 'S' for graphene@Bi_2Te_3 composites were obtained as a function of graphene concentration. Negative values of 'S' are seen in both series of composite samples, indicating n-type semiconductor behaviour of the composite. The 'S' values grow with increasing graphene concentration till a maximum value is obtained and then decrease with increase in graphene loading, and then they fall as graphene loading increases as shown in Figure 9(e). According to the electron transport model, a material's 'S' value is usually considered to be inversely proportional to carrier concentration(n). As a result of 'S', the 'PF' rises with increasing graphene content until it reaches a maximum value at 0.5 wt.% graphene content, after which it decreases with increase in graphene content as seen in Figure 9(f). The dopant of graphene may provide extra transmission channels for electrons, which results in high 'σ' and higher 'ZT' (0.4) at 300K for 1 wt% of graphene dopant as seen in Figure 7(g).

Zhang *et al.*[126] obtained the Bi_2Te_3 nanoparticles by a typical surfactant mediated hydrothermal method and showed that the increase in concentration of dopant particles may reduce the grain size of particles. Zhang *et al.*[126] discovered that raising the concentration of dopant (Ag) can enhance 'σ', which potentially promotes electrical connection and increases electronic transport. Because of the low lattice 'k', nanoplates coupled to nanorods create a significant number of grain-grain interactions, resulting in intense phonon scattering.

An *et al.*[127] synthesized Cu-doped Bi_2Te_3 nanoparticles by a redox reaction of Cu(I) salt. Cu–doped Bi_2Te_3 samples have shown higher Seebeck coefficients and power factor as compared to pure sample. As a result, a high ZT of 0.67 at 415 K has been obtained for 15.6 at% Cu doped sample. The increase in the power factor and the reduced thermal conductivity are attributed to the ZT enhancements. Song *et al.*[120] developed Bi_2Te_3 hierarchical nano strings using a solvothermal process. They also showed how the reaction is time-dependent; as time progresses, the nanorods become rougher and the void inside becomes clearer, yielding a variety of morphologies at different time intervals. They showed that low lattice thermal conductivity induces a large number of grain-grain interactions caused by nanoplates attached to nanorods which leads to strong phonon scattering.

Cao *et al.*[128] showed that by doping $SbTe_3$ with Bi_2Te_3 the structure of the particles can be modified and they obtained a quasi-layered crystal and there is also an observation of flake like structures and rod-shaped structures that exhibited very good thermoelectric properties.

They showed that the quantum confinement effect is responsible for obtaining a high 'PF', which is created by enhanced phonon scattering and contributes to boosting of 'ZT'.

Kwang *et al.*[129] studied the TE properties for ZnO coated Bi_2Te_3 pellets and obtained good results. Figure 9(r) shows 'σ' for all the ZnO coated samples, and the value obtained was increased at 5 cycle ZnO coating samples. The 'S' value increases initially till 400K and decreases due to bipolar conduction as shown in Figure 9(s). Since increase in 'σ' and slight decrease in 'S' they obtained enhanced 'PF' for 10 cycle ZnO coating of Bi_2Te_3 pellets of 4.3 $mWm^{-1}K^{-2}$ at 300K as depicted in Figure 9(t). All the ZnO coated samples exhibited very low '*k*' and lattice thermal conductivity (k_L) as increase in temperature, and obtained '*k*' value of 0.85 W/mK for 10 cycled ZnO coating as shown in Figure 9(u) and 'k_L' value of 0.35 W/mKfor 10 cycled ZnO coating at 345 K a depicted in Figure 9(v). A high 'ZT' value of 1.15 has been obtained for 10 cycled ZnO coating at 329 K as shown in Figure 9(w).

SnTe nanoparticles can be synthesized in various ways, such as solvothermal, mechanical, and high temperature sintering process, etc. For example, Wang *et al.*[121] used solvothermal method to obtain an octahedral morphology of Se/Cd co-doped SnTe samples of size ranging from ~0.8 μm to ~1.5 μm as portrayed in Figure 10(a,b,c). The SEM images of sintered SnTe, $SnTe_{0.90}Se_{0.10}$ and $Sn_{0.98}Cd_{0.02}Te_{0.9}Se_{0.1}$ representing that Se and Cd are uniformly doped into SnTe samples which can be seen in Figure 10(d,e,f). The EDS map of $Sn_{0.98}Cd_{0.02}Te_{0.9}Se_{0.1}$ which shows different elements in the sample is given in Figure 10(g-j). Figure 10(l,m,n) depicts the electrical transport characteristics,'σ','S' and 'PF' of sintered pellets of $SnTe_{1-x}Se_x$ (x = 0, 0.05, 0.10) and Se/Cd co-doped $Sn_{1-y}Cd_yTe_{0.90}Se_{0.10}$ (y = 0.01, 0.02, 0.03) as a function of temperature. High value of 'σ' of 3350 Scm^{-1} was observed at 323 K for $Sn_{0.97}Cd_{0.03}Te_{0.9}Se_{0.1}$, and a remarkable value of 'S' of 156 μVK^{-1} at 823 K for $Sn_{0.98}Cd_{0.02}Te_{0.9}Se_{0.1}$ was obtained. As a result, a high 'PF' of 23.1 $\mu Wcm^{-1}K^{-2}$ at 823 K was recorded for $Sn_{0.99}Cd_{0.01}Te_{0.9}Se_{0.1}$.

Han *et al.*[122] used aqueous solution method and SPS technique to obtain round shaped nanoparticles with average size distribution of 95 nm. The study showed that when riveted confinement is compared to PXRD, the result contains cubic SnTe and two minority phases of tetragonal SnO_2 trigonal Te. Due to the huge concentration of Sn vacancies in SnTe, the carrier concentration is extremely high, resulting in p-type semiconductors with a 'ZT' value of 0.081 at 530 K.

Due to its applicability and chemical stability, lead telluride, a distinctive IV–VI semiconducting compound with a narrow band gap and a high Bohr exciton radius, holds considerable promise for relieving the energy and environmental crises[130]. It is one of the best thermoelectric candidates at intermediate temperature range (400–800 K) [131]. PbTe nanoparticles can also be synthesized by several methods such as hydrothermal method, wet chemical synthesis, reaction of solid solution, melt milling and hot pressing. Jin *et al.*[130] synthesized PbTe by a simple hydrothermal method to obtain flower-like dendritic structure of size 2-5 μm. They obtained an S value of 349 μV/K at 400 K. The separation of higher energy electrons from lower energy electrons, as well as selective electron scattering, may contribute to the increase in S.

By using a simple solvothermal process, Zhou *et al.*[132] were able to create n-type Ag_2Te nanoparticles with a uniform size distribution. Sulphur doping occurs when dodecane thiol is used as a surfactant during the synthesis process. As a result, the concentration of charge carriers rises. They were able to synthesise Ag_2Te nanoparticles with a size of about 15 nm after characterization. The size and morphology of Ag_2Te nanoparticles can be altered by altering the reaction time and temperature. At 550 K, Ag_2Te nanoparticles had a higher 'ZT' than bulk Ag_2Te, which was 0.62. Due to copper vacancies, copper-based chalcogenides have p-type semiconductor properties and are prospective materials for a variety of applications including thermoelectric batteries, photothermal treatment, and photovoltaics. Copper telluride, one of the copper chalcogenides, has attracted attention due to its direct band gap (1.1 eV-1.5 eV), thermoelectric power and superionic conductivity [133]. $Cu_{1.75}Te$ 2D nanosheets were generated by colloidal dispersion of dodecylsulfate and solvothermal technique by Nethravathi *et al.*[133]. The single-crystalline nanosheets have large lateral dimensions. Nanosheets with a thickness of 5-20 nm were obtained. $Cu_{1.75}Te$ nanosheets are big, transparent, and irregularly formed. At 650 K, the 'PF' of the $Cu_{1.75}Te$ nanosheet sample increases monotonically, reaching a maximum of 6×10^{-5} $Wm^{-1}K^{-2}$. At 650 K, a 'ZT' of 0.04 was obtained.

5.2.2. High temperature fabrication

Feng *et al.*[134] obtained n-type $Bi_2Te_{2.4}Se_{0.6}$ bulk samples with larger grain size and layered morphology to improvise the TE properties. Backscattered electron (BSE) image mapping and elemental distribution of $Bi_2Te_{2.4}Se_{0.6}$ bulk sample is shown in Figure 9(i-l). They used an annealing method following SPS sintering to obtain a pure n-type $Bi_2Te_{2.4}Se_{0.6}$ sample

with all three elements equally scattered since elemental segregation may be obtained for these materials by cooling them down. Authors investigated the TE characteristics of two products: one is $Bi_2Te_{2.4+\delta}Se_{0.6}$ (δ = 0, 0.01, and 0.02) and the other is $Bi_2Te_{2.4-x}I_xSe_{0.6}$ (x = 0.01 and 0.02). Figure 7(l) displays a 'σ' graph were increasing the dopant content in the sample results in an increase in 'σ'. At 300 K, the greatest value achieved when both Te and I are doped in the sample, i.e. when x = 0.02, is 2.6 x 10^5 Sm^{-1}. Negative 'S' value is obtained for every sample since the dominant carriers are electrons. The better 'S' value obtained was 76 μVK^{-1} at 300K and when x=0.02 as shown in Figure 9(m). The 'σ' was enhanced by excessive doping of Te, the 'PF' obtained was 31.3 $\mu Wcm^{-1}K^{-2}$ at 300K as depicted in Figure 7(n). The 'k' and electronic thermal conductivity (k_e) are shown in Figure 9(o) and Figure 7(p) respectively which results in high conductivity due to doping of Te and excessive doping of I. They obtained a very good 'ZT' value by excess doping of Te i.e. $Bi_2Te_{2.41}Se_{0.6}$ of 1 at 420K as shown in Figure 9(q).

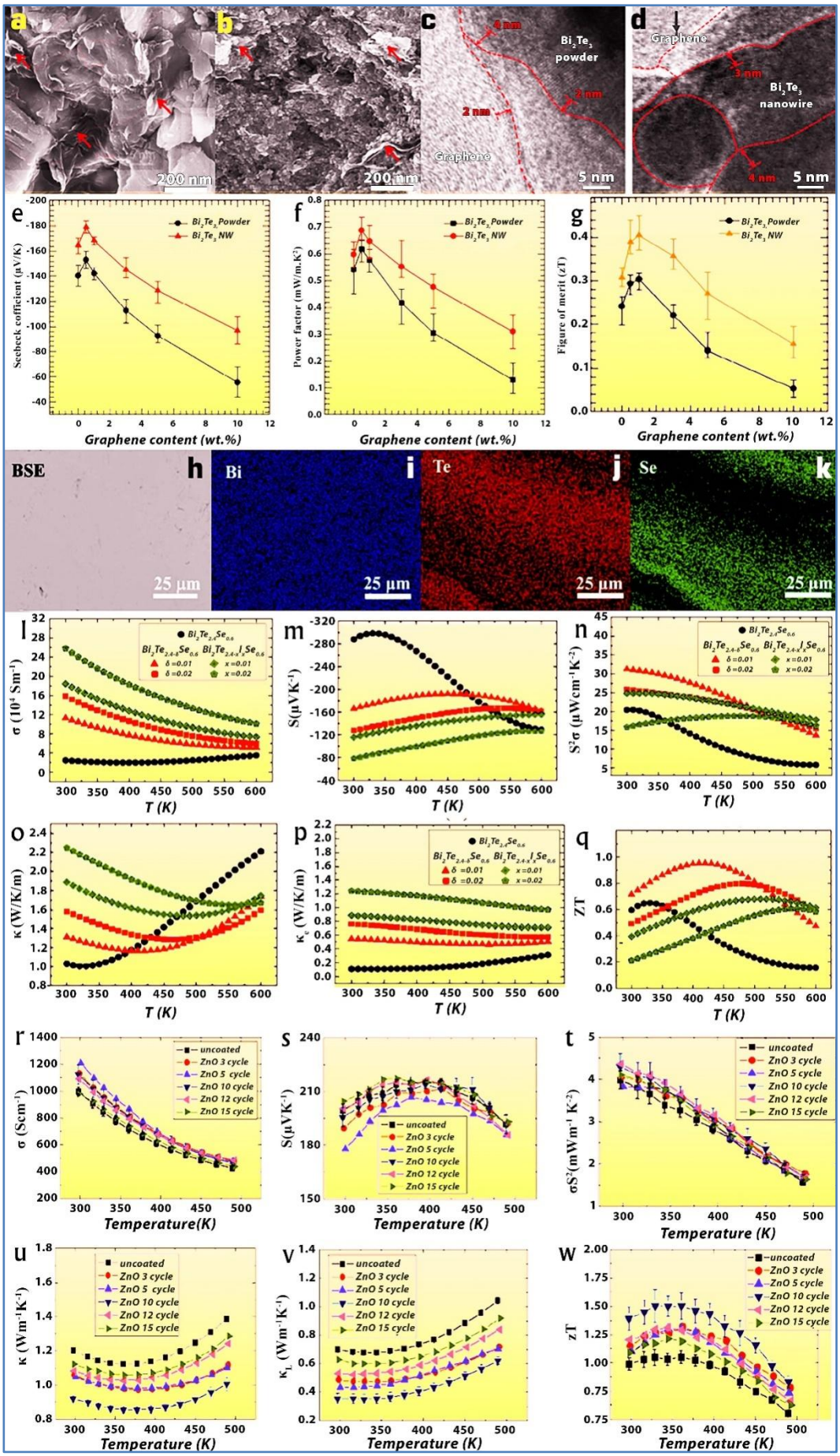
a
200 nm
b
200 nm
c
4 nm
Bi2Te3 powder
2 nm
2 nm
Graphene
5 nm
d
Graphene
3 nm
Bi2Te3 nanowire
4 nm
5 nm
e
Seebeck cofficient (μV/K)
Bi2Te3 Powder
Bi2Te3 NW
Graphene content (wt.%)
f
Power factor (mW/m.K2)
Bi2Te3 Powder
Bi2Te3 NW
Graphene content (wt.%)
g
Figure of merit (zT)
Bi2Te3 Powder
Bi2Te3 NW
Graphene content (wt.%)
BSE
h
25 μm
Bi
i
25 μm
Te
j
25 μm
Se
k
25 μm
l
σ (10⁴ Sm⁻¹)
T (K)
m
S(μVK⁻¹)
T (K)
n
S²σ (μWcm⁻¹K⁻²)
T (K)
o
κ (W/K/m)
T (K)
p
κe (W/K/m)
T (K)
q
ZT
T (K)
r
σ (Scm⁻¹)
uncoated
ZnO 3 cycle
ZnO 5 cycle
ZnO 10 cycle
ZnO 12 cycle
ZnO 15 cycle
Temperature(K)
s
S(μVK⁻¹)
uncoated
ZnO 3 cycle
ZnO 5 cycle
ZnO 10 cycle
ZnO 12 cycle
ZnO 15 cycle
Temperature (K)
t
σS²(mWm⁻¹ K⁻²)
uncoated
ZnO 3 cycle
ZnO 5 cycle
ZnO 10 cycle
ZnO 12 cycle
ZnO 15 cycle
Temperature (K)
u
κ (Wm⁻¹K⁻¹)
uncoated
ZnO 3 cycle
ZnO 5 cycle
ZnO 10 cycle
ZnO 12 cycle
ZnO 15 cycle
Temperature (K)
v
κL (Wm⁻¹K⁻¹)
uncoated
ZnO 3 cycle
ZnO 5 cycle
ZnO 10 cycle
ZnO 12 cycle
ZnO 15 cycle
Temperature (K)
w
zT
uncoated
ZnO 3 cycle
ZnO 5 cycle
ZnO 10 cycle
ZnO 12 cycle
ZnO 15 cycle
Temperature (K)

Figure 9. FE-SEM images of the graphene/Bi_2Te_3-powder composite (a) before and (b) after sintering process. FE-SEM images for the graphene/Bi_2Te_3-NW composite (c) before and (d) after sintering. Red arrows indicate the graphene sheets distributed in the Bi_2Te_3 matrices. (e) S and (f) PF of the synthesized graphene/Bi_2Te_3 composites with different graphene content. (g) ZT of the fabricated graphene/Bi_2Te_3 composites with varied graphene content at a temperature of 300 K. (Reprinted with permission from [125] Copyright © 2016, Elsevier), (h-k) Backscattered electron (BSE) imaging map and elemental distribution in the sintered $Bi_2Te_{2.4}Se_{0.6}$ bulk sample. Temperature dependences of (l) σ, (m) S, (n) PF, (o) κ, (p) κe, and (q) ZT for the $Bi_2Te_{2.4+\delta}Se_{0.6}$ (δ = 0, 0.01, and 0.02) and $Bi_2Te_{2.4-x}I_xSe_{0.6}$ (x = 0.01 and 0.02) samples. (Reprinted with permission from [134]Copyright © 2018, American Chemical Society), Temperature dependence of the (r) σ, (s) S, (t) PF, (u) 'k', (v) lattice contribution of the thermal conductivity, and (w) ZT of the SPS BST with various ZnO thicknesses. The thermal conductivity and the other data of the 10-cycle-ZnO-coated BST were obtained from the average of 8 and 16 samples, respectively. (Reprinted with permission from [129] Copyright © 2019, American Chemical Society)

Malik *et al.*[135] studied the properties of sulfur-doped Bi_2Te_3 compounds synthesized via a melting method. Sulfur creates dislocation and increase of the lattice strain in the compounds. Therefore, the combination of these defects help strong scattering of phonons and gives a low k_l. This observed k_l value is almost 40% lower compared to pristine Bi_2Te_3. Further, a Seebeck coefficient (240 μV/K) and a low *k*have resulted in a high ZT value of 1.12 at 413 K.

Jiang *et al.*[136] synthesized the nanoparticles by mechanical techniques and hot press sintering to obtain multiscale hierarchical structure of octahedral shape of size range 0.4 μm – 2.4 μm. According to their observations, the stacking faults, SeTe point defects, $Cu_{1.75}Te$ nano inclusions, and grain size effectively scatter the phonons into short, medium, and long wavelengths. They obtained a multiscale hierarchical structure with a size range of 1-2 μm with 'ZT' of 1.02 at 873 K. The study showed that the carrier concentration of the product increases with increasing dopants. There are also other synthesis ways of nano SnTe such as hydrothermal method [137] and self-propagating high temperature synthesis (SHS) [138]. Krishna *et al.*[138] studied the TE properties of doped SnTe with Mg and In. Figure 10(n) depicts 'S' varying with temperature, its trend to increase with doping and increase in temperature and obtained around 218 μvK^{-1} at 840K when x = 0.03 in $Sn_{1.04-2x}Mg_xIn_xTe$. They obtained a maximum 'ZT' of 1.5 for x = 0.03 in $Sn_{1.04-2x}Mg_xIn_xTe$ at 840K as depicted in Figure 10(o) and compared them with optimized doping and obtained 'ZT' of 1.5 as shown in Figure 10(p).

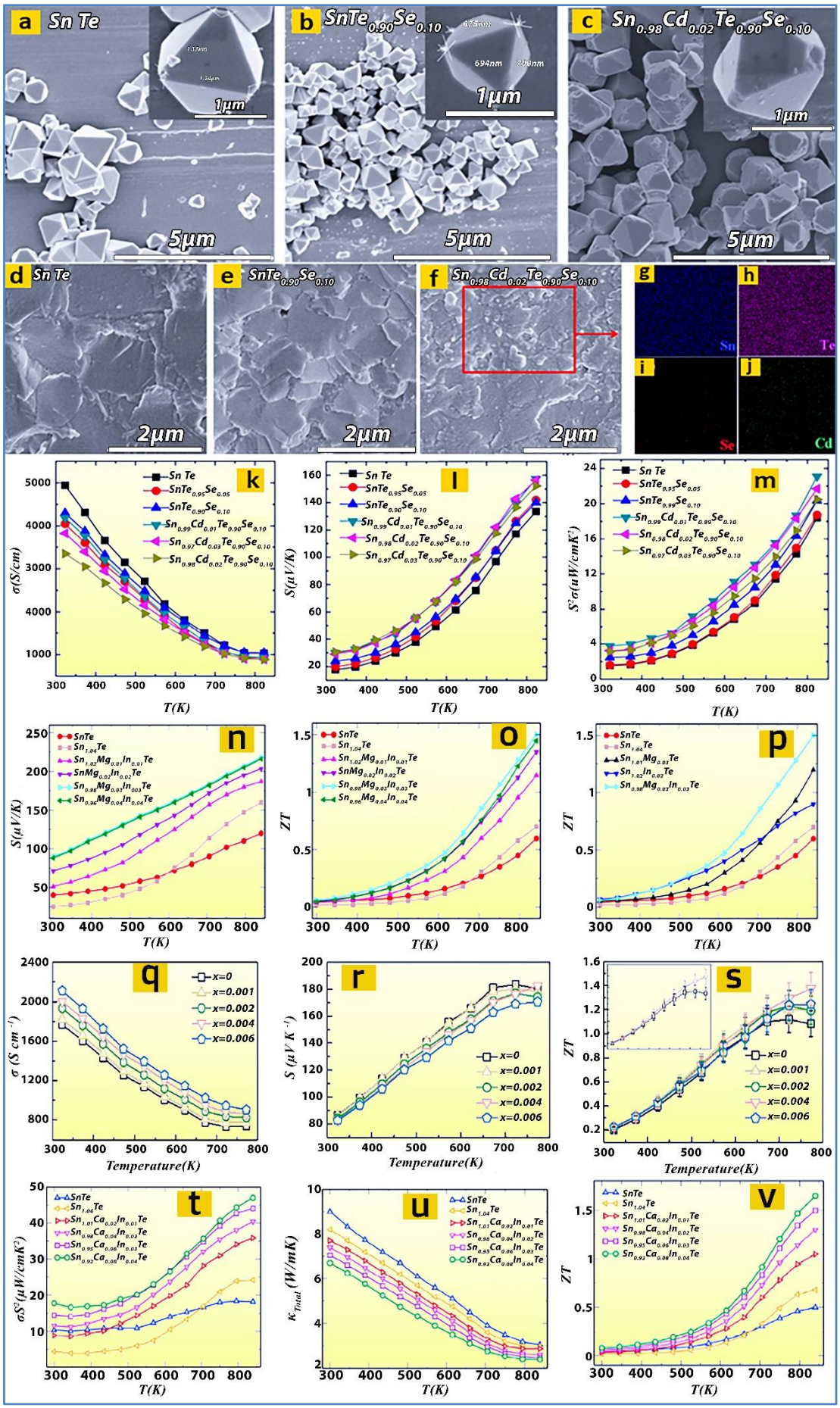
a Sn Te
b SnTe0.90Se0.10
c Sn0.98Cd0.02Te0.90Se0.10
1μm
5μm
d Sn Te
e SnTe0.90Se0.10
f Sn0.98Cd0.02Te0.90Se0.10
2μm
g Sn
h Te
i Se
j Cd
k
l
m
n
o
p
q
r
s
t
u
v
T(K)
Temperature(K)
x=0
x=0.001
x=0.002
x=0.004
x=0.006

Figure 10. *SEM images show the morphologies of SnTe; (a), $SnTe_{0.90}Se_{0.10}$; (b) and $Sn_{0.98}Cd_{0.02}Te_{0.9}Se_{0.1}$; (c) with the insets high magnification SEM images; (d), (e) and (f) SEM images show the grains of sintered SnTe, $SnTe_{0.90}Se_{0.10}$ and $Sn_{0.98}Cd_{0.02}Te_{0.9}Se_{0.1}$ samples, (g)–(j) the EDS maps of different elements as marked of $Sn_{0.98}Cd_{0.02}Te_{0.9}Se_{0.1}$ sample. Electrical transport properties as a function of temperature for Se doped $SnTe_{1-x}Se_x$ (x = 0, 0.05, 0.10) and Se/Cd co-doped $Sn_{1-y}Cd_yTe_{0.90}Se_{0.10}$ (y = 0.01, 0.02, 0.03) samples: (k) σ, (l) S, (m) PF. (Reprinted with permission from[121] Copyright © 2017, American Chemical Society) (n) Seebeck coefficient with temperature in $Sn_{1.04-2x}Mg_xIn_xTe$. (o) ZT with temperature in $Sn_{1.04-2x}Mg_xIn_xTe$. (p) Comparison of variation of ZT with temperature of samples with optimized concentration. (Reprinted with permission from [138]Copyright © 2017, American Chemical Society) The temperature dependence of (q) σ, (r) S, and (s) ZT value of $Sb_2Te_3(Sn_{1-x}Re_xTe)n$ samples. (Reprinted with permission from [139] Copyright © 2020, The Royal Society of Chemistry) Variation of (t) PF and (u) total thermal conductivity (v) ZT with temperature in $Sn_{1.04-3x}Ca_{2x}In_xTe$. Adopted from (Reprinted with permission from [140] Copyright © 2018, Elsevier)*

G. Han*et al.*[122] obtained SnTe nanoparticles of octahedron shape of 0.4 µm - 2.4 µm which results in 'ZT' value of 0.79 (873 K), demonstrating that Sn is easily volatilized during the sintering process, resulting in Sn vacancies and positive holes. Xiao *et al.*[139] studied the TE properties of $Sb_2Te_3(SnTe)_n$ samples where 'σ' decreases with increase in temperature and decrease in concentration(n) and obtained value of 1800 Scm^{-1} at RT as shown in Figure 10(q). 'S' increases as temperature increases and as n decreases and obtains a value of 90 µV/K as shown in Figure 10(r). And Figure 10(s) illustrates an optimum 'ZT' value of 1.12 at 723 K for $Sb_2Te_3(SnTe)_8$ sample. The Se/Cd co-doped material has a 'k' of 1.8 W/mK, which results in a very good 'ZT' of 0.78 at 773 K. It is also evident from the figure that the 'ZT' value of Se/Cd doped SnTe samples are more superior to any other SnTe doped with a single element at high temperature. Bhat *et al.*[138] confirmed that when multiple bands coexist at the Fermi level, the carriers move from one valley to another by means of complex inter valley scattering. Krishna *et al.*[140] studied the TE properties of doped Ca and In in SnTe sample. Figure 8(t) shows 'PF' varying with temperature and obtained a very high 'PF' for $x = 0.04$ in $Sn_{1.01-3x}Ca_{2x}In_xTe$ sample. For all Sn doped samples exhibit a decreasing trend of '*k*' as increase in temperature as shown in Figure 10(u). The maximum 'ZT' obtained is 1.65 at 840 K for $x = 0.04$ in $Sn_{1.01-3x}Ca_{2x}In_xTe$ sample as shown in Figure 10(v).

During the past several years, TE performance of lead chalcogenides has been enhanced[141]. Recently,nanostructured PbTe doped with SrTe has been fabricated by a high temperature synthesis using elemental sources and a very high ZT of 2.5 (923 K) was achieved for heavily alloyed PbTe–x%SrTe [142]. The higher levels of Sr in the PbTe matrix widen its bandgap and

produce convergence of the two valence bands. Such modifications greatly enhance the PF with maximum values over 3000 $\mu W/mK^2$. From exceeding the solubility limit of Sr in PbTe, SrTe nanostructures have been observed in the PbTe matrix which produce extremely low lattice thermal conductivity of 0.5 W/ m K. Alongside, it also preserves high charge mobilities valence band alignments between the PbTe and SrTe.

Yang *et al.*[131] synthesized n - type Bi-doped PbTe nanoparticles by a solvothermal method followed by SPS to obtain cubic shaped $Pb_{1-x}Bi_xTe$ (x=0.05) structures of 50-500 nm as represented in Figure 11(d,e). These doped specimens were compared with un-doped PbTe nanocubes as in Figure 11(a,b), of size range 100-150 nm without sharp edges and it was observed that the cubic shaped structures consist of elongation due to large pressure applied by SPS technique. The HRTEM images show that the nanocubes have a defect-free FCC structure as seen in Figure 11(c) where the selected area electron diffraction (SAED) pattern confirms FCC structure with [111] zone axis. Pure PbTe sample and Bi-doped sample show 0.32 nm of lattice spacing as represented in Figure 11(f) where obtained SAED pattern shows single crystal nano cubes with no sharp edges with [001] zone axis.A high cyclodextrin concentration causes the stem to produce additional branches, resulting in the formation of PbTe Dentrix flowers. Authors studied thermoelectric properties for a temperature range of 300 K to 800 K. They obtained decreasing 'σ' with increasing temperature for Bi-doped pellets. Figure 11(g) shows the bipolar conductivity of the samples which have been depressed indicating increasing 'S' with increasing temperature. They observed due to low electronic contribution the un-doped PbTe has lower 'k' then Bi-doped PbTe showing decreasing trend as increasing temperature as represented in Figure 11(h) and obtained the 'ZT' value ~1.35 at 675 K for $Pb_{0.99}Bi_{0.01}Te$ pellets as shown in Figure 11(i).

The thermoelectric properties of PbTe are remarkable but due to its toxic nature, an alternative to replace Pb is necessary. Zhang *et al.*[143] discovered that at higher temperatures, heavy valence bands predominate, contributing to a large effective mass and increasing the S through doping. The significant decrease in lattice k caused by the addition of Se is thought to create a multiscale hierarchical structure scattering phonons with a broad frequency spectrum. Due to increased grain boundaries, in sub-micro scale the scattering of phonons has a long mean free path. Maria *et al.*[144] discovered that nanocrystal-based doping resulted in higher σ but somewhat lower absolute values of the S, which is associated with lower k values. Synergic interactions between charge carriers in each phase alter ZT, resulting in nanocomposites with electrical conductivities up to one order of magnitude higher than pure

material. Wang *et al.*[145] studied Ga doped PbTe samples. They studied EDS results for different sets of samples which showed clear phase distributions due to distinct boundaries and grains of Ga, Pb and Te as shown in Figure 11(j-m). The results show that the doped products have very good TE properties. Figure 11(n) depicts 'PF' varying with temperature and shows better results for $Pb_{1-x}Ga_xTe$ at $x = 0.03$. Due to thermal excitation the 'S' value decreases with increase in temperature as shown inFigure 11(o), andobtained a high 'ZT' value of 1.3 at 823 K for $Pb_{1-x}Ga_xTe$ at $x = 0.03$ as depicted in Figure 11(p).

Sun *et al.*[117] studied Sb_2Te_3, a layered semiconductor with a tetradymite structure, is a p-type semiconductor with a narrow band gap. One of the finest options for near-room temperature thermoelectric applications is the Sb_2Te_3 molecule and its doped variants with nanoscale size. They used the solvothermal method to obtain Sb_2Te_3 nanosheet powders, then used the SPS to create nanosheet bulk samples. They obtained hexagonal-based sheets with an edge length of 200-300 nm and a thickness of 18-20nm. The nanosheets were extremely thin and virtually transparent, with lattice fringes spaced at 0.217 nm. Nanostructures may have a higher 'S' than bulk thermoelectric materials due to their intense interface scattering. Because of the large number of crystal interfaces present in Sb_2Te_3, and the low density of Sb_2Te_3 nanosheets, the 'k' of Sb_2Te_3 nanosheet sintered bulk samples is low. At 565 K, the Sb_2Te_3 nanosheet sintered bulk sample has a 'ZT' value of 0.57.

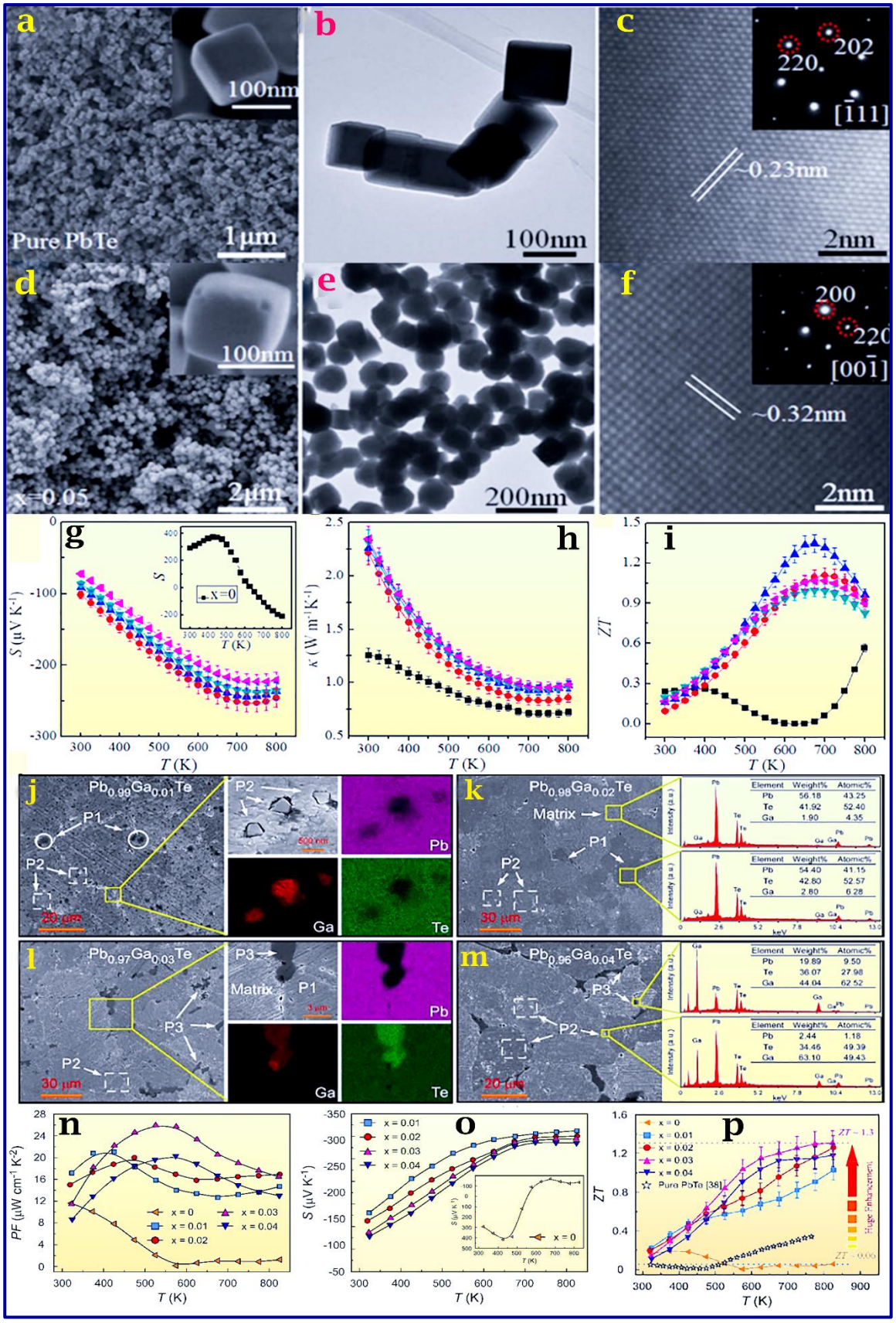

Figure 11. (a) SEM image with inset high magnification SEM image; (b) typical TEM image and (c) HRTEM image with the corresponding SAED pattern; and characterizations of $Pb_{1-x}Bi_xTe$ (x=0.05): (d) SEM image with inset high magnification SEM image; (e) typical

TEM image and (f) HRTEM image with the corresponding SAED pattern; Temperature dependent properties of as-sintered un-doped and Bi-doped PbTe samples: (a) σ; (b) S; (c) κ and (d) ZT values. (Reprinted with permission from [131] Copyright © 2016, Elsevier) Surface morphology and corresponding EDS mapping for (j) x = 0.01; (k) x = 0.02, along with EDS and the corresponding quantitative results of matrix and P1, respectively; (l) x = 0.03; (m) x = 0.04, along with the EDS spectrum and the corresponding quantitative results of P2 and P3, respectively (n) PF; (o) S; (p) ZT for $Pb_{1-x}Ga_xTe$, compared with ref [143] (Reprinted with permission from[145] Copyright © 2018, American Chemical Society)

5.2.3. Chemical/Physical deposition

Thin film thermoelectric devices are usually obtained from chemical or physical deposition methods. The motivation behind several thin film based thermoelectric studies was based on the prediction that quantum confinement of in-plane charge transport could significantly enhance ZT. Enhanced TE properties have been achieved in different thin films, including Bi_2Te_3[146], n-PbTe/pSnTe/n-PbTe structures[147], PbTe/Ag_2Te thin films[148], and many other films.

Fan *et al.*[149]fabricated stoichiometric Bi_2Te_3 thin films via a two-step thermal vapour process with a single source. Further, a rapid thermal process was used to improve the crystallinity and thermoelectric properties of the films. The Seebeck coefficient of the films increased after rapid thermal treatment, leading to enhanced power factor and they also exhibited low thermal conductivity due to their nano grains, resulting in high ZT of 0.51 at 400 K.Bassi *et al.*[150]grown Bi-Te thin films with different structures and morphologies using pulsed laser deposition (PLD). Among others, films with layered structures have shown better results, with Seebeck coefficients of about -250 μV/K and power factors in the range 20-45 $\mu W/cm\,K^2$, with a predicted ZT greater than 1.5.Jin *et al.* [151] developed high ZT Bi_2Te_3 thin films with excellent flexibility for highly ordered nanocrystals on carbon nanotube (CNT) bundles via the sputtering process. These films have shown a power factor of ~1,600 $\mu W/mK^2$ with a low in-plane lattice thermal conductivity of 0.26 W/mK, resulting in a maximum ZT of 0.89 at room temperature.

Karthikeyan *et al.*[152] developed flexible thin films of PbTe and SnTe on flexible polyimide substrates by thermal evaporation method. A maximum power density of 8.4 mW/cm^2 has been observed from a thermoelectric device designed with these films. Beyer et al. reported high ZT of about 1.2 in PbTe and Bi_2Te_3-based superlattices grown by molecular beam epitaxy (MBE) technique.Similarly, Bala *et al.*[153]PbTe, and Ag incorporated PbTe thin films were fabricated by thermal evaporation method. The measured properties show that the Ag

addition improves the crystalline nature of the PbTe films and results in enhanced thermoelectric properties. The details of synthesis methods, crystal structures and particle size/structures along with their TE performances have been summarized in Table 1. Since improved performances were achieved from all synthesis methods, it is bit difficult to comment on the best suitable method for material fabrication. However, based on the cost-effectiveness and simplicity of the synthesis process, a suitable method can be utilized for the applications. It is also true that in many cases desired material design may not be possible with simple low-cost methods and may involve sophisticated and expensive fabrication processes to obtain desired materials.

Table 1: Summary on different thermoelectric inorganic chalcogenides

Chalcogenides	Synthesis Procedure	Crystalline phase, particle structure/ size	'S' (μV/K)	PF (μW/mK^2)	ZT	Ref
BiSe	Spark Plasma Sintering (SPS)	Rhombo-hedral structure	-60 @ 300K	680 @ 300K	0.36 @425K	81
BiSe	Wet chemical synthesis	Layered heterostructures/Nano sheets	-70 @ 300K	--	--	87
$Bi_{0.7}Sb_{0.3}Se$	Spark Plasma Sintering (SPS)	Hexagonal structure	-136 @ 300K	854 @ 300K	0.8 @425k	81
Bi_2Se_3	Solvothermal	Rhombo-hedral/ nanoflakes of sizes ranging 150-400 nm	-115 @ 300K	152 @ 523K	0.096 @ 523K	154
Ag_2Se	Colloidal Synthesis method	Orthorho-mbic/ nanocom	-85.9 @ 389K	2340 @ 360K	0.89 @ 343K	95

		posites				
$SnCu_{0.01}Se_2$	A melt quenching, mechanical milling process, and SPS method	Hexagonal / nanocomposites	136 @ 300K	1960 @ 300K	0.75 @ 300K	[108]
$Sn_{0.94}Bi_{0.06}Se$	Solution-phase synthesis	Orthorhombic/ few-layer nanosheets	-285 @ 719K	100 @ 719K	0.21 @ 719K	[97]
(Na, K) doped SnSe	Ball Milling and SPS	Orthorhombic/ polycrystalline	383 @ 700K	492 @ 773K	1.2 @ 773K	[155]
vol% Ag/Bi_2Te_3 (x = 0.0, 0.5, 1.0, 1.5, 2.0, 2.5, 5.0)	Hydrothermal method	Rhombohedral/sphere and plate like structure	−89.4 @RT for x=5	1140 @ 475K for x=1.5	0.77 @475K for x=2	[156]
Bi_2Te_3 nano strings	Solvothermal method	Rod shape with 1µm length and 300nm diameter	-134 @ 460K	430 @ 460K	0.35 @ 460K	[157]
$Sn_{1-x}Cd_xTe_{0.90}Se_{0.10}$ (x = 0.01, 0.02, 0.03)	Microwave-stimulated wet-chemical method and SPS Method	Octahedral with size of 1.2µm	156 @ 823K	2310 @ 823K	0.78 @ 773K	[121]
$Sn_{1.04-2x}Mg_xIn_xTe$ (x=0.03)	High temperature synthesis and SPS process.	Cubic	218 @840K	4200 @ 840K	1.5 @ 840K	[138]

p- type SnTe	SPS		55.8 @ 530K	430 @ 530K	0.081 @ 530K	[122]
$Bi_{0.05}Ge_{0.95}Te$	Ball Milling and SPS	Rhombo hedral structures	250 @ 650K	4460 @ 650K	1.45 @ 650K	[158]
$Cu_2Se_{1-x}Te_x$ Nanostructure	Solvothermal and SPS	Hexagonal Structure	~312 @ 850K		1.76 @ 850 K	[159]
$Cu_{1.75}Te$	Solvothermal	single-crystalline nanosheets	31 @ 650 K	60 @ 650 K	0.04 @ 650 K	[133]
Ag_2Te	Solvothermal	Single crystalline structures	147 @ 570 K	477 @ 570 K	0.62 @ 550 K	[160]
PbTe–x%SrTe	High temperature synthesis	Rock salt structure	300 @ 923 K	3000 @ 923 K	2.5 @ 923 K	[142]
Sb_2Te_3	Solvothermal	Rhombo-hedral	199 @ 565 K	838 @ 565 K	0.57 @ 565 K	[117]
$Bi_2 Se_3$	High temperature melting + SPS	Rhombo-hedral phase of particle size 100 nm	121 @ 533K	739 @ *533K*	0.41 at 533K	[161]
$Gd_{3-x}Se_4$ (x- 0.16, 0.21, and 0.25)	Ball milling process	Cubic phase	-86 at RT for x=0.25	420 at 850K for x=0.16	0.27 at 850K for x=0.16	[162]

Cu_2 Se	Microwave assisted thermal decomposition	cubic berzelian ite phase of particle size 200 nm	220 at 875K	1400 at 875K	1.9 at 875K	[163]

Negative values of Seebeck coefficient indicate n type semiconductor, RT=Room Temperature

6. Approaches to improve the performance of thermoelectrics

The performance of a thermoelectric material is strongly correlated with 'PF', 'S', and 'k' of material. In this respect, the degenerate and highlydegenerate semiconductor materials are most suitable as their charge transport characteristics can be tuned by altering the electronic structure. This section briefly discusses about the strategies that can be used to effectively enhance the thermoelectric properties of materials

6.1 Alloying

Alloying is a process in which two or more elements are melted together in a predetermined compositional combination to form a specific material known as alloy that exhibits a different set of electrical and thermal properties. Alloying can be used to improve the thermoelectric performance viz., increase in 'PF', and decrease in '*k*'. Alloying brings disorder at the atomic site *via* strain field effect, which significantly reduces the lattice '*k*' [164-165]. An optimal carrier concentration is required to maximize electrical transport and thus thermoelectric performance of a material. For illustration, Kunpeng *et al.*[166] proposed a novel strategy of bonding energy variation to control the carrier concentrations in Cu_2Se-based compounds. Using this approach, they have employed alloyed S at the Se sites and fix Cu atoms in the crystal lattice to suppress the formation of Cu vacancies that led to significantly lesser carrier concentrations toward the optimal value.

6.2 Doping

The incorporation of suitable species/impurities into thermoelectric host material can significantly increase the carrier concentration and alter the electronic band structure of the material. As a consequence of an increase in the number of states, the density of states (DOS) get altered such that the energy level close to Fermi level (within an order of K_BT) can easily promote electron transport. In addition, the uniform doping changes the carrier concentration and improves the PF. In some cases, dopants not only alter the carrier concentration but also

the type of carriers. For example, an increase in the amount of Mg can change MgSb based compounds from p- to n-type. [167] The excess Mg in $Mg_3(Sb, Bi_2)$ forms n-type Mg interstitial defects, which suppress the effects of hole-producing Mg vacancies. Therefore, depending on the role of the dopants within the host material, the electrical transport properties of the resulting compounds can be altered to make them suitable for particular applications. The ability of the dopants to transfer a p-type material into n-type or vice versa can help design TE devices with only one type material having different levels of dopant levels.

Efforts have been made to incorporate rare earth species into chalcogenides to improve its thermoelectric performance [168]. Doping of lanthanide elements can reduce the electrical resistivity and provide additional phonon-scattering centres for reducing the thermal conductivities. Wu *et al.* studied the effect of incorporation of lanthanides in $R_{0.2}Bi_{1.8}Se_{0.3}Te_{2.7}$ (where R = Ce, Y, and Sm) and achieved a 'ZT' of 1.21 at 140 ℃ for $Y_{0.2}Bi_{1.8}Se_{0.3}Te_{2.7}$ [168].Incorporation of dopant ions into thermoelectric materials (e.g., PbSe: Al, PbTe: Cr, and PbSe: Cu) distort the crystal structure of host material and modify the electronic DOS by creating resonant states within the forbidden gap. This assists in electron transport and results in an improvement in thermoelectric characteristics of TE materials. Addition of aluminium into PbSe introduces resonant states in the forbidden gap of the host resulting in high 'ZT' leading to enhancement of 'ZT" [169]. The 'S' is dependent on the doping concentration. Further detailed information about the influence of doping K, Na, B, Al, Ga, In, Tl, Ce, Sb, on the thermoelectric properties such as 'S', 'ZT', 'σ' and 'k' in various chalcogenides (e.g. PbSe, $TiNiSn_{1-x}Sb_x$, $PbTe1\text{-}xSe_x$) can be found in existing literature.[170-172]

6.3 Superlattices

Superlattices are highly anisotropic layered structures of two or different materials in which the thickness of one layer is several nanometres. Such highly anisotropic layered TE materials exhibit high 'ZT', although the presence of different orientations/interfaces reduces the 'k' because of phonon scattering [173]. Sofo and Mahan suggested that alternating barrier layers of superlattices have finite 'k' and tunnelling probability in the quantum wells. Further, the quantum mixing in the well changes DOS from 2D to 3D and predicts an increase in 'ZT'[173].

Superlattices can be fabricated using various physical and chemical methods such as sputtering, thermal evaporation, molecular beam epitaxy, pulsed laser deposition, electrodeposition, chemical vapour deposition (CVD), metal organic CVD etc [174]. Venkata Subramaniam *et al.* have developed a p-type multiple-quantum-well Bi_2Te_3/Sb_2Te_3

superlattice device with a 'ZT' value of 2.4. The enhancement 'ZT' value can be achieved by controlling the transport of phonons and electrons in the superlattices. High 'ZT' values were obtained by limiting the 'k' in the range 0.4–0.6 W/m K by controlling the transport of phonons and electrons [175]. The thermoelectric properties of a few bismuth and antimony based chalcogenide superlattices are listed in Table below. The major drawbacks of using superlattices are the complex synthesis routes, high cost, inability to support a large temperature difference across the material, and also less thermal stability of these special nanostructures.

Table 2. Thermoelectric characteristics of a few chalcogenide superlattices

Material	'k' (W/m.K)	'σ' (S/cm)	'S' (μV/K)	PF (μW/mK^2)	ZT	Reference
p-$Sb_{1.5}Bi_{0.5}Te_3$	0.3	96	86	71	0.05	[176]
p-Sb_2Te_3/Bi_2Te_3	0.58	105.4	210	4650	2.4	[175]
n-$(SeTe)_3$ $(BiSb)_2$	1.36	806	-228	4190	0.9	[177]
n-type $Bi_2Te_3/Bi_2Te_{2.83}Se_{0.17}$	0.94	813	-238	4600	1.5	[175]

6.4 Nano structuring

Nano structuring can introduce heterogeneities at nanoscale dimension and plays a significant role in reducing 'k'. When the size of nanostructure is brought down to length scale comparable to the mean free path of electrons, energy-filtering effect and quantum confinement effect are prevalent. An increase in DOS eventually causes an increase in 'S'. Besides, 'k' is also decreased due to scattering of phonons from the nanostructure surfaces. Nanostructured materials possess a number of interfaces that can play a crucial role in reducing the lattice 'k' [178].

Zhou *et al.*[178]have fabricated $Ag_{0.8}Pb_{m+x}SbTe_{m+2}$ (m = 18, x = 4.5) nanostructured system using combined MA and SPS methods followed by annealing for several days. They investigated the influence of heat treatment on the nano structuring $Ag_{0.8}Pb_{m+x}SbTe_{m+2}$ (m = 18, x = 4.5) compound that determines the thermoelectric properties. The heat treatment

introduces the nanoscopic inhomogeneities within the grains, which in turns, increases the phonon scattering and reduces 'k' as compared to that of an unannealed sample. However, they did not observe any change in 'PF' due to the nano structuring effect. A 'ZT' value of 1.5 at 700 K is obtained for $Ag_{0.8}Pb_{m+x}SbTe_{m+2}$ (m = 18, x = 4.5) compound heat treated for 30 days. This value is 50% higher than that of the unannealed sample [178]. Using nano structuring approach Xie *et al.* have developed a p-type Bi_2Te_3 system that exhibit a low lattice 'k' ($\boldsymbol{\kappa}_{lattice}$ ~ 0.5 W/mK), good 'σ' (**S** ~225 μV/K, $\boldsymbol{\sigma}$ ~ 625 S/cm) and a high 'ZT' of 1.5 [179]. Employing the nano structuring approach, the 'ZT' was increased by 50% vis-a-vis that achieved for commercially available zone-melted materials. In a similar way, Xie *et al.*[180]incorporated melt spinning and SPS techniques to synthesize $Bi_{0.5}Sb_{1.5}Te_3$ compound that offered a maximum 'ZT' of 1.56 at 300 K.

6.5.Band engineering

The tuning of transport properties in TE materials through band engineering is another way to improve the thermoelectric performance.[181] It is a well-known fact that S and σ are directly related to the carrier concentration and thus they are strongly dependent on each other. With all-scale hierarchical architectures, it is possible to enhance TE power factor defined as PF = $S^2\sigma$ by decoupling these physical quantities, which will provide new opportunities to achieve enhanced ZT[182]. Modern heterostructures such as core-shell nanostructures offer additional electronic tuneability due to band alignment at the interface between the core and shell regions.[183] Further, these structures cause the localization of the some phonon modes and thus reduce phonon transport through the materials. Therefore, the band engineering strategy with phonon engineering effect provides a new avenue to reduce the thermal conductivity of the heterostructures.[181]

6.6. Grain boundary engineering

Grain boundary engineering has been established as one of the effective ways to enhance TE performance of materials[184]. The approach has been successful in many conventional TE materials such as Bi_2Te_3, PbTe, SiGe and their alloys.[184] With this approach, their thermal and electronic transport properties can be controlled separately. The short-wavelength phonons can be scattered by alloy scattering or point-defect scattering and therefore, it is an effective way to improve ZT. However, mid and long-wavelength phonons can still travel easily as they transfer heat. Using the formation of structures of larger characteristic length than that of point defects, a further reduction of lattice thermal conductivity is possible. In

such cases, forming high-density grain boundaries for phonon scattering can help achieve further enhanced thermoelectric performances. Secondary phase formation at grain boundaries is a recent promising approach where phonons are effectively scattered along with energy filtering effects which enhance Seebeck effect in the materials.

6.7. Bulk materials with nanoinclusions

In order to obtain high performance TE materials, new materials are being synthesized via various strategies.Compared to nanomaterials, composite materials and bulk materials containing nanoinclusions are relatively easy to fabricate.[126, 185] With new synthesis methods and procedures, different bulk TE materials have been developed that contain nanoinclusions.[185-187] The addition of these foreign nanostructures or nanoinclusions into bulk materials creates high density interfaces/boundaries, dislocations, lattice distortion, and defects.[185] Inside these compounds, phonons with medium and long wavelengths can be strongly scattered by these nanoinclusions which have comparable sizes to that of phonon wavelengths, alongside the short wavelength phonons can be scattered by the point defects or dislocations.[185] Such materials can achieve significant reduction in thermal conductivity with maintaining good electrical conductivity and thus high TE performance.

7. Critical factors evaluating performance of thermoelectrics

The thermoelectric characteristics of a material are strongly dependent upon the grain size, crystal structure, densification, grain orientation and so forth. Therefore, these parameters need to be optimized to achieve the best performance. This section briefly discusses the various critical factors that determine the properties of TE materials.

7.1 Grain size and orientation

In polycrystalline bulk materials, the grain orientation and interfacial microstructure play a crucial role in determining the thermoelectric characteristics of a material. If the preferential alignment of grains are random and not aligned in the direction of electron transport (Fig. 12a), the electrical properties of the material get diminished. A proper heat treatment such as sintering or annealing can be able to preferentially align the domains in the direction of electron transport (Fig. 12b). Evolution of more grain boundaries as a result of decrease in grain size results in scattering of phonons in a more effective manner, thereby reducing thermal conduction *via* the interfacial scattering process (Fig. 12c). Much attention is paid toward nanocomposite material which combines multiple phases of nanoscale dimensions.

The other way to improve grain boundary properties relies on forming thin layers of a second phase at the boundaries (Fig. 12d). Besides, the nanoscale inclusions can also be incorporated within the grain interiors (Fig. 12e). The approaches to produce lamellar nanostructures (Fig. 12f) seek to replicate in bulk materials the advances demonstrated previously in multilayer thin-film thermoelectric materials.

Nanostructured materials have a large number of grain boundaries that enhance the phonon-scattering and thus help reducethermal conductivity. When the average grain size (d_s) is much largerthan the mean free path of phonon(l_t), the lattice thermal conductivity (κ_s) is expressed as[188]

$$\kappa_l = \kappa_s - \frac{2}{3}\kappa_0\sqrt{\frac{l_t}{3d_s}} \qquad [6]$$

where κ_s is the lattice thermal conductivity,large grain size means negligible boundary scattering. κ_0 is the lattice thermal conductivity when there is no alloy scattering related to l_t.If the grain size is comparable or smaller thanl_t, the dependence of κ_l on d_s is described by

$$\kappa_l = \left(\frac{2\kappa_s}{3}\right)\left[\left(\frac{3d_s}{l_t}\right)\left(\frac{\kappa_s}{2\kappa_0}\right)^2\right]^{1/4} \qquad [7]$$

Similarly, grain-oriented materials obtained from microstructure control and achieving specific orientations can help achieve improvements in TE properties[189-190]. The detailed information about the approaches to engineer the grain and interfacial structure i.e nano inclusions, lamellar/multilayer structure and nanocoated grains are described elsewhere. [191]

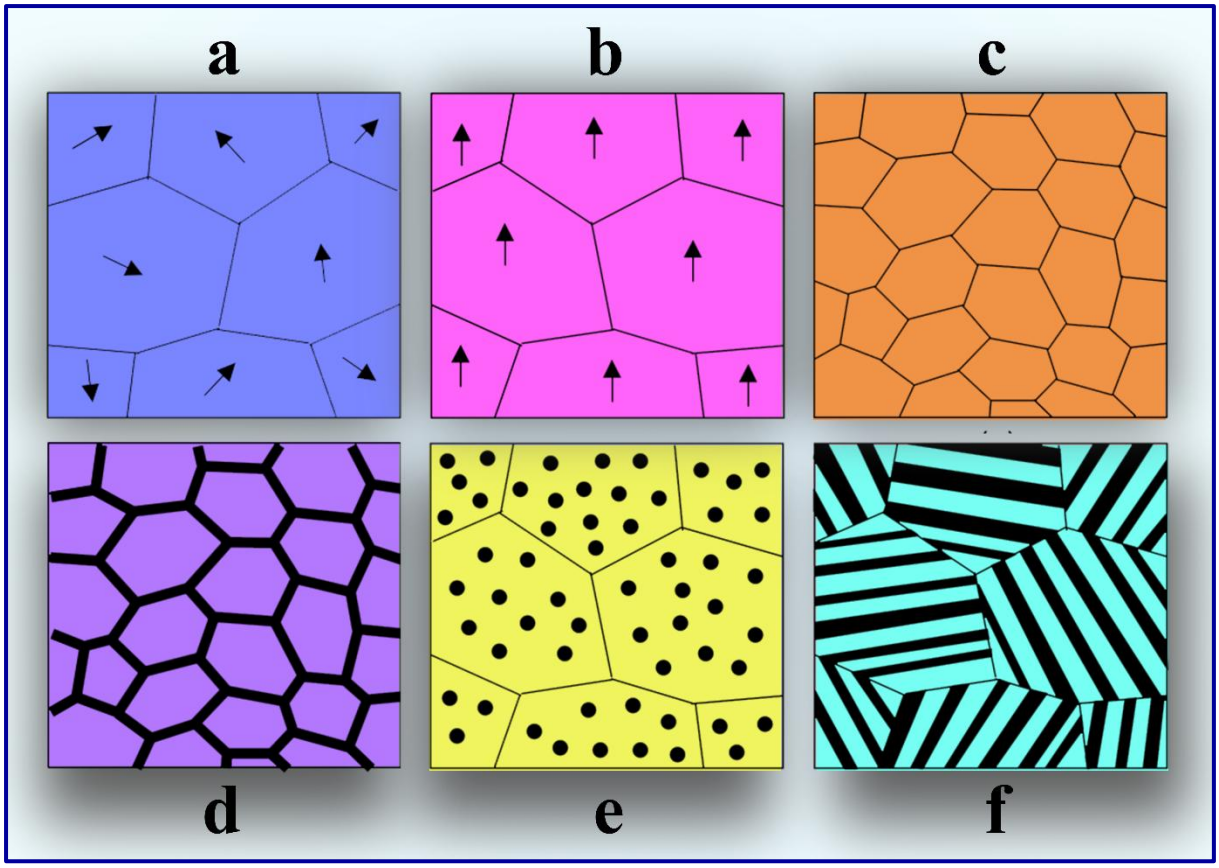

Figure 12. Structural characteristics of a material with several distinct classes of grain and interfacial microstructure: (a) polycrystalline microstructure, (b) preferential alignment of grains along the transport direction, (c) and reduced grain size for favourable interfacial scattering process; (d) nanocoated grains, (e) nano inclusions, and (f) lamellar/multilayer structure. (Reprinted with permission from [191] Copyright © 2009, Elsevier)

7.2 Crystal structure

Creating complex crystal structures is recent promising strategy in thermoelectric research. These complex crystal structures can show simultaneously low thermal conductivity because of structural complexity and high electrical conductivity because of periodic crystal ordering.[192-193] G. Slack termed such an approach as "phonon-glass electron-crystal" (PGEC concept).[194] Many new compounds such as clathrates and skutterudites have emerged as a new type of TE materials because of their unique complex crystal structures.

Hong *et al.* fabricated films of $Ge_2Sb_2Te_5$ (GST) over SiO_2 (250 nm)/Si substrate at room temperature and annealed them at different temperatures to investigate the structural variations. The GST films underwent a transformation from an amorphous to face-centred cubic (FCC) and hexagonal closed packed (HCP) crystalline phases with an increase in annealing temperature increases. Interestingly, the samples annealed at 380 °C showed co-existence of both the FCC and the HCP phases and exhibit highest charge carrier

concentration, the lowest resistivity, and the highest 'PF'. Further, the 'S' of the films decreased linearly with an increase of annealing temperature from 200 to 350 °C (FCC structure) while samples annealed at 380 °C exhibit a mixture of FCC and HCP phases and showed a slow decreasing rate of the 'S', as compared to that of pure FCC and HCP phase(s) [195]. The other example includes Cu_2Se system in which **α**-phase crystallizes into a monoclinic system at lower annealing temperature (127 ℃) in contrast to high temperature FCC **β**-phase. Figure shows the variation inthermoelectric properties (e.g., 'k', 'S' and electrical resistivity) of copper selenide system with annealing temperature, crystalline phase, and composition [196]. This clearly demonstrates the crucial role of crystal structure on the thermoelectric properties of chalcogenides.

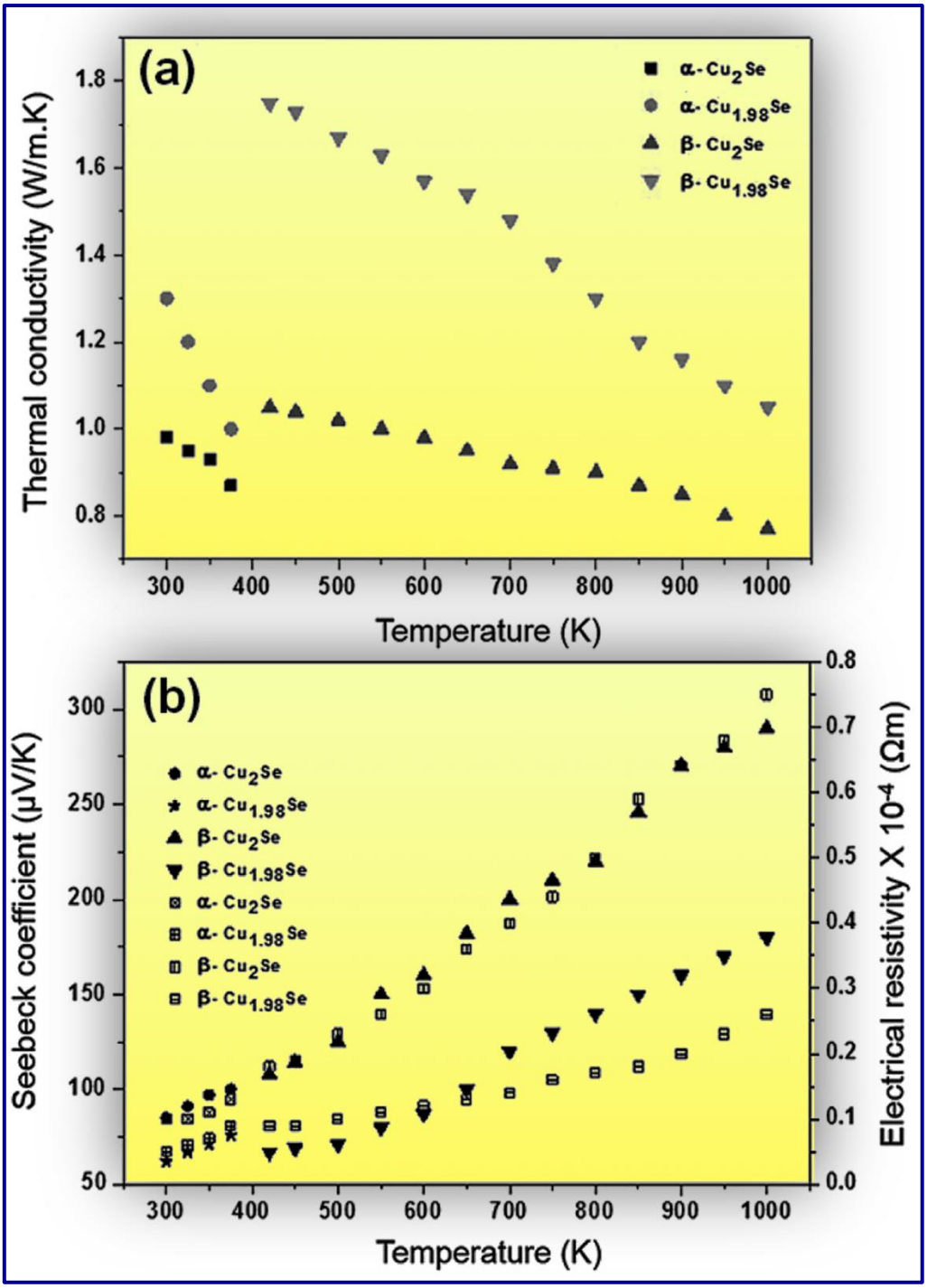

Figure 13. Plots showing variation in (a) 'k', (b) 'S' and electrical resistivity as a function of annealing temperature for **α** and **β** phases of Cu_2Se system with different compositions. (Reprinted with permission from [197] Copyright © 2012 Macmillan Publishers Limited)

7.3 Densification

The microstructure of a material is the key to determine its thermoelectric performance. As the thermal conductivity depends on the density and microstructure of the material, materials processing techniques play crucial roles in determining the 'k'. As reported in available literature samples prepared by SPS exhibit greater densification than those synthesized by hot

pressing (HP) method[198]. Consequently, the net 'k' as well as 'σ' of samples prepared using SPS technique are higher as compared to that of prepared by hot press method. Also, the materials with smaller particle size are found to exhibit low 'k' due to the effect of grain size, as smaller grains cause increased scattering of phonons. The processing temperature is also found to affect the 'k' of materials as it influences grain size, shape and orientation. In general, nanostructured materials display high 'ZT' values and low 'k_{lat}' as compared to their counterparts. The 'ZT' value can be increased by a microstructural engineering approach that can assist in maintaining a smaller mean free path for the phonons and larger mean free path for the charge carriers [174]. Optimization between k and σ can be achieved with controlled density of the compounds during the SPS or hot press process which can result in better ZT from the materials. Further, achieving highly dense materials is important for practical applications as it helps maintain good charge flow and therefore better TE performance.

8. Device applications

Considering the global energy demand, it is judicious to recover and utilise maximum energy that goes unrecovered as waste heat. Thermoelectric devices are one of the promising technologies that can recover the waste heat and widely used in various applications due to their advantageous efficiencies. In all the above discussed sections, different materials have been reviewed for their excellent properties. In this section, focus lies on recent developments in different thermoelectric devices that have been introduced for various applications. [199]

8.1 Medical and Wearable Devices

In the medical field, various measurement devices, health monitoring and tracking systems, sports and fitness wearable devices utilize thermoelectric generators. Torfs *et al.*[200] reported a successful wearable autonomous pulse oximeter for measurement of human pulse and blood saturation levels in the body. This device was fabricated in the form of a watch which used TEG as a power source powered by body heat. Using Bi_2Te_3 thermopiles, it could generate a power of 100**μ**W at an ambient of 22 ºC. [200] Huu *et al.*[201] reported a human body powered flexible TEG by using electro-deposition technique to fabricate a bi-composite of Bi_2Te_3 and Sb_2Te_3 TE materials on flexible substrate that could generate upto 3μW/cm² of output power density from body temperature and ambient conditions. The power output was a promising result for this fabrication to be used in health-monitoring devices such as ECG. Leonov *et al.*[202]have developed a CMOS-based TEG fibre which when placed between skin and a T-shirt, acts as a flexible radiator that is capable of keeping the body warm during winters using body heat. Casado *et al.*[203] examined a fabricated TEC-based conditioned

mattress consistent with affording required sleep conditions. The operation of the system was testified as 3.4 ^{o}C difference in temperature between the mattress external and ambient with coefficient of performance (COP) of 0.58. Personal thermoregulation devices are highly useful in the military field to provide thermal protection and it is also capable of concealing thermal infrared (IR) signature from material body for thermal camouflage to avoid detection by IR.[204]

8.2 Sensor devices

In wireless sensor TEGs are applied, thermoelectric materials help in reduction of maintenance duties and their expenses while ignoring the utilization of batteries and reduction in environment pollution from chemical products discharged. Most commercial/residential buildings have numerous heating devices, such as Heating, Ventilation and Air Conditioning (HVAC) units, boilers, water-heaters, and hot water pipes that all come under Building energy management (BEM) of that building which uses wireless sensor networks (WSN) for all its controls. Wang *et al.* reported theoretical and experimental work of Bismuth Telluride based TEG for powering WSN nodes for BEM applications.[205] Iezzi *et al.*[206] discussed a flexible planar TEG fabricated from screen printed silver and nickel inks that was capable of extracting thermal energy from industrial hot pipes to power a WSN like temperature sensing circuit. Reports suggest development of a new form of unified microsensor for detecting water condensation. Thermal oscillation caused by the Peltier effect was used to power the sensor. The thermal oscillation was disrupted when water droplets formed due to cooling of the junction sensitive area, resulting in shift of the frequency. This shift was documented so that the conditions for mist production may be predicted ahead of time.[207]

8.3 Electronic devices

In electronic devices, a lot of heat is wasted and therefore reusing this thermal energy has gained more attention. Rosales *et al.* developed a TEG-based energy garnering system for mobile phones. This system was capable of utilising all the heat lost in the mobile devices due to the display, the cover, the camera device, and a printed circuit board (PCB) and a dye to power the battery. Li *et al.*[208] reported a chip-level vertical micro-TEG based on a high-density Si nanowire array fabricated with CMOS technology to be used under clean energy source. Suarez *et al.*[209] demonstrated the fabrication of a TEG device that provides power to wearable electronics from the human body using flexible thermoelectric materials of Bismuth compounds showing a p-type behaviour and n-type Bi_2Se_3 legs. Song *et al.*[210] reported the

potential of lighting up diodes by a paddler through attaching a TEG and diode circuits into a helmet. As the cycling speed is increased, the body heat arises and produces more voltages to power up the diodes. Currently, few progressive techniques such as those based on electrochemical deposition have been developed to manufacture micro legs [211] and 3D printed legs.[212] European Telco Orange company successfully manufactured thermoelectric boots that could charge mobile phones. The bottom of the boot was designed along with a TEG that would use the heat from the wearer's foot to generate electricity that could charge any device with a battery. [213]

8.4 Aerospace devices

In the aerospace industry, Radioisotope TEGs (abbreviated as RTGs) are extensively applied in spacecraft, probes, and satellites. RTGs utilize the heat produced by the natural decay of radioactive materials for conversion into electric power. In 1989, NASA launched the first modular General-Purpose Heat Source RTG on Galileo spacecraft[214]. Multi Mission Radioisotope TEG is regarded as the next generation of the RTG used in space missions. It was first conceived in June 2003 and planned to work on planetary bodies in the vacuum of space. [215] TEGs are potential enough to be used on the surface of spacesuits that utilises the temperature difference between human body and space to act as power source. Similarly, they are used on the shells of spacecraft that utilizes the power generated due to the difference in temperature between the spacecraft environment and space. PbTe-based modules have been used in RTGs to provide electrical power using heat from natural radioactive decay for space missions for a long time now. Using a radioisotope as a heat source, the minimum efficiency of such modules was found to be around 5.1% for T_h = 783 K and Tc = 366 K.[216] Another module based on $Yb_{14}MnSb_{11}$ has been demonstrated for RTGs in space missions. [217]

8.5 Automobile machines

Luo *et al.*[218] demonstrated a new air conditioning system for a truck that works on the principles of thermoelectric phenomenon. Choi et al [219] engineered a thermoelectric car seat temperature control system for heating and cooling purposes. This product has been further advanced technically and developed commercially by Gentherm Company as Climate Control Seat (CCS®). The renewable energy laboratory in 2010 tested a TEG on a BMW engine in the US Energy Department. The experimental results demonstrated that the TEG was successful in recovering approximately 5% thermal energy from the exhaust pipe and can be used as a substitute for the vehicle alternator thus improving the vehicle fuel

efficiency by about 10%. Thermoelectric devices integrated with transpired solar collector systems are installed in many new generation cars of Jaguar and Land rover to enable an increasing amount of power generation from the heat by near infrared and to increase efficiency of the system.

8.6 Heat Exchange Devices

Thermoelectric materials are used to improve the accuracy of sophisticated electronic instruments like a cooled CdZnTe detector used in X-ray astronomy. These materials operate by reducing the thermal noise of the electric components and the leakage current of the electronic devices.[220] Naphon and Wiriyasart [221] studied liquid cooling in a fin type heat sink adjunct with the thermoelectric conduction system and showed that the thermoelectric cooler operates more efficiently at small heat loads.[221] Gould *et al.*[222] reported a thermoelectric based cooling system employed for a desktop computer. It was explained that this cooling technique helped to keep the temperature of the CPU lower than the ambient temperature. Cheng *et al.*[223] designed a solar thermoelectric cooling unit for sustainable building utilization. Hara *et al.*[224]designed a headgear which was solar cell-driven with thermoelectric cooling to cool the forehead. This trivial headgear provides thermal comfort by achieving the required temperature difference of 4-5^{o}C between the ambient and cooling temperature.

9. Future prospects

The fast-emerging thermoelectric science and technology has been successful in drawing its attention for future research and design development. Although thermoelectric applications have great advantages over conventional techniques, it has to be noted that thermoelectric devices have to face considerable challenges for their large-scale applications and development.

- In the thermoelectric field, investing on recent nuances in thermoelectric materials from the laboratory and industry to build sustainable, system-level demonstrable equipment that can largely facilitate the acceptance of the thermoelectric science and technology across various business sectors remains an unsolved challenge.
- Thermoelectric materials have been intensively explored providing a wide range of materials for selection to suit a particular application. Whilst integration of these materials into thermoelectric device designs without degrading the performance of the TE materials in manufacturing sets is still a challenging issue.

- Thermoelectric properties are temperature sensitive. In recent decades, numerous novel techniques for enhancing TE properties by bandgap engineering, nanostructure engineering, surface engineering and others have been reported. While achieving a high 'ZT' value for greater performance is still being explored, obtaining a high average value of 'ZT' for a device over a wide temperature profile is also an important goal.
- Commercialisation of TEGs for recovery of heat from exhaust gas for fuel efficiency and heat shielding and cooling in automotive industry, electrical powering devices in aerospace industry, TE devices in cooling of electronic apparatus, devices for powering wireless sensors for Internet of Things (IoT) applications and other major devices have to be executed.
- Exploitation of the global market and opportunities for thermoelectric devices require investment and support on new generation reported research materials, designs and system integration which can be obtained only on popularisation of existing devices that can be achieved by improving efficiency of fabricated devices.
- Introduction of earth abundant materials in thermoelectric devices for cost effectiveness is considered a novel method and research based on the same is reported but it has not been successful in fabrication. Overcoming this challenge would reduce the cost and hence, build a greater market for thermoelectric devices.

10. Conclusions

The current priority in the TE research is yet to develop high ZT materials and reduce manufacturing/material cost. If achieved, TE technology can be a more promising alternative energy source[185]. In order to construct better TE devices, superior materials have to be developed via various approaches. The development of high ZT thermoelctrics can improve the TE market and help boost interest in TE research. Optimization of manipulation of carrier concentration and band structures are very useful strategies in achieving enhancements in TE performance. The future focus can be on to synergistically optimize all the effective TE parameters with new and novel strategies to further enhance TE performance.

In this review, we have summarised the recent developments in thermoelectric materials especially metal selenides and tellurides along with their performance characteristics. Engineering of electrical transport properties through different approaches is the key to enhance 'ZT'. Enhancement of 'ZT' has been attempted via different approaches

while obtaining a 'ZT' > 2 is a challenge because of the strong coupling between the TE parameters. It is also important to note that when developing TE power generation modules in mid- or high-temperature region, the mechanical properties as well as power output should be simultaneously optimized. Since TE properties are temperature dependent, they generally possess their best ZT under certain temperature ranges.[225-226] To achieve a maximum performance, studies need to focus on design and fabrication of devices with suitable materials based on their properties and suitable operating temperature range in order to use them successfully for applications at different temperatures while maintaining the highest ZT. Therefore, in addition to achieving better performance from thermoelectric devices, materials mechanical properties are important for successful working of devices.[227] The strength, fracture toughness, and elasticity are some of the crucial parameters for designing of TE devices.[228] These parameters provide details about different mechanical properties such as material's stiffness, mechanical stresses, thermal expansion coefficients, thermal and chemical stability, and compatibility of the segmented materials used in the device.[225] All these factors may affect and reduce the TE efficiency of the devices over time. Therefore, understanding and optimizing the mechanical properties of TE materials are also very important for practical TE applications.[228]

Further, careful tailoring of morphology of nanostructures has been proven to be a promising way to enhance thermoelectric properties of materials. Insights on transport properties and associated mechanisms are crucial for optimization of thermoelectric efficiency of materials. Recent strategies such as band structure engineering, grain boundary engineering, and nano inclusions in bulk materials are some of the interesting methods to achieve high ZT materials. Doping and alloying are yet some standard ways to tune the band gap and enhance the thermoelectric properties of materials. Overcoming major challenges associated with manufacturing cost and abundance and developing new technologies could result in a better global market for thermoelectric devices.

Acknowledgment

The author (CM) is grateful to the Management, Rashtreeya Sikshana Samithi Trust, and the Principal, RV College of Engineering for constant support and encouragement. This study was also supported by Rashtreeya Sikshana Samithi Trust (RSST) Bengaluru, India under RVCE sustainability fund (Seed money grant no:RVE/A/c/116/2021-22/ Dated 08 July 2021). Authors (RM and CWD) are thankful to the Welsh Government (EU European

Regional Development Fund) for funding the RICE (Reducing Industrial Carbon Emission) project (Grant Number: 81435).

Conflicts of interest

There are no conflicts to declare.

References

1. He, J.; Kanatzidis, M. G.; Dravid, V. P., High performance bulk thermoelectrics via a panoscopic approach. *Materials Today* **2013,** *16* (5), 166-176.
2. Novak, T. G.; Kim, J.; Kim, J.; Tiwari, A. P.; Shin, H.; Song, J. Y.; Jeon, S., Complementary n-Type and p-Type Graphene Films for High Power Factor Thermoelectric Generators. *Advanced Functional Materials* **2020,** *30* (28), 2001760.
3. Tian, Q.; Deng, D.; Zhang, Z.; Li, Y.; Yang, Y.; Guo, X., Facile synthesis of Ag2Se quantum dots and their application in Dye/Ag2Se co-sensitized solar cells. *Journal of Materials Science* **2017,** *52* (20), 12131-12140.
4. Ahmad, H.; Kamarudin, S. K.; Minggu, L. J.; Hasran, U. A.; Masdar, S.; Daud, W. R. W., Enhancing methanol oxidation with a TiO2-modified semiconductor as a photo-catalyst. *International Journal of Hydrogen Energy* **2017,** *42* (14), 8986-8996.
5. Thakur, A. K.; Majumder, M.; Singh, S. B., Graphene and its derivatives for secondary battery application. In *Surface Engineering of Graphene*, Springer: 2019; pp 53-80.
6. Selvan, K. V.; Hasan, M. N.; Mohamed Ali, M. S., State-of-the-art reviews and analyses of emerging research findings and achievements of thermoelectric materials over the past years. *Journal of Electronic Materials* **2019,** *48* (2), 745-777.
7. Zaferani, S. H.; Sams, M. W.; Ghomashchi, R.; Chen, Z.-G., Thermoelectric coolers as thermal management systems for medical applications: Design, optimization, and advancement. *Nano Energy* **2021,** *90*, 106572.
8. Dusastre, V., *Materials for sustainable energy: a collection of peer-reviewed research and review articles from Nature Publishing Group*. World Scientific: 2010.
9. Gonçalves, A. P.; Godart, C., New promising bulk thermoelectrics: intermetallics, pnictides and chalcogenides. *The European Physical Journal B* **2014,** *87* (2), 1-29.
10. Kuroki, T.; Kabeya, K.; Makino, K.; Kajihara, T.; Kaibe, H.; Hachiuma, H.; Matsuno, H.; Fujibayashi, A., Thermoelectric generation using waste heat in steel works. *Journal of electronic materials* **2014,** *43* (6), 2405-2410.
11. Bell, L. E., Cooling, heating, generating power, and recovering waste heat with thermoelectric systems. *Science* **2008,** *321* (5895), 1457-1461.
12. Mulla, R.; Dunnill, C. W., Powering the Hydrogen Economy from Waste Heat: A Review of Heat-to-Hydrogen Concepts. *ChemSusChem* **2019,** *12* (17), 3882-3895.
13. Petsagkourakis, I.; Tybrandt, K.; Crispin, X.; Ohkubo, I.; Satoh, N.; Mori, T., Thermoelectric materials and applications for energy harvesting power generation. *Science and Technology of Advanced Materials* **2018,** *19* (1), 836-862.
14. Xu, S.; Hong, M.; Li, M.; Sun, Q.; Yin, Y.; Liu, W.; Shi, X.; Dargusch, M.; Zou, J.; Chen, Z.-G., Two-dimensional flexible thermoelectric devices: Using modeling to deliver optimal capability. *Applied Physics Reviews* **2021,** *8* (4), 041404.
15. Chen, W.-Y.; Shi, X.-L.; Zou, J.; Chen, Z.-G., Wearable fiber-based thermoelectrics from materials to applications. *Nano Energy* **2021,** *81*, 105684.
16. Armin Razmjoo, A.; Sumper, A.; Davarpanah, A., Energy sustainability analysis based on SDGs for developing countries. *Energy Sources, Part A: Recovery, Utilization, and Environmental Effects* **2020,** *42* (9), 1041-1056.

17. Allen, C.; Metternicht, G.; Wiedmann, T., Initial progress in implementing the Sustainable Development Goals (SDGs): A review of evidence from countries. *Sustainability Science* **2018,** *13* (5), 1453-1467.
18. Pizzi, S.; Caputo, A.; Corvino, A.; Venturelli, A., Management research and the UN sustainable development goals (SDGs): A bibliometric investigation and systematic review. *Journal of cleaner production* **2020,** *276*, 124033.
19. Han, C.; Li, Z.; Lu, G. Q. M.; Dou, S. X., Robust scalable synthesis of surfactant-free thermoelectric metal chalcogenide nanostructures. *Nano Energy* **2015,** *15*, 193-204.
20. Mulla, R.; Jones, D. R.; Dunnill, C. W., Thermoelectric Paper: Graphite Pencil Traces on Paper to Fabricate a Thermoelectric Generator. *Advanced Materials Technologies* **2020,** *5* (7), 2000227.
21. LaLonde, A. D.; Pei, Y.; Wang, H.; Snyder, G. J., Lead telluride alloy thermoelectrics. *Materials today* **2011,** *14* (11), 526-532.
22. Sootsman, J. R.; Chung, D. Y.; Kanatzidis, M. G., New and old concepts in thermoelectric materials. *Angewandte Chemie International Edition* **2009,** *48* (46), 8616-8639.
23. Franco, I. B.; Power, C.; Whereat, J., SDG 7 affordable and clean energy. In *Actioning the Global Goals for Local Impact*, Springer: 2020; pp 105-116.
24. Elavarasan, R. M.; Pugazhendhi, R.; Jamal, T.; Dyduch, J.; Arif, M. T.; Kumar, N. M.; Shafiullah, G.; Chopra, S. S.; Nadarajah, M., Envisioning the UN Sustainable Development Goals (SDGs) through the lens of energy sustainability (SDG 7) in the post-COVID-19 world. *Applied Energy* **2021,** *292*, 116665.
25. Vaidya, H.; Chatterji, T., SDG 11 sustainable cities and communities. In *Actioning the Global Goals for Local Impact*, Springer: 2020; pp 173-185.
26. Charnock, R.; Hoskin, K., SDG 13 and the entwining of climate and sustainability metagovernance: an archaeological–genealogical analysis of goals-based climate governance. *Accounting, Auditing & Accountability Journal* **2020**.
27. Yousefi, R., Metal-selenide nanostructures: growth and properties. *Metal Chalcogenide Nanostructures for Renewable Energy Applications* **2014**, 43-81.
28. Su, S.; Wu, W.; Gao, J.; Lu, J.; Fan, C., Nanomaterials-based sensors for applications in environmental monitoring. *Journal of Materials Chemistry* **2012,** *22* (35), 18101-18110.
29. Mulla, R.; Dunnill, C. W., Enhanced thermal sensitivity in single metal thermocouple: significance of thickness-engineering of the metal layers. *Engineering Research Express* **2021,** *3* (3), 035015.
30. Franklin, A. D., Nanomaterials in transistors: From high-performance to thin-film applications. *Science* **2015,** *349* (6249), aab2750.
31. Saadi, S.; Nazari, B., Recent developments and applications of nanocomposites in solar cells: a review. *Journal of Composites and Compounds* **2019,** *1* (1), 41-50.
32. Manjunatha, C.; Srinivasa, N.; Chaitra, S.; Sudeep, M.; Kumar, R. C.; Ashoka, S., Controlled synthesis of nickel sulfide polymorphs: studies on the effect of morphology and crystal structure on OER performance. *Materials Today Energy* **2020,** *16*, 100414.
33. Jena, M.; Manjunatha, C.; Shivaraj, B.; Nagaraju, G.; Ashoka, S.; Aan, M. S., Optimization of parameters for maximizing photocatalytic behaviour of Zn1-xFexO nanoparticles for methyl orange degradation using Taguchi and Grey relational analysis Approach. *Materials Today Chemistry* **2019,** *12*, 187-199.
34. Ansari, S. A.; Manjunatha, C.; Parveen, N.; Shivaraj, B.; Krishna, R. H., Mechanistic insights into defect chemistry and tailored photoluminescence and photocatalytic properties of aliovalent cation substituted Zn 0.94 M 0.06− x Li x O (M: Fe 3+, Al 3+, Cr 3+) nanoparticles. *Dalton Transactions* **2021,** *50* (41), 14891-14907.
35. Channegowda, M., Recent advances in environmentally benign hierarchical inorganic nano-adsorbents for the removal of poisonous metal ions in water: a review with mechanistic insight into toxicity and adsorption. *Nanoscale Advances* **2020,** *2* (12), 5529-5554.

36. Subana, P.; Manjunatha, C.; Rao, B. M.; Venkateswarlu, B.; Nagaraju, G.; Suresh, R., Surface functionalized magnetic α-Fe2O3 nanoparticles: Synthesis, characterization and Hg2+ ion removal in water. *Surfaces and Interfaces* **2020,** *21*, 100680.
37. Wang, Z. L., ZnO nanowire and nanobelt platform for nanotechnology. *Materials Science and Engineering: R: Reports* **2009,** *64* (3), 33-71.
38. Huang, L.; Chen, J.; Yu, Z.; Tang, D., Self-Powered Temperature Sensor with Seebeck Effect Transduction for Photothermal–Thermoelectric Coupled Immunoassay. *Analytical Chemistry* **2020,** *92* (3), 2809-2814.
39. Wang, J.; Cao, P.; Li, X.; Song, X.; Zhao, C.; Zhu, L., Experimental study on the influence of Peltier effect on the output performance of thermoelectric generator and deviation of maximum power point. *Energy Conversion and Management* **2019,** *200*, 112074.
40. Zhang, M.; Tian, Y.; Xie, H.; Wu, Z.; Wang, Y., Influence of Thomson effect on the thermoelectric generator. *International Journal of Heat and Mass Transfer* **2019,** *137*, 1183-1190.
41. Han, C.; Sun, Q.; Li, Z.; Dou, S. X., Thermoelectric Enhancement of Different Kinds of Metal Chalcogenides. *Advanced Energy Materials* **2016,** *6* (15), 1600498.
42. Witting, I. T.; Chasapis, T. C.; Ricci, F.; Peters, M.; Heinz, N. A.; Hautier, G.; Snyder, G. J., The Thermoelectric Properties of Bismuth Telluride. *Advanced Electronic Materials* **2019,** *5* (6), 1800904.
43. Wang, X.; Wang, H.; Su, W.; Mehmood, F.; Zhai, J.; Wang, T.; Chen, T.; Wang, C., Geometric structural design for lead tellurium thermoelectric power generation application. *Renewable Energy* **2019,** *141*, 88-95.
44. Adam, A. M.; El-Khouly, A.; Lilov, E.; Ebrahim, S.; Keshkh, Y.; Soliman, M.; El Maghraby, E. M.; Kovalyo, V.; Petkov, P., Ultra thin bismuth selenide-bismuth telluride layers for thermoelectric applications. *Materials Chemistry and Physics* **2019,** *224*, 264-270.
45. Chen, L.-C.; Chen, P.-Q.; Li, W.-J.; Zhang, Q.; Struzhkin, V. V.; Goncharov, A. F.; Ren, Z.; Chen, X.-J., Enhancement of thermoelectric performance across the topological phase transition in dense lead selenide. *Nature Materials* **2019,** *18* (12), 1321-1326.
46. Tian, B.-Z.; Chen, J.; Jiang, X.-P.; Tang, J.; Zhou, D.-L.; Sun, Q.; Yang, L.; Chen, Z.-G., Enhanced Thermoelectric Performance of SnTe-Based Materials via Interface Engineering. *ACS Applied Materials & Interfaces* **2021,** *13* (42), 50057-50064.
47. Wang, D.-Z.; Liu, W.-D.; Shi, X.-L.; Gao, H.; Wu, H.; Yin, L.-C.; Zhang, Y.; Wang, Y.; Wu, X.; Liu, Q.; Chen, Z.-G., Se-alloying reducing lattice thermal conductivity of Ge0.95Bi0.05Te. *Journal of Materials Science & Technology* **2022,** *106*, 249-256.
48. Li, M.; Sun, Q.; Xu, S.-D.; Hong, M.; Lyu, W.-Y.; Liu, J.-X.; Wang, Y.; Dargusch, M.; Zou, J.; Chen, Z.-G., Optimizing Electronic Quality Factor toward High-Performance Ge1−x−yTaxSbyTe Thermoelectrics: The Role of Transition Metal Doping. *Advanced Materials* **2021,** *33* (40), 2102575.
49. Shutoh, N.; Sakurada, S., Thermoelectric properties of the TiX(Zr0.5Hf0.5)1−XNiSn half-Heusler compounds. *Journal of Alloys and Compounds* **2005,** *389* (1), 204-208.
50. Sun, H.-L.; Yang, C.-L.; Wang, M.-S.; Ma, X.-G., Remarkably High Thermoelectric Efficiencies of the Half-Heusler Compounds BXGa (X = Be, Mg, and Ca). *ACS Applied Materials & Interfaces* **2020,** *12* (5), 5838-5846.
51. Guin, S. N.; Banik, A.; Biswas, K., Thermoelectric Energy Conversion in Layered Metal Chalcogenides. In *2D Inorganic Materials beyond Graphene*, pp 239-274.
52. He, J.; Liu, Y.; Funahashi, R., Oxide thermoelectrics: The challenges, progress, and outlook. *Journal of Materials Research* **2011,** *26* (15), 1762-1772.
53. Yin, Y.; Tudu, B.; Tiwari, A., Recent advances in oxide thermoelectric materials and modules. *Vacuum* **2017,** *146*, 356-374.
54. Sharma, V.; Kagdada, H. L.; Jha, P. K.; Śpiewak, P.; Kurzydłowski, K. J., Thermal transport properties of boron nitride based materials: A review. *Renewable and Sustainable Energy Reviews* **2020,** *120*, 109622.

55. Mulla, R.; Jones, D. R.; Dunnill, C. W., Economical and Facile Route to Produce Gram-Scale and Phase-Selective Copper Sulfides for Thermoelectric Applications. *ACS Sustainable Chemistry & Engineering* **2020,** *8* (37), 14234-14242.
56. Kerdsongpanya, S.; Hellman, O.; Sun, B.; Koh, Y. K.; Lu, J.; Van Nong, N.; Simak, S. I.; Alling, B.; Eklund, P., Phonon thermal conductivity of scandium nitride for thermoelectrics from first-principles calculations and thin-film growth. *Physical Review B* **2017,** *96* (19), 195417.
57. Reshak, A. H., Thermoelectric properties for AA- and AB-stacking of a carbon nitride polymorph (C3N4). *RSC Advances* **2014,** *4* (108), 63137-63142.
58. Beretta, D.; Neophytou, N.; Hodges, J. M.; Kanatzidis, M. G.; Narducci, D.; Martin- Gonzalez, M.; Beekman, M.; Balke, B.; Cerretti, G.; Tremel, W.; Zevalkink, A.; Hofmann, A. I.; Müller, C.; Dörling, B.; Campoy-Quiles, M.; Caironi, M., Thermoelectrics: From history, a window to the future. *Materials Science and Engineering: R: Reports* **2019,** *138*, 100501.
59. Seebeck, T. J., *Magnetische polarisation der metalle und erze durch temperatur-differenz*. W. Engelmann: 1895.
60. Altenkirch, E., About the Efficiency of the Thermal Columns. *Physikalische Zeitschrift* **1909,** *10* (16), 560-580.
61. Altenkirch, E., Electro-thermal generation of coldness and reversible electric heating. *Physikalische Zeitschrift* **1911,** *12*, 920-924.
62. Vedernikov, M.; Iordanishvili, E. In *AF Ioffe and origin of modern semiconductor thermoelectric energy conversion*, Seventeenth International Conference on Thermoelectrics. Proceedings ICT98 (Cat. No. 98TH8365), IEEE: 1998; pp 37-42.
63. Goldsmid, H. J.; Douglas, R. W., The use of semiconductors in thermoelectric refrigeration. *British Journal of Applied Physics* **1954,** *5* (11), 386-390.
64. Jia, N.; Cao, J.; Tan, X. Y.; Dong, J.; Liu, H.; Tan, C. K. I.; Xu, J.; Yan, Q.; Loh, X. J.; Suwardi, A., Thermoelectric materials and transport physics. *Materials Today Physics* **2021,** *21*, 100519.
65. Mostafa, M. H.; Abdel Aleem, S. H. E.; Ali, S. G.; Abdelaziz, A. Y., Chapter 20 - Energy-management solutions for microgrids. In *Distributed Energy Resources in Microgrids*, Chauhan, R. K.; Chauhan, K., Eds. Academic Press: 2019; pp 483-515.
66. Dargusch, M.; Liu, W.-D.; Chen, Z.-G., Thermoelectric Generators: Alternative Power Supply for Wearable Electrocardiographic Systems. *Advanced Science* **2020,** *7* (18), 2001362.
67. Twaha, S.; Zhu, J.; Yan, Y.; Li, B., A comprehensive review of thermoelectric technology: Materials, applications, modelling and performance improvement. *Renewable and Sustainable Energy Reviews* **2016,** *65*, 698-726.
68. Freer, R.; Powell, A. V., Realising the potential of thermoelectric technology: a Roadmap. *Journal of Materials Chemistry C* **2020,** *8* (2), 441-463.
69. Chen, Q.; Longtin, J. P.; Tankiewicz, S.; Sampath, S.; Gambino, R. J., Ultrafast laser micromachining and patterning of thermal spray multilayers for thermopile fabrication. *Journal of Micromechanics and Microengineering* **2004,** *14* (4), 506-513.
70. Endrődi, B.; Mellár, J.; Gingl, Z.; Visy, C.; Janáky, C., Molecular and Supramolecular Parameters Dictating the Thermoelectric Performance of Conducting Polymers: A Case Study Using Poly(3-alkylthiophene)s. *The Journal of Physical Chemistry C* **2015,** *119* (16), 8472-8479.
71. ter Haar, D.; Neaves, A., On the thermal conductivity and thermoelectric power of semiconductors. *Advances in Physics* **1956,** *5* (18), 241-269.
72. Shi, X.-L.; Zou, J.; Chen, Z.-G., Advanced Thermoelectric Design: From Materials and Structures to Devices. *Chemical Reviews* **2020,** *120* (15), 7399-7515.
73. Masood, K. B.; Kumar, P.; Giri, R.; Singh, J., Controlled synthesis of two-dimensional (2-D) ultra-thin bismuth selenide (Bi2Se3) nanosheets by bottom-up solution-phase chemistry and its electrical transport properties for thermoelectric application. *FlatChem* **2020,** *21*, 100165.
74. Hasan, M. N.; Wahid, H.; Nayan, N.; Mohamed Ali, M. S., Inorganic thermoelectric materials: A review. *International Journal of Energy Research* **2020,** *44* (8), 6170-6222.

75. Li, Y.-d.; Fan, P.; Zheng, Z.-h.; Luo, J.-t.; Liang, G.-x.; Guo, S.-z., The influence of heat treatments on the thermoelectric properties of copper selenide thin films prepared by ion beam sputtering deposition. *Journal of Alloys and Compounds* **2016,** *658*, 880-884.
76. Wei, T.-R.; Wu, C.-F.; Li, F.; Li, J.-F., Low-cost and environmentally benign selenides as promising thermoelectric materials. *Journal of Materiomics* **2018,** *4* (4), 304-320.
77. C, M.; P, P. R.; Bhardwaj, P.; H, R.; D, R., New insights into synthesis, morphological architectures and biomedical applications of elemental selenium nanostructures. *Biomedical Materials* **2020**.
78. Zeier, W. G.; Zevalkink, A.; Gibbs, Z. M.; Hautier, G.; Kanatzidis, M. G.; Snyder, G. J., Thinking Like a Chemist: Intuition in Thermoelectric Materials. *Angewandte Chemie International Edition* **2016,** *55* (24), 6826-6841.
79. Yadav, G. G.; Susoreny, J. A.; Zhang, G.; Yang, H.; Wu, Y., Nanostructure-based thermoelectric conversion: an insight into the feasibility and sustainability for large-scale deployment. *Nanoscale* **2011,** *3* (9), 3555-3562.
80. Yamauchi, K.; Mori, R.; Yamaguchi, M.; Takashiri, M., Thermoelectric properties including thermal conductivity of electrodeposited bismuth selenide thin films fabricated using different acid solutions. *Journal of Alloys and Compounds* **2019,** *792*, 222-229.
81. Samanta, M.; Pal, K.; Pal, P.; Waghmare, U. V.; Biswas, K., Localized vibrations of Bi bilayer leading to ultralow lattice thermal conductivity and high thermoelectric performance in weak topological insulator n-type BiSe. *Journal of the American Chemical Society* **2018,** *140* (17), 5866-5872.
82. Wang, H.; Liu, X.; Zhang, B.; Huang, L.; Yang, M.; Zhang, X.; Zhang, H.; Wang, G.; Zhou, X.; Han, G., General surfactant-free synthesis of binary silver chalcogenides with tuneable thermoelectric properties. *Chemical Engineering Journal* **2020,** *393*, 124763.
83. Gao, J.; Miao, L.; Lai, H.; Zhu, S.; Peng, Y.; Wang, X.; Koumoto, K.; Cai, H., Thermoelectric Flexible Silver Selenide Films: Compositional and Length Optimization. *iScience* **2020,** *23* (1), 100753.
84. Ge, Z.-H.; Song, D.; Chong, X.; Zheng, F.; Jin, L.; Qian, X.; Zheng, L.; Dunin-Borkowski, R. E.; Qin, P.; Feng, J.; Zhao, L.-D., Boosting the Thermoelectric Performance of (Na,K)-Codoped Polycrystalline SnSe by Synergistic Tailoring of the Band Structure and Atomic-Scale Defect Phonon Scattering. *Journal of the American Chemical Society* **2017,** *139* (28), 9714-9720.
85. Zhang, Y.; Liu, Y.; Xing, C.; Zhang, T.; Li, M.; Pacios, M.; Yu, X.; Arbiol, J.; Llorca, J.; Cadavid, D.; Ibáñez, M.; Cabot, A., Tin Selenide Molecular Precursor for the Solution Processing of Thermoelectric Materials and Devices. *ACS Applied Materials & Interfaces* **2020,** *12* (24), 27104-27111.
86. Protsak, I. S.; Champet, S.; Chiang, C.-Y.; Zhou, W.; Popuri, S. R.; Bos, J.-W. G.; Misra, D. K.; Morozov, Y. M.; Gregory, D. H., Toward New Thermoelectrics: Tin Selenide/Modified Graphene Oxide Nanocomposites. *ACS Omega* **2019,** *4* (3), 6010-6019.
87. Samanta, M.; Biswas, K., 2D Nanosheets of Topological Quantum Materials from Homologous (Bi2)m(Bi2Se3)n Heterostructures: Synthesis and Ultralow Thermal Conductivity. *Chemistry of Materials* **2020,** *32* (20), 8819-8826.
88. Tumelero, M. A.; Martins, M. B.; Souza, P. B.; Della Pace, R. D.; Pasa, A. A., Effect of electrolyte on the growth of thermoelectric Bi2Se3 thin films. *Electrochimica Acta* **2019,** *300*, 357-362.
89. Kadel, K.; Kumari, L.; Li, W. Z.; Huang, J. Y.; Provencio, P. P., Synthesis and Thermoelectric Properties of Bi2Se3 Nanostructures. *Nanoscale Res Lett* **2010,** *6* (1), 57.
90. Sarguru, M.; Kumar, R. T., Synthesis, characterization and applications of Aniline passivated bismuth selenide thermoelectric nanoparticles. *Materials Today: Proceedings* **2020,** *33*, 2187-2192.
91. Ahmed, R.; Xu, Y.; Sales, M. G.; Lin, Q.; McDonnell, S.; Zangari, G., Synthesis and Material Properties of Bi2Se3 Nanostructures Deposited by SILAR. *The Journal of Physical Chemistry C* **2018,** *122* (22), 12052-12060.
92. Andzane, J.; Buks, K.; Strakova, M. N.; Zubkins, M.; Bechelany, M.; Marnauza, M.; Baitimirova, M.; Erts, D., Structure and Doping Determined Thermoelectric Properties of

Bi₂Se₃ Thin Films Deposited by Vapour–Solid Technique. *IEEE Transactions on Nanotechnology* **2019,** *18*, 948-954.
93. Musah, J.-D.; Linlin, L.; Guo, C.; Novitskii, A.; Ilyas, A. O.; Serhiienko, I.; Khovaylo, V.; Roy, V. A. L.; Lawrence Wu, C.-M., Enhanced Thermoelectric Performance of Bulk Bismuth Selenide: Synergistic Effect of Indium and Antimony Co-doping. *ACS Sustainable Chemistry & Engineering* **2022,** *10* (12), 3862-3871.
94. Li, Y.; Liu, Y.; Gao, G.; Zhu, Y.; Wang, D.; Ding, M.; Yao, T.; Liu, M.; You, W., L-cysteine and urea synergistically-mediated one-pot one-step self-transformed hydrothermal synthesis of p-Ag2S/n-AgInS2 core-shell heteronanoflowers for photocatalytic MO degradation. *Applied Surface Science* **2021,** *548*, 149279.
95. Lim, K. H.; Wong, K. W.; Liu, Y.; Zhang, Y.; Cadavid, D.; Cabot, A.; Ng, K. M., Critical role of nanoinclusions in silver selenide nanocomposites as a promising room temperature thermoelectric material. *Journal of Materials Chemistry C* **2019,** *7* (9), 2646-2652.
96. Lisi, H., Facile in situ solution synthesis of SnSe/rGO nanocomposites with enhanced thermoelectric performance. *Journal of materials chemistry A* **2020,** *v. 8* (no. 3), pp. 1394-1402-2020 v.8 no.3.
97. Chandra, S.; Banik, A.; Biswas, K., n-Type Ultrathin Few-Layer Nanosheets of Bi-Doped SnSe: Synthesis and Thermoelectric Properties. *ACS Energy Letters* **2018,** *3* (5), 1153-1158.
98. Bohra, A. K.; Bhatt, R.; Singh, A.; Basu, R.; Bhattacharya, S.; Meshram, K. N.; Ahmad, S.; Debnath, A. K.; Chauhan, A. K.; Bhatt, P.; Shah, K.; Bhotkar, K.; Sharma, S.; Aswal, D. K.; Muthe, K. P.; Gadkari, S. C., Tellurium-free thermoelectrics: Improved thermoelectric performance of n-type Bi2Se3 having multiscale hierarchical architecture. *Energy Conversion and Management* **2017,** *145*, 415-424.
99. Hegde, G. S.; Prabhu, A. N.; Yang, C. F.; Kuo, Y. K., Reduction in electrical resistivity of bismuth selenide single crystal via Sn and Te co-doping. *Materials Chemistry and Physics* **2022,** *278*, 125675.
100. Bayesteh, S.; Sailler, S.; Schlörb, H.; He, R.; Schierning, G.; Nielsch, K.; Pérez, N., Mobility-enhanced thermoelectric performance in textured nanograin Bi2Se3, effect on scattering and surface-like transport. *Materials Today Physics* **2022,** *24*, 100669.
101. He, J.; Xu, J.; Tan, X.; Liu, G.-Q.; Shao, H.; Liu, Z.; Jiang, H.; Jiang, J., Synthesis of SnTe/AgSbSe2 nanocomposite as a promising lead-free thermoelectric material. *Journal of Materiomics* **2016,** *2* (2), 165-171.
102. Liu, W.-D.; Yang, L.; Chen, Z.-G., Cu2Se thermoelectrics: property, methodology, and device. *Nano Today* **2020,** *35*, 100938.
103. Han, G.; Chen, Z.-G.; Drennan, J.; Zou, J., Indium Selenides: Structural Characteristics, Synthesis and Their Thermoelectric Performances. *Small* **2014,** *10* (14), 2747-2765.
104. Wu, C.-F.; Wei, T.-R.; Li, J.-F., Enhancing average ZT in pristine PbSe by over-stoichiometric Pb addition. *APL Materials* **2016,** *4* (10), 104801.
105. Zhao, L.-D.; Hao, S.; Lo, S.-H.; Wu, C.-I.; Zhou, X.; Lee, Y.; Li, H.; Biswas, K.; Hogan, T. P.; Uher, C.; Wolverton, C.; Dravid, V. P.; Kanatzidis, M. G., High Thermoelectric Performance via Hierarchical Compositionally Alloyed Nanostructures. *Journal of the American Chemical Society* **2013,** *135* (19), 7364-7370.
106. Liu, H.; Yuan, X.; Lu, P.; Shi, X.; Xu, F.; He, Y.; Tang, Y.; Bai, S.; Zhang, W.; Chen, L.; Lin, Y.; Shi, L.; Lin, H.; Gao, X.; Zhang, X.; Chi, H.; Uher, C., Ultrahigh Thermoelectric Performance by Electron and Phonon Critical Scattering in Cu2Se1-xIx. *Advanced Materials* **2013,** *25* (45), 6607-6612.
107. Zhao, K.; Blichfeld, A. B.; Chen, H.; Song, Q.; Zhang, T.; Zhu, C.; Ren, D.; Hanus, R.; Qiu, P.; Iversen, B. B.; Xu, F.; Snyder, G. J.; Shi, X.; Chen, L., Enhanced Thermoelectric Performance through Tuning Bonding Energy in Cu2Se1–xSx Liquid-like Materials. *Chemistry of Materials* **2017,** *29* (15), 6367-6377.
108. Wang, J.; Jia, X.; Lou, S.; Li, G.; Zhou, S., Cu-Embedded SnSe2 with a High Figure of Merit at Ecofriendly Temperature. *ACS omega* **2020,** *5* (21), 12409-12414.

109. Shu, Y.; Su, X.; Xie, H.; Zheng, G.; Liu, W.; Yan, Y.; Luo, T.; Yang, X.; Yang, D.; Uher, C.; Tang, X., Modification of Bulk Heterojunction and Cl Doping for High-Performance Thermoelectric SnSe2/SnSe Nanocomposites. *ACS Applied Materials & Interfaces* **2018,** *10* (18), 15793-15802.
110. Shi, X.-L.; Tao, X.; Zou, J.; Chen, Z.-G., High-Performance Thermoelectric SnSe: Aqueous Synthesis, Innovations, and Challenges. *Advanced Science* **2020,** *7* (7), 1902923.
111. Jindal, S.; Singh, S.; Saini, G. S. S.; Tripathi, S. K., Low temperature thermoelectric power factors of thermally evaporated Ag2Se thin films. *AIP Conference Proceedings* **2020,** *2220* (1), 090008.
112. Wu, J.-K.; Hofmann, M.; Hsieh, W.-P.; Chen, S.-H.; Yen, Z.-L.; Chiu, S.-K.; Luo, Y.-R.; Chiang, C.-C.; Huang, S.-Y.; Chang, Y.-H.; Hsieh, Y.-P., Enhancing Thermoelectric Properties of 2D Bi2Se3 by 1D Texturing with Graphene. *ACS Applied Energy Materials* **2019,** *2* (12), 8411-8415.
113. Jia, B.; Liu, S.; Li, G.; Liu, S.; Zhou, Y.; Wang, Q., Study on thermoelectric properties of co-evaporated Sn-Se films with different phase formations. *Thin Solid Films* **2019,** *672*, 133-137.
114. Burton, M. R.; Liu, T.; McGettrick, J.; Mehraban, S.; Baker, J.; Pockett, A.; Watson, T.; Fenwick, O.; Carnie, M. J., Thin Film Tin Selenide (SnSe) Thermoelectric Generators Exhibiting Ultralow Thermal Conductivity. *Advanced Materials* **2018,** *30* (31), 1801357.
115. Jamwal, D.; Mehta, S. K., Metal Telluride Nanomaterials: Facile Synthesis, Properties and Applications for Third Generation Devices. *ChemistrySelect* **2019,** *4* (6), 1943-1963.
116. Hong, M.; Zou, J.; Chen, Z.-G., Thermoelectric GeTe with Diverse Degrees of Freedom Having Secured Superhigh Performance. *Advanced Materials* **2019,** *31* (14), 1807071.
117. Sun, S.; Peng, J.; Jin, R.; Song, S.; Zhu, P.; Xing, Y., Template-free solvothermal synthesis and enhanced thermoelectric performance of Sb2Te3 nanosheets. *Journal of alloys and compounds* **2013,** *558*, 6-10.
118. Bao, D.; Sun, Q.; Huang, L.; Chen, J.; Tang, J.; Zhou, D.; Hong, M.; Yang, L.; Chen, Z.-G., Thermoelectric performance of p-type (Bi,Sb)2Te3 incorporating amorphous Sb2S3 nanospheres. *Chemical Engineering Journal* **2022,** *430*, 132738.
119. Hong, M.; Chen, Z.-G.; Zou, J., Fundamental and progress of Bi ₂ Te ₃ -based thermoelectric materials. *Chinese Physics B* **2018,** *27* (4), 048403.
120. Liu, Y.; Wang, Q.; Pan, J.; Sun, Y.; Zhang, L.; Song, S., Hierarchical Bi2Te3 Nanostrings: Green Synthesis and Their Thermoelectric Properties. *Chemistry – A European Journal* **2018,** *24* (39), 9765-9768.
121. Wang, L.; Chang, S.; Zheng, S.; Fang, T.; Cui, W.; Bai, P.-p.; Yue, L.; Chen, Z.-G., Thermoelectric performance of Se/Cd codoped SnTe via microwave solvothermal method. *ACS Applied Materials & Interfaces* **2017,** *9* (27), 22612-22619.
122. Han, G.; Zhang, R.; Popuri, S. R.; Greer, H. F.; Reece, M. J.; Bos, J.-W. G.; Zhou, W.; Knox, A. R.; Gregory, D. H., Large-scale surfactant-free synthesis of p-Type SnTe nanoparticles for thermoelectric applications. *Materials* **2017,** *10* (3), 233.
123. Moshwan, R.; Yang, L.; Zou, J.; Chen, Z.-G., Eco-Friendly SnTe Thermoelectric Materials: Progress and Future Challenges. *Advanced Functional Materials* **2017,** *27* (43), 1703278.
124. Bao, D.; Chen, J.; Yu, Y.; Liu, W.; Huang, L.; Han, G.; Tang, J.; Zhou, D.; Yang, L.; Chen, Z.-G., Texture-dependent thermoelectric properties of nano-structured Bi2Te3. *Chemical Engineering Journal* **2020,** *388*, 124295.
125. Ju, H.; Kim, J., Preparation and structure dependent thermoelectric properties of nanostructured bulk bismuth telluride with graphene. *Journal of Alloys and Compounds* **2016,** *664*, 639-647.
126. Zhang, Q.; Ai, X.; Wang, L.; Chang, Y.; Luo, W.; Jiang, W.; Chen, L., Improved Thermoelectric Performance of Silver Nanoparticles-Dispersed Bi2Te3 Composites Deriving from Hierarchical Two-Phased Heterostructure. *Advanced Functional Materials* **2015,** *25* (6), 966-976.
127. An, J.; Han, M.-K.; Kim, S.-J., Synthesis of heavily Cu-doped Bi2Te3 nanoparticles and their thermoelectric properties. *Journal of Solid State Chemistry* **2019,** *270*, 407-412.

128. Cao, Y. Q.; Zhao, X. B.; Zhu, T. J.; Zhang, X. B.; Tu, J. P., Syntheses and thermoelectric properties of Bi2Te3/Sb2Te3 bulk nanocomposites with laminated nanostructure. *Applied Physics Letters* **2008,** *92* (14), 143106.
129. Kim, K.-C.; Lim, S.-S.; Lee, S. H.; Hong, J.; Cho, D.-Y.; Mohamed, A. Y.; Koo, C. M.; Baek, S.-H.; Kim, J.-S.; Kim, S. K., Precision Interface Engineering of an Atomic Layer in Bulk Bi2Te3 Alloys for High Thermoelectric Performance. *ACS Nano* **2019,** *13* (6), 7146-7154.
130. Jin, R.; Chen, G.; Pei, J.; Yan, C.; Zou, X.; Deng, M.; Sun, S., Facile solvothermal synthesis and growth mechanism of flower-like PbTe dendrites assisted by cyclodextrin. *CrystEngComm* **2012,** *14* (6), 2327-2332.
131. Yang, L.; Chen, Z.-G.; Hong, M.; Wang, L.; Kong, D.; Huang, L.; Han, G.; Zou, Y.; Dargusch, M.; Zou, J., n-type Bi-doped PbTe Nanocubes with Enhanced Thermoelectric Performance. *Nano Energy* **2017,** *31*, 105-112.
132. Zhou, W.; Zhao, W.; Lu, Z.; Zhu, J.; Fan, S.; Ma, J.; Hng, H. H.; Yan, Q., Preparation and thermoelectric properties of sulfur doped Ag2Te nanoparticles via solvothermal methods. *Nanoscale* **2012,** *4* (13), 3926-3931.
133. Nethravathi, C.; Rajamathi, C. R.; Rajamathi, M.; Maki, R.; Mori, T.; Golberg, D.; Bando, Y., Synthesis and thermoelectric behaviour of copper telluride nanosheets. *Journal of Materials Chemistry A* **2014,** *2* (4), 985-990.
134. Hao, F.; Xing, T.; Qiu, P.; Hu, P.; Wei, T.; Ren, D.; Shi, X.; Chen, L., Enhanced Thermoelectric Performance in n-Type Bi2Te3-Based Alloys via Suppressing Intrinsic Excitation. *ACS Applied Materials & Interfaces* **2018,** *10* (25), 21372-21380.
135. Malik, I.; Srivastava, T.; Surthi, K. K.; Gayner, C.; Kar, K. K., Enhanced thermoelectric performance of n-type Bi2Te3 alloyed with low cost and highly abundant sulfur. *Materials Chemistry and Physics* **2020,** *255*, 123598.
136. Jiang, Q.; Hu, H.; Yang, J.; Xin, J.; Li, S.; Viola, G.; Yan, H., High Thermoelectric Performance in SnTe Nanocomposites with All-Scale Hierarchical Structures. *ACS Applied Materials & Interfaces* **2020,** *12* (20), 23102-23109.
137. Feng, D.; Ge, Z.-H.; Chen, Y.-X.; Li, J.; He, J., Hydrothermal synthesis of SnQ (Q = Te, Se, S) and their thermoelectric properties. *Nanotechnology* **2017,** *28* (45), 455707.
138. Bhat, D. K.; Shenoy U, S., High Thermoelectric Performance of Co-Doped Tin Telluride Due to Synergistic Effect of Magnesium and Indium. *The Journal of Physical Chemistry C* **2017,** *121* (13), 7123-7130.
139. Xu, X.; Cui, J.; Yu, Y.; Zhu, B.; Huang, Y.; Xie, L.; Wu, D.; He, J., Constructing van der Waals gaps in cubic-structured SnTe-based thermoelectric materials. *Energy & Environmental Science* **2020,** *13* (12), 5135-5142.
140. Bhat, D. K.; Shenoy, U. S., Enhanced thermoelectric performance of bulk tin telluride: Synergistic effect of calcium and indium co-doping. *Materials Today Physics* **2018,** *4*, 12-18.
141. Zhou, M.; Snyder, G. J.; Li, L.; Zhao, L.-D., Lead-free tin chalcogenide thermoelectric materials. *Inorganic Chemistry Frontiers* **2016,** *3* (11), 1449-1463.
142. Tan, G.; Shi, F.; Hao, S.; Zhao, L.-D.; Chi, H.; Zhang, X.; Uher, C.; Wolverton, C.; Dravid, V. P.; Kanatzidis, M. G., Non-equilibrium processing leads to record high thermoelectric figure of merit in PbTe–SrTe. *Nature Communications* **2016,** *7* (1), 12167.
143. Zhang, Q.; Chere, E. K.; Wang, Y.; Kim, H. S.; He, R.; Cao, F.; Dahal, K.; Broido, D.; Chen, G.; Ren, Z., High thermoelectric performance of n-type PbTe1− ySy due to deep lying states induced by indium doping and spinodal decomposition. *Nano Energy* **2016,** *22*, 572-582.
144. Ibáñez, M.; Zamani, R.; Gorsse, S.; Fan, J.; Ortega, S.; Cadavid, D.; Morante, J. R.; Arbiol, J.; Cabot, A., Core–Shell Nanoparticles As Building Blocks for the Bottom-Up Production of Functional Nanocomposites: PbTe–PbS Thermoelectric Properties. *ACS Nano* **2013,** *7* (3), 2573-2586.
145. Wang, Z.; Wang, G.; Wang, R.; Zhou, X.; Chen, Z.; Yin, C.; Tang, M.; Hu, Q.; Tang, J.; Ang, R., Ga-doping-induced carrier tuning and multiphase engineering in n-type PbTe with enhanced thermoelectric performance. *ACS applied materials & interfaces* **2018,** *10* (26), 22401-22407.

146. Chowdhury, I.; Prasher, R.; Lofgreen, K.; Chrysler, G.; Narasimhan, S.; Mahajan, R.; Koester, D.; Alley, R.; Venkatasubramanian, R., On-chip cooling by superlattice-based thin-film thermoelectrics. *Nature Nanotechnology* **2009,** *4* (4), 235-238.
147. Rogacheva, E. I.; Nashchekina, O. N.; Meriuts, A. V.; Lyubchenko, S. G.; Dresselhaus, M. S.; Dresselhaus, G., Quantum size effects in n-PbTe/p-SnTe/n-PbTe heterostructures. *Applied Physics Letters* **2005,** *86* (6), 063103.
148. Urban, J. J.; Talapin, D. V.; Shevchenko, E. V.; Kagan, C. R.; Murray, C. B., Synergism in binary nanocrystal superlattices leads to enhanced p-type conductivity in self-assembled PbTe/Ag2Te thin films. *Nature Materials* **2007,** *6* (2), 115-121.
149. Fan, P.; Zhang, P.-c.; Liang, G.-x.; Li, F.; Chen, Y.-x.; Luo, J.-t.; Zhang, X.-h.; Chen, S.; Zheng, Z.-h., High-performance bismuth telluride thermoelectric thin films fabricated by using the two-step single-source thermal evaporation. *Journal of Alloys and Compounds* **2020,** *819*, 153027.
150. Bassi, A. L.; Bailini, A.; Casari, C. S.; Donati, F.; Mantegazza, A.; Passoni, M.; Russo, V.; Bottani, C. E., Thermoelectric properties of Bi–Te films with controlled structure and morphology. *Journal of Applied Physics* **2009,** *105* (12), 124307.
151. Jin, Q.; Jiang, S.; Zhao, Y.; Wang, D.; Qiu, J.; Tang, D.-M.; Tan, J.; Sun, D.-M.; Hou, P.-X.; Chen, X.-Q.; Tai, K.; Gao, N.; Liu, C.; Cheng, H.-M.; Jiang, X., Flexible layer-structured Bi2Te3 thermoelectric on a carbon nanotube scaffold. *Nature Materials* **2019,** *18* (1), 62-68.
152. Karthikeyan, V.; Surjadi, J. U.; Wong, J. C. K.; Kannan, V.; Lam, K.-H.; Chen, X.; Lu, Y.; Roy, V. A. L., Wearable and flexible thin film thermoelectric module for multi-scale energy harvesting. *Journal of Power Sources* **2020,** *455*, 227983.
153. Bala, M.; Gupta, S.; Tripathi, T. S.; Varma, S.; Tripathi, S. K.; Asokan, K.; Avasthi, D. K., Enhancement of thermoelectric power of PbTe: Ag nanocomposite thin films. *RSC Advances* **2015,** *5* (33), 25887-25895.
154. Kadel, K.; Kumari, L.; Li, W.; Huang, J. Y.; Provencio, P. P., Synthesis and thermoelectric properties of Bi2Se3 nanostructures. *Nanoscale Res Lett* **2011,** *6* (1), 1-7.
155. Ge, Z.-H.; Song, D.; Chong, X.; Zheng, F.; Jin, L.; Qian, X.; Zheng, L.; Dunin-Borkowski, R. E.; Qin, P.; Feng, J., Boosting the thermoelectric performance of (Na, K)-codoped polycrystalline SnSe by synergistic tailoring of the band structure and atomic-scale defect phonon scattering. *Journal of the American Chemical Society* **2017,** *139* (28), 9714-9720.
156. Zhang, Q.; Ai, X.; Wang, L.; Chang, Y.; Luo, W.; Jiang, W.; Chen, L., Improved thermoelectric performance of silver nanoparticles-dispersed Bi2Te3 composites deriving from hierarchical two-phased heterostructure. *Advanced Functional Materials* **2015,** *25* (6), 966-976.
157. Liu, Y.; Wang, Q.; Pan, J.; Sun, Y.; Zhang, L.; Song, S., Hierarchical Bi2Te3 Nanostrings: Green Synthesis and Their Thermoelectric Properties. *Chemistry–A European Journal* **2018,** *24* (39), 9765-9768.
158. Hwang, J.; Kim, H.; Han, M.-K.; Hong, J.; Shim, J.-H.; Tak, J.-Y.; Lim, Y. S.; Jin, Y.; Kim, J.; Park, H.; Lee, D.-K.; Bahk, J.-H.; Kim, S.-J.; Kim, W., Gigantic Phonon-Scattering Cross Section To Enhance Thermoelectric Performance in Bulk Crystals. *ACS Nano* **2019,** *13* (7), 8347-8355.
159. Yang, L.; Chen, Z.-G.; Han, G.; Hong, M.; Huang, L.; Zou, J., Te-Doped Cu 2 Se nanoplates with a high average thermoelectric figure of merit. *Journal of Materials Chemistry A* **2016,** *4* (23), 9213-9219.
160. Zhou, W.; Zhao, W.; Lu, Z.; Zhu, J.; Fan, S.; Ma, J.; Hng, H. H.; Yan, Q., Preparation and thermoelectric properties of sulfur doped Ag 2 Te nanoparticles via solvothermal methods. *Nanoscale* **2012,** *4* (13), 3926-3931.
161. Ali, Z.; Butt, S.; Cao, C.; Butt, F. K.; Tahir, M.; Tanveer, M.; Aslam, I.; Rizwan, M.; Idrees, F.; Khalid, S., Thermochemically evolved nanoplatelets of bismuth selenide with enhanced thermoelectric figure of merit. *AIP Advances* **2014,** *4* (11), 117129.
162. Qin, F.; Nikolaev, S. A.; Suwardi, A.; Wood, M.; Zhu, Y.; Tan, X.; Aydemir, U.; Ren, Y.; Yan, Q.; Hu, L., Crystal structure and atomic vacancy optimized thermoelectric properties in gadolinium selenides. *Chemistry of Materials* **2020,** *32* (23), 10130-10139.

163. Hamawandi, B.; Ballikaya, S.; Råsander, M.; Halim, J.; Vinciguerra, L.; Rosén, J.; Johnsson, M.; S Toprak, M., Composition tuning of nanostructured binary copper selenides through rapid chemical synthesis and their thermoelectric property evaluation. *Nanomaterials* **2020,** *10* (5), 854.
164. Yang, J.; Li, H.; Wu, T.; Zhang, W.; Chen, L.; Yang, J., Evaluation of half-Heusler compounds as thermoelectric materials based on the calculated electrical transport properties. *Advanced Functional Materials* **2008,** *18* (19), 2880-2888.
165. Qiu, P.; Yang, J.; Huang, X.; Chen, X.; Chen, L., Effect of antisite defects on band structure and thermoelectric performance of ZrNiSn half-Heusler alloys. *Applied Physics Letters* **2010,** *96* (15), 152105.
166. Zhao, K.; Blichfeld, A. B.; Chen, H.; Song, Q.; Zhang, T.; Zhu, C.; Ren, D.; Hanus, R.; Qiu, P.; Iversen, B. B., Enhanced Thermoelectric Performance through Tuning Bonding Energy in Cu2Se1–x S x Liquid-like Materials. *Chemistry of Materials* **2017,** *29* (15), 6367-6377.
167. Imasato, K.; Wood, M.; Anand, S.; Kuo, J. J.; Snyder, G. J., Understanding the High Thermoelectric Performance of Mg3Sb2-Mg3Bi2 Alloys. *Advanced Energy and Sustainability Research n/a* (n/a), 2100208.
168. Wu, F.; Song, H.; Jia, J.; Hu, X., Thermoelectric properties of rare earth-doped n-type Bi2Se0. 3Te2. 7 nanocomposites. *Bulletin of Materials Science* **2014,** *37* (5), 1007-1012.
169. Zhang, Q.; Wang, H.; Liu, W.; Wang, H.; Yu, B.; Zhang, Q.; Tian, Z.; Ni, G.; Lee, S.; Esfarjani, K., Enhancement of thermoelectric figure-of-merit by resonant states of aluminium doping in lead selenide. *Energy & Environmental Science* **2012,** *5* (1), 5246-5251.
170. Zhang, Q.; Cao, F.; Liu, W.; Lukas, K.; Yu, B.; Chen, S.; Opeil, C.; Broido, D.; Chen, G.; Ren, Z., Heavy doping and band engineering by potassium to improve the thermoelectric figure of merit in p-type pbte, pbse, and pbte1–y se y. *Journal of the American chemical society* **2012,** *134* (24), 10031-10038.
171. Bhattacharya, S.; Pope, A.; Littleton IV, R.; Tritt, T. M.; Ponnambalam, V.; Xia, Y.; Poon, S., Effect of Sb doping on the thermoelectric properties of Ti-based half-Heusler compounds, TiNiSn 1− x Sb x. *Applied Physics Letters* **2000,** *77* (16), 2476-2478.
172. Li, J.; Li, S.; Wang, Q.; Wang, L.; Liu, F.; Ao, W., Effect of Ce-doping on thermoelectric properties in PbTe alloys prepared by spark plasma sintering. *Journal of electronic materials* **2011,** *40* (10), 2063-2068.
173. Dresselhaus, M. S.; Chen, G.; Tang, M. Y.; Yang, R.; Lee, H.; Wang, D.; Ren, Z.; Fleurial, J. P.; Gogna, P., New directions for low-dimensional thermoelectric materials. *Advanced materials* **2007,** *19* (8), 1043-1053.
174. Gayner, C.; Kar, K. K., Recent advances in thermoelectric materials. *Progress in Materials Science* **2016,** *83*, 330-382.
175. Venkatasubramanian, R.; Siivola, E.; Colpitts, T.; O'quinn, B., Thin-film thermoelectric devices with high room-temperature figures of merit. *Nature* **2001,** *413* (6856), 597-602.
176. Makala, R. S.; Jagannadham, K.; Sales, B. C., Pulsed laser deposition of Bi 2 Te 3-based thermoelectric thin films. *Journal of Applied physics* **2003,** *94* (6), 3907-3918.
177. Harman, T.; Taylor, P.; Walsh, M.; LaForge, B., Quantum dot superlattice thermoelectric materials and devices. *science* **2002,** *297* (5590), 2229-2232.
178. Zhou, M.; Li, J.-F.; Kita, T., Nanostructured AgPb m SbTe m+ 2 system bulk materials with enhanced thermoelectric performance. *Journal of the American Chemical Society* **2008,** *130* (13), 4527-4532.
179. Xie, W.; He, J.; Kang, H. J.; Tang, X.; Zhu, S.; Laver, M.; Wang, S.; Copley, J. R.; Brown, C. M.; Zhang, Q., Identifying the specific nanostructures responsible for the high thermoelectric performance of (Bi, Sb) 2Te3 nanocomposites. *Nano letters* **2010,** *10* (9), 3283-3289.
180. Xie, W.; Tang, X.; Yan, Y.; Zhang, Q.; Tritt, T. M., High thermoelectric performance BiSbTe alloy with unique low-dimensional structure. *Journal of Applied Physics* **2009,** *105* (11), 113713.

181. Ouyang, Y.; Zhang, Z.; Li, D.; Chen, J.; Zhang, G., Emerging Theory, Materials, and Screening Methods: New Opportunities for Promoting Thermoelectric Performance. *Annalen der Physik* **2019,** *531* (4), 1800437.
182. Mulla, R.; Dunnill, C. W., Core–shell nanostructures for better thermoelectrics. *Materials Advances* **2022,** *3* (1), 125-141.
183. Jang, Y.; Shapiro, A.; Isarov, M.; Rubin-Brusilovski, A.; Safran, A.; Budniak, A. K.; Horani, F.; Dehnel, J.; Sashchiuk, A.; Lifshitz, E., Interface control of electronic and optical properties in IV–VI and II–VI core/shell colloidal quantum dots: a review. *Chemical Communications* **2017,** *53* (6), 1002-1024.
184. Mun, H.; Choi, S. M.; Lee, K. H.; Kim, S. W., Boundary engineering for the thermoelectric performance of bulk alloys based on bismuth telluride. *ChemSusChem* **2015,** *8* (14), 2312-2326.
185. Yang, L.; Chen, Z.-G.; Dargusch, M. S.; Zou, J., High Performance Thermoelectric Materials: Progress and Their Applications. *Advanced Energy Materials* **2018,** *8* (6), 1701797.
186. Biswas, K.; He, J.; Blum, I. D.; Wu, C.-I.; Hogan, T. P.; Seidman, D. N.; Dravid, V. P.; Kanatzidis, M. G., High-performance bulk thermoelectrics with all-scale hierarchical architectures. *Nature* **2012,** *489* (7416), 414-418.
187. Yang, L.; Chen, Z.-G.; Hong, M.; Han, G.; Zou, J., Enhanced Thermoelectric Performance of Nanostructured Bi2Te3 through Significant Phonon Scattering. *ACS Applied Materials & Interfaces* **2015,** *7* (42), 23694-23699.
188. Takashiri, M.; Miyazaki, K.; Tanaka, S.; Kurosaki, J.; Nagai, D.; Tsukamoto, H., Effect of grain size on thermoelectric properties of n-type nanocrystalline bismuth-telluride based thin films. *Journal of Applied Physics* **2008,** *104* (8), 084302.
189. Shi, Z.; Su, T.; Zhang, P.; Lou, Z.; Qin, M.; Gao, T.; Xu, J.; Zhu, J.; Gao, F., Enhanced thermoelectric performance of Ca3Co4O9 ceramics through grain orientation and interface modulation. *Journal of Materials Chemistry A* **2020,** *8* (37), 19561-19572.
190. Van Nong, N.; Pryds, N.; Linderoth, S.; Ohtaki, M., Enhancement of the Thermoelectric Performance of p-Type Layered Oxide Ca3Co4O9+δ Through Heavy Doping and Metallic Nanoinclusions. *Advanced Materials* **2011,** *23* (21), 2484-2490.
191. Snyder, G., Interfaces in bulk thermoelectric materials. *Curr. Opin. Colloid Interface Sci* **2009,** *14*, 226-235.
192. SNYDER, G. J.; TOBERER, E. S., Complex thermoelectric materials. In *Materials for Sustainable Energy*, pp 101-110.
193. Mulla, R.; Rabinal, M. H. K., Copper Sulfides: Earth-Abundant and Low-Cost Thermoelectric Materials. *Energy Technology* **2019,** *7* (7), 1800850.
194. Rowe, D. M., *CRC handbook of thermoelectrics*. CRC press: 2018.
195. Hong, J.-E.; Yoon, S.-G., Effect of structural change on thermoelectric properties of the chalcogenide Ge2Sb2Te5 thin films. *ECS Journal of Solid State Science and Technology* **2014,** *3* (10), P298.
196. Yu, B.; Liu, W.; Chen, S.; Wang, H.; Wang, H.; Chen, G.; Ren, Z., Thermoelectric properties of copper selenide with ordered selenium layer and disordered copper layer. *Nano Energy* **2012,** *1* (3), 472-478.
197. Liu, H.; Shi, X.; Xu, F.; Zhang, L.; Zhang, W.; Chen, L.; Li, Q.; Uher, C.; Day, T.; Snyder, G. J., Copper ion liquid-like thermoelectrics. *Nature materials* **2012,** *11* (5), 422-425.
198. Zevalkink, A.; Smiadak, D. M.; Blackburn, J. L.; Ferguson, A. J.; Chabinyc, M. L.; Delaire, O.; Wang, J.; Kovnir, K.; Martin, J.; Schelhas, L. T., A practical field guide to thermoelectrics: Fundamentals, synthesis, and characterization. *Applied Physics Reviews* **2018,** *5* (2), 021303.
199. Li, C.; Jiang, F.; Liu, C.; Liu, P.; Xu, J., Present and future thermoelectric materials toward wearable energy harvesting. *Applied Materials Today* **2019,** *15*, 543-557.
200. Torfs, T.; Leonov, V.; Van Hoof, C.; Gyselinckx, B. In *Body-heat powered autonomous pulse oximeter*, SENSORS, 2006 IEEE, IEEE: 2006; pp 427-430.

201. Huu, T. N.; Van, T. N.; Takahito, O., Flexible thermoelectric power generator with Y-type structure using electrochemical deposition process. *Applied energy* **2018,** *210*, 467-476.
202. Leonov, V., Thermoelectric energy harvesting of human body heat for wearable sensors. *IEEE Sensors Journal* **2013,** *13* (6), 2284-2291.
203. Rincón-Casado, A.; Martinez, A.; Araiz, M.; Pavón-Domínguez, P.; Astrain, D., An experimental and computational approach to thermoelectric-based conditioned mattresses. *Applied Thermal Engineering* **2018,** *135*, 472-482.
204. Hong, S.; Gu, Y.; Seo, J. K.; Wang, J.; Liu, P.; Meng, Y. S.; Xu, S.; Chen, R., Wearable thermoelectrics for personalized thermoregulation. *Science advances* **2019,** *5* (5), eaaw0536.
205. Wang, W.; Cionca, V.; Wang, N.; Hayes, M.; O'Flynn, B.; O'Mathuna, C., Thermoelectric energy harvesting for building energy management wireless sensor networks. *International journal of distributed sensor networks* **2013,** *9* (6), 232438.
206. Iezzi, B.; Ankireddy, K.; Twiddy, J.; Losego, M. D.; Jur, J. S., Printed, metallic thermoelectric generators integrated with pipe insulation for powering wireless sensors. *Applied energy* **2017,** *208*, 758-765.
207. Vancauwenberghe, O.; Short, J.; Giehler, E.; Bildstein, P.; Ancey, P.; Gschwind, M., Microsensor for the preventive detection of water condensation: operating principle and interface electronics. *Sensors and Actuators A: Physical* **1996,** *53* (1-3), 304-308.
208. Li, Y.; Buddharaju, K.; Tinh, B. C.; Singh, N.; Lee, S. J., Improved vertical silicon nanowire based thermoelectric power generator with polyimide filling. *IEEE electron device letters* **2012,** *33* (5), 715-717.
209. Suarez, F.; Parekh, D. P.; Ladd, C.; Vashaee, D.; Dickey, M. D.; Öztürk, M. C., Flexible thermoelectric generator using bulk legs and liquid metal interconnects for wearable electronics. *Applied energy* **2017,** *202*, 736-745.
210. Lv, S.; He, W.; Wang, L.; Li, G.; Ji, J.; Chen, H.; Zhang, G., Design, fabrication and feasibility analysis of a thermo-electric wearable helmet. *Applied Thermal Engineering* **2016,** *109*, 138-146.
211. Brown, S. R.; Kauzlarich, S. M.; Gascoin, F.; Snyder, G. J., Yb14MnSb11: New high efficiency thermoelectric material for power generation. *Chemistry of materials* **2006,** *18* (7), 1873-1877.
212. Recatala-Gomez, J.; Suwardi, A.; Nandhakumar, I.; Abutaha, A.; Hippalgaonkar, K., Toward accelerated thermoelectric materials and process discovery. *ACS Applied Energy Materials* **2020,** *3* (3), 2240-2257.
213. Harcourt, R.; Bruine de Bruin, W.; Dessai, S.; Taylor, A., Investing in a good pair of wellies: how do non-experts interpret the expert terminology of climate change impacts and adaptation? *Climatic change* **2019,** *155* (2), 257-272.
214. O'Brien, R.; Ambrosi, R.; Bannister, N.; Howe, S.; Atkinson, H. V., Safe radioisotope thermoelectric generators and heat sources for space applications. *Journal of Nuclear Materials* **2008,** *377* (3), 506-521.
215. Ritz, F.; Peterson, C. E. In *Multi-mission radioisotope thermoelectric generator (MMRTG) program overview*, 2004 IEEE aerospace conference proceedings (IEEE Cat. No. 04TH8720), IEEE: 2004; pp 2950-2957.
216. Tan, G.; Ohta, M.; Kanatzidis, M. G., Thermoelectric power generation: from new materials to devices. *Philosophical Transactions of the Royal Society A* **2019,** *377* (2152), 20180450.
217. Brown, S. R.; Kauzlarich, S. M.; Gascoin, F.; Snyder, G. J., Yb14MnSb11: New High Efficiency Thermoelectric Material for Power Generation. *Chemistry of Materials* **2006,** *18* (7), 1873-1877.
218. Luo, Q.; Wang, Y.; Zhang, P. In *A novel thermoelectric air-conditioner for a truck cab*, 2010 International Conference on Advances in Energy Engineering, 19-20 June 2010; 2010; pp 178-181.
219. Choi, H.-S.; Yun, S.; Whang, K.-i., Development of a temperature-controlled car-seat system utilizing thermoelectric device. *Applied Thermal Engineering* **2007,** *27* (17), 2841-2849.
220. Redus, R. H.; Huber, A. C.; Pantazis, J. A., Improved thermoelectrically cooled X/γ-ray detectors and electronics. *Nuclear Instruments and Methods in Physics Research Section A: Accelerators, Spectrometers, Detectors and Associated Equipment* **2001,** *458* (1), 214-219.

221. Naphon, P.; Wiriyasart, S., Liquid cooling in the mini-rectangular fin heat sink with and without thermoelectric for CPU. *International Communications in Heat and Mass Transfer* **2009,** *36* (2), 166-171.
222. Gould, C. A.; Shammas, N. Y. A.; Grainger, S.; Taylor, I., Thermoelectric cooling of microelectronic circuits and waste heat electrical power generation in a desktop personal computer. *Materials Science and Engineering: B* **2011,** *176* (4), 316-325.
223. Cheng, T.-C.; Cheng, C.-H.; Huang, Z.-Z.; Liao, G.-C., Development of an energy-saving module via combination of solar cells and thermoelectric coolers for green building applications. *Energy* **2011,** *36* (1), 133-140.
224. Hara, T.; Azuma, H.; Shimizu, H.; Obora, H.; Sato, S., Cooling performance of solar cell driven, thermoelectric cooling prototype headgear. *Applied Thermal Engineering* **1998,** *18* (11), 1159-1169.
225. Jaziri, N.; Boughamoura, A.; Müller, J.; Mezghani, B.; Tounsi, F.; Ismail, M., A comprehensive review of Thermoelectric Generators: Technologies and common applications. *Energy Reports* **2020,** *6*, 264-287.
226. Tan, G.; Ohta, M.; Kanatzidis, M. G., Thermoelectric power generation: from new materials to devices. *Philosophical Transactions of the Royal Society A: Mathematical, Physical and Engineering Sciences* **2019,** *377* (2152), 20180450.
227. Yan, Q.; Kanatzidis, M. G., High-performance thermoelectrics and challenges for practical devices. *Nature Materials* **2022,** *21* (5), 503-513.
228. Gelbstein, G. M. G. Y., Mechanical Properties of Thermoelectric Materials for Practical Applications. In *Bringing Thermoelectricity into Reality*, Aranguren, P., Ed. IntechOpen: 2018.